International Scientific-Technical and Production Journal

The Paton WELDING JOURNAL

April 2011 # 4

English translation of the monthly «Avtomaticheskaya Svarka» (Automatic Welding) journal published in Russian since 1948

Founders: *E.O. Paton Electric Welding Institute of the NAS of Ukraine International Association «Welding»* **Publisher:** *International Association «Welding»*

Address:
E.O. Paton Electric Welding Institute,
International Association «Welding»,
11, Bozhenko str., 03680, Kyiv, Ukraine
Tel.: (38044) 200 67 57, 200 82 77
Fax: (38044) 200 04 86, 200 82 77
E-mail: journal@paton.kiev.ua
http://www.nas.gov.ua/pwj

State Registration Certificate
KV 4790 of 09.01.2001

Subscriptions:
$324, 12 issues per year,
postage and packaging included.
Back issues available.

CONTENTS

INFLUENCE OF REPEATED LOADING ON THE EFFICIENCY OF ELECTRODYNAMIC TREATMENT OF ALUMINIUM ALLOY AMg6 AND ITS WELDED JOINTS

L.M. LOBANOV, N.A. PASHCHIN, V.P. LOGINOV and **O.L. MIKHODUJ**
E.O. Paton Electric Welding Institute, NASU, Kiev, Ukraine

The mechanism of reduction of preliminary stresses in repeated loading and electrodynamic treatment of AMg6 alloy and its welded joints were investigated on the basis of the developed procedure. It was established that the history of loading of AMg6 alloy has no substantial effect on relaxation characteristics of metal subjected to repeated impact by current pulses.

Keywords: *aluminium alloy, welded joint, residual stress, electric current pulse, electrodynamic treatment, efficiency of treatment, relative yield strength, tensile strength*

During service of welded structures of aluminium-magnesium alloys operating under conditions of influence of pulse electric and magnetic fields, the residual stresses causing fracture of single elements can arise at certain conditions. The beginning of plastic flow of metal begins at values of working stresses below the relative yield strength [1–3].

Since the end of the last century a number of domestic and foreign scientific organizations conduct research works on optimization of structure and properties of structural materials and welded joints using their treatment by pulse electromagnetic fields. It was established that pulse influence of current on metals and alloys affects the fatigue resistance, static strength and other mechanical characteristics [4]. At the same time the data of work [3] evidence negative role of electromagnetic effect on the strength of metals and alloys.

One of the methods of electric current impact on the metals is electrodynamic treatment (EDT) based on initiating of electrodynamic forces in the material, which are formed during passing of electric charge through the current conducting material [5]. While summing them with outer loadings, applied to the structure being treated, the local fields of plastic yielding of metal arise in the zone of current impact [6].

During investigation of EDT influence on aluminium alloys and low-carbon steels the main attention was paid on studying mechanism of stress state relaxation [7–9] and evolution of structure of base metal and welded joint [10]. It should be noted that questions about changing strength characteristics of welded joints under the impact of energy of current charges initiated by EDT practically were not studied. At the same time in the works [3, 4] different opinions about influence of pulse electromagnetic fields on the strength of structural materials are given. Besides there are no data in modern literature about the effect of repeated loading on relaxation of stresses in metal at electromagnetic effects.

The purpose of this work is investigation of influence of EDT on mechanical properties of aluminium alloy AMg6 and its welded joints at uniaxial tension as well as on relaxation of stresses at repeated loading of metal.

The EDT of specimens of base metal and welded joints of annealed aluminium alloy AMg6 of 4 mm thickness with a size of 110 × 30 mm working area loaded by uniaxial tension at the speed of 0.1 mm/s were carried out. Three levels of tensile loadings were preset: at the low elastic stresses of 52–60 MPa; at the stresses of 116–147 MPa close to elasticity limit of AMg6 alloy (which approximately correlates with the level of residual welding stresses in the alloy being investigated); at the stresses beyond elasticity limit. The tension in elastic-plastic zone was brought to 260–280 MPa, i.e. till generating Portevin–Le Chatelier effect which is manifested in the discontinuous yielding of metal in the zone of prefracture [11].

EDT was performed using laboratory machine, the description of which is given in the work [9]. EDT of specimens after tension was performed using contact of working electrode with a surface of a metal according to the scheme presented in [7]. The specimens were subjected to tension till generating stresses of preset value in them and treated with a series of current discharges, after each pulse the drop of tensile force in the material was controlled. The EDT was conducted at the energy of current discharge E = 140, 300 and 800 J.

After termination of EDT, the 50 % of investigated specimens were subjected to fracture and remained part was again subjected to tension and treatment under similar conditions to determine influence of repeated cycle of EDT on stress relaxation.

The changes of mechanical properties of AMg6 alloy and its welded joints at different levels of loading and energy of current discharge are given in the Table. Analyzing its data it can be concluded that EDT at E = 140–300 J of specimens loaded up to 140 MPa (series Nos. 2, 3, 5, 6) practically does not influence the characteristics of static strength as compared with initial values (series No.1). The same concerns the variant of treatment at E = 800 J and σ_{in} = 60 MPa (series No.8). The EDT at E = 800 J at increasing σ_{in} to the values close to elasticity limit of AMg6 alloy, 15–20 % increases $\sigma_{0.2}$ of base metal and welded joint (series No.9). The values of σ_t of a welded joint are increased approximately by 15 %. The combined impact of electric current pulses and elastic-plastic loading enhances yielding processes in the specimens being studied which are determined according to increase of values $\sigma_{0.2}$ by 45–50 % (series Nos. 4, 7, 10). The tensile strength of base metal increases approximately by 8, and that of welded joint — by 20 %.

Figure 1 shows dependence of the level of initial tensile stresses of specimens of welded joints on the number of discharges at the first and repeated tensions. Figure 1, *a* shows that at E = 140 J negligible decrease of values σ_{in} after the first EDT (curves *1* and *3*) and repeated (curves *2* and *4*) occurs in elastic loading area. At σ_{in} < 60 MPa the relative decrease of values of stresses at the first and repeated EDT was respectively 16 and 21 %. For specimens at tensile stresses up to 120 MPa the similar values after two series of EDT did not exceed 20 %. In elastic-plastic area at σ_{in} = 260 MPa after the first (Figure 1, curve *5*) and repeated (Figure 1, curve *6*) EDT the decrease of stresses amounted, respectively, to 11 and 14 %, i.e. lower than at small loads (Figure 1, curves *1* and *2*).

More efficient is EDT of welded joints at E = = 800 J. After the first and repeated series of EDT of specimens after tension at tensile stresses of up to 60 MPa (Figure 1, *b*, curves *1*, *2*) the relative decrease of applied loading in both cases was 55 %. The increase of tensile forces to the values close to elasticity limit of 140 MPa (Figure 1, curves *3*, *4*) practically does

Mechanical properties of AMg6 alloy and its welded joints after EDT

No. of series of specimen	Energy of current discharge E, J	Initial tensile stresses σ_{in}, MPa	Relative yield strength $\sigma_{0.2}$, MPa	Tensile strength σ_t, MPa
1	–	–	140/130	305/246
2	140	60	140/130	305/245
3	140	140	145/131	304/248
4	140	260	253/232	330/303
5	300	55	145/130	305/246
6	300	135	144/132	310/245
7	300	265	258/237	330/303
8	800	60	145/133	305/245
9	800	146	170/152	310/285
10	800	260	261/256	332/305

Note. 1. Numerator denotes the data for base metal, while denominator gives data for welded joint. 2. Series of specimens Nos. 7, 9 and 10 obtained increment of values $\sigma_{0.2}$ and σ_t under the effect of EDT.

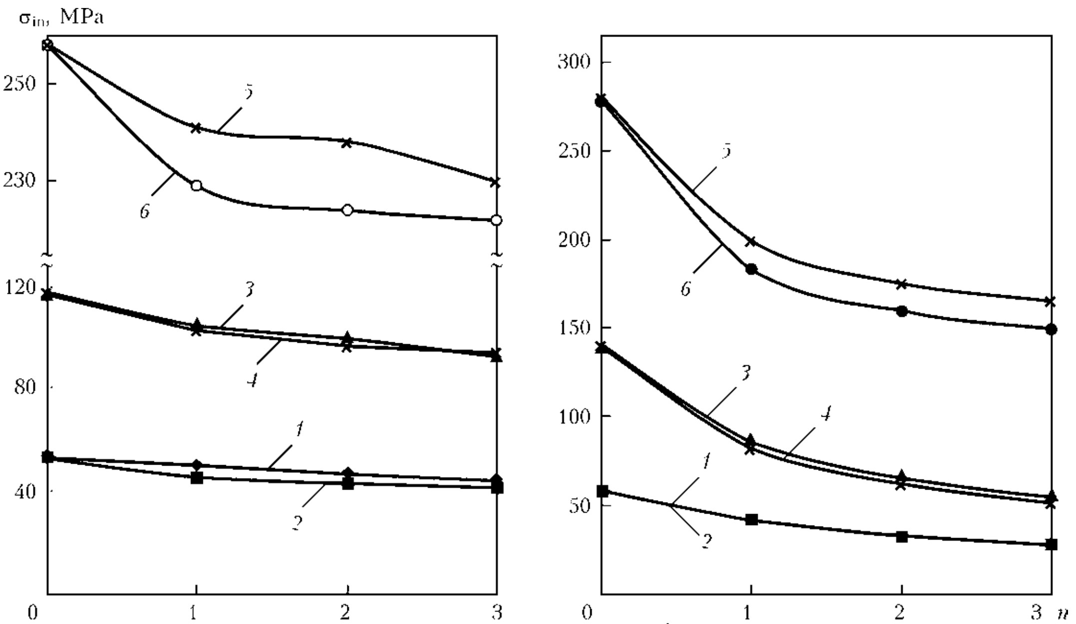

Figure 1. Dependence of level of tensile stresses σ_{in} on number of discharges n in specimens of welded joints of AMg6 alloy at E = 140 (*a*) and 800 (*b*) J after the first (*1*, *3*, *5*) and repeated (*2*, *4*, *6*) EDT

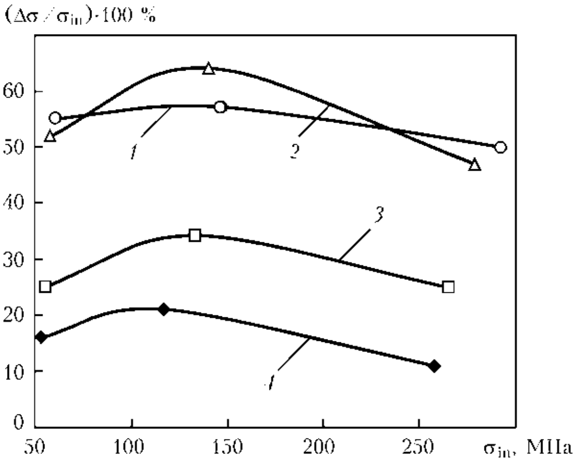

Figure 2. Dependence of relative efficiency $\Delta\sigma/\sigma_{in}$ of EDT in specimens of AMg6 alloy (*1*, *3*) and its welded joints (*2*, *4*) on the level of tensile stresses σ_{in} at E = 800 (*1*, *2*), 300 (*3*) and 140 (*4*) J

not influence the efficiency of current impact. Therefore after two series of EDT the relative decrease of loading was respectively 60 and 65 %. In elastic-plastic area the level of tensile stresses reaches 280 MPa as well as at EDT with E = 140 J (Figure 1, *a*), the efficiency of treatment is somewhat decreased. Here, the difference is observed in values of drops of loading after first and second EDT (Figure 1, curves *5*, *6*), relative efficiency of these processes is respectively 40 and 50 %.

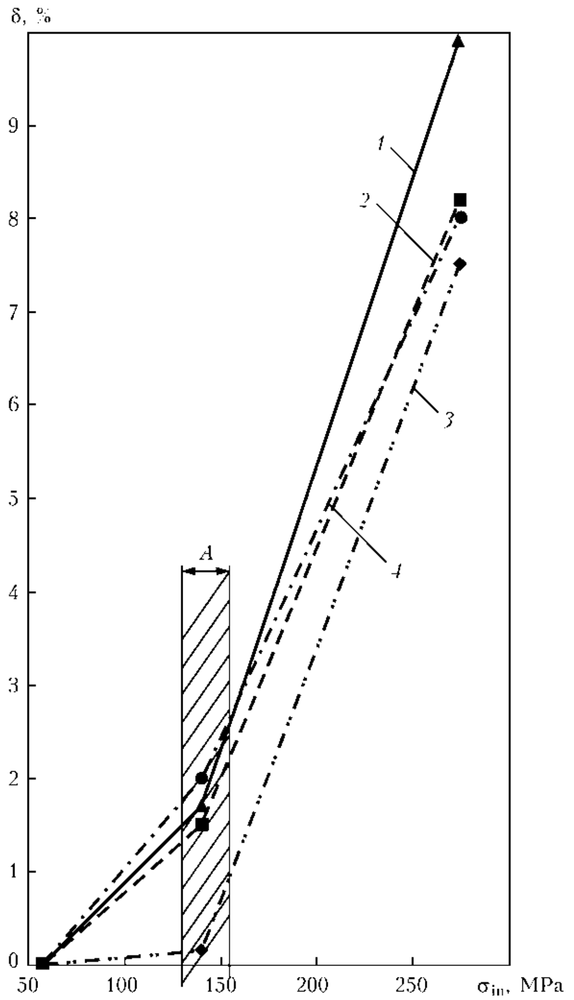

Figure 3. Dependence of residual elongation δ on the level of tensile stresses σ_{in} in the specimens of base metal of AMg6 alloy (*1*, *2*) and its welded joints (*3*, *4*) at E = 800 (*1*, *4*), 300 (*2*) and 140 (*3*) J: *A* — region of maximal $\Delta\sigma/\sigma_{in}$ values

After EDT the values of δ_{in} in the specimens of base metal (AMg6 alloy) were practically the same as in Figure 1 which evidences the similarity of relaxation mechanisms in welded joints.

Figure 2 shows that resulting efficiency of the process of treatment is directly proportional to the energy of current discharge in the range being investigated. EDT with E = 800 J provides maximal decrease of applied tensile stresses in the whole range of loadings being investigated. The highest effect at all the values of energy of current discharge used in this work is achieved at the level of initial tensile stresses close to limit of elasticity for AMg6 alloy (150 MPa) which is approximately in compliance with the peaks of tensile stresses for AMg6 alloy. The comparison of efficiency of current impact on the specimens of base metal and welded joints (Figure 2) showed that cast structure of a weld is more subjected to EDT impact with E = 800 J at σ_{in} = 130–150 MPa. This is expressed in the higher level of efficiency of reducing stresses after EDT in the specimens of welded joints as compared to the base metal (accordingly 60 and 55 %) which makes the premises for the development of EDT technology to control the stressed state of welded structures of aluminium-magnesium alloys. At the same time the decrease of values of relative efficiency of EDT at σ_{in} = 260–280 MPa (Figure 2) can be connected with deformational strengthening initiated by current discharges in AMg6 alloy [10].

The evaluation of residual elongation δ of base metal and welded joints initiated by current discharges in the specimens at EDT was carried out. In accordance with the data of the works [4, 6] the passing of current pulse through the loaded material results in formation of plastic deformation in it which can influence the characteristics of static strength. Figure 3 shows that at E = 140 J the residual elongation of specimens is stimulated by EDT process at tensile stresses of more than 120 MPa, and at σ_{in} = 150 MPa δ = 1.5 % and can reach 7.5 % in elastic-plastic area of loading at σ_{in} = 275 MPa. At σ_{in} = 60 MPa the use of the whole range of energies of current discharge did not result in increase of elongation that proves a low efficiency of EDT process of AMg6 alloy with a low level of initial stresses. At the same time at σ_{in} > 125 MPa the current discharges with energy of 300 and 800 J lead to the increase in elongation up to 1.5 % and with increase in tensile stresses up to 150 MPa the residual plastic deformation increases up to 2.0. The further increase in $\sigma_{in} \geq 290$ MPa results in elongation of specimens up to 8–10 %, it is difficult to share EDT contribution and plastic yielding of material under load. According to Figure 2 maximal efficiency of EDT in the whole range of values of energy of current discharge occurred at tensile stresses up to 150 MPa, to which the elongation of up to 2 % of a specimen of AMg6 corresponds. Its further elongation deteriorates efficiency of treatment which is, as described above, connected with development of deformational strengthening processes, initiated by current discharges [9], which negatively influence the efficiency of EDT process.

CONCLUSIONS

1. EDT has no influence on decrease of values of relative yield strength $\sigma_{0.2}$ and tensile strength σ_t of AMg6 alloy and its welded joints. At EDT of specimens after tension until elasticity limit, the parameters $\sigma_{0.2}$ and σ_t are increased by 15–20 %, and elastic-plastic state is increased, respectively, by 50 and 20 %.

2. The repeated loading of specimens of AMg6 alloy has no substantial influence on efficiency of current impact. At EDT with E = 140 J the relative decrease of level of applied stresses in AMg6 alloy is 20 %, and at E = 800 J it is 65 %.

3. The maximal efficiency of EDT of specimens of AMg6 alloy and its welded joints is observed at σ_{in} = = 150 MPa.

1. Pisarenko, G.S. (1984) About mechanical strength of materials of structure elements. *Problemy Prochnosti*, **1**, 3–5.
2. Pisarenko, G.S., Agarev, V.A., Kvitka, A.L. et al. (1986) *Strength of materials*. Ed. by G.S. Pisarenko. Kiev: Vyshcha Shkola.
3. Strizhalo, V.A., Novogrudsky, L.S., Vorobiov, E.V. (2008) *Strength of materials at cryogenic temperatures taking into account the action of electromagnetic fields*. Kiev: G.S. Pisarenko IPP.
4. Lobanov, L.M., Pashchin, N.A., Loginov, V.P. et al. (2005) Application of electric pulse treatment of structural elements to extend their service life (Review). *The Paton Welding J.*, **11**, 19–23.
5. Aleksandrov, G.N., Borisov, V.V., Ivanov, V.L. et al. (1985) *Theory of electric apparatuses*. Moscow: Vysshaya Shkola.
6. Bataronov, I.L. (1999) Mechanisms of electroplasticity. *Sorosov. Obrazovat. Zhurnal*, **10**, 93–99.
7. Lobanov, L.M., Pashchin, N.A., Loginov, V.P. et al. (2007) Change of the stress-strain state of welded joints of aluminium alloy AMg6 after electrodynamic treatment. *The Paton Welding J.*, **6**, 7–14.
8. Lobanov, L.M., Makhnenko, V.I., Pashchin, N.A. et al. (2007) Features of formation of plastic deformations at electrodynamic treatment of welded joints of St3 steel. *Ibid.*, **10**, 7–11.
9. Lobanov, L.M., Pashchin, N.A., Skulsky, V.Yu. et al. (2006) Influence of electrodynamic treatment on the stress-strain state of heat-resistant steels. *Ibid.*, **5**, 8–11.
10. Lobanov, L.M., Pashchin, N.A., Loginov, V.P. et al. (2007) Influence of electrodynamic treatment on the features of fracture micromechanism of welded joints on aluminium alloy AMg6. *Ibid.*, **2**, 2–6.
11. Bell, J.F. (1984) *Experimental principles of mechanics of deformed solids*. Pt 2: Finite deformations. Moscow: Nauka.

EFFECT OF ALLOYING OF THE WELDS ON STRUCTURE AND PROPERTIES OF WELDED JOINTS ON STEEL 17Kh2M

L.I. MARKASHOVA, V.D. POZNYAKOV, T.A. ALEKSEENKO, E.N. BERDNIKOVA, S.L. ZHDANOV, O.S. KUSHNARYOVA and **A.A. MAKSIMENKO**

E.O. Paton Electric Welding Institute, NASU, Kiev, Ukraine

Structural-phase state of metal of the welded joints on high-strength low-carbon steel 17Kh2M ($w_{6/5}$ = 20–23 °C/s) produced by using welding wires of different chemical compositions and structural types (Sv-08G2S, Sv-08Kh20N9G7T, Sv-10KhN2GSMFTYu) was investigated. Analytical estimation of differential contribution of each structural parameter to a change in the set of mechanical properties (strength, ductility) of the HAZ and weld metal, as well as of a character of distribution and localisation of strain, level of local internal stresses, intensity and size of the stress raisers, which are potential sources of cracks forming during the welding process, was carried out on the basis of experimental data.

Keywords: *arc welding, high-strength steel, welded joints, weld and HAZ metal, type of weld alloying, structural-phase parameters, mechanical properties, localised strain, local internal stresses, crack resistance*

High-strength steels with yield stress σ_y = 590 MPa or more are used in the national and foreign practice to fabricate critical welded structures. With the rational utilisation of these steels it is possible to substantially improve technical and economic indices of machines, mechanisms and engineering structures. However, the main problems in welding of high-strength steels are related not only to the requirement to ensure the sufficient strength level, but also to the need to prevent cold cracking of the welded joints. This is determined to a considerable degree by formation of optimal structures in the weld and HAZ metal, which can improve not only strength but also brittle fracture resistance of the welded joints [1–3].

The effect of the structure of metal of the welded joints on their properties is evidenced by the fact that welding of high-strength steels is performed, as a rule, by using consumables that provide welds with the bainitic (B) or bainitic-martensitic (B-M) structures. However, the low- or high-alloyed consumables are used in certain cases to increase cold crack resistance of the welded joints, the resulting welds having the

Table 1. Chemical composition (wt.%) of steel 17Kh2M and metal of the welds made by using welding wires of different grades

Material	C	Mn	Si	Cr	Ni	Mo	Al	Ti	S	P
Steel 17Kh2M	0.19	0.60	0.20	1.55	0.11	0.30	–	–	0.006	0.014
Welding wire grade:										
Sv-10KhN2GSMFTYu	0.08	1.08	0.30	0.92	1.72	0.43	0.02	–	0.019	0.023
Sv-08G2S	0.08	1.30	0.80	–	–	–	–	–	0.017	0.019
Sv-08Kh20N9G7T	0.08	6.60	0.55	20.70	8.43	–	–	0.40	0.012	0.018

ferritic-pearlitic (F-P) or austenitic-ferritic (A-F) structures. As proved by practice, the processes of structural-phase transitions and their effect on properties of different zones of the welded joints on high-strength steels are little studied as yet. This is attributable to a complicated mechanism of transformation of austenite in the high-strength steel HAZ metal taking place during cooling over a wide range of temperatures [4–6]. Moreover, the phase formation processes and, hence, properties of the welded joints are greatly affected by the composition of the deposited metal.

This study is dedicated to investigation of peculiarities of phase and structural transformations in metal of the high-strength steel welded joints produced by using welding consumables of different compositions, as well as to estimation and prediction of properties of such joints depending on the above factors.

Butt joints on steel 17Kh2M, 20 mm thick, with V-groove (C21 according to GOST 14471–76) and multilayer welds were chosen as the investigation objects. The welded joints were made by mechanised arc welding in a shielding atmosphere of the Ar + + 22 % CO_2 gas mixture by using 1.2 mm diameter solid wires of the Sv-08G2S (weld of the F-P type), Sv-08Kh20N9G7T (weld of the A-F type) and Sv-10KhN2GSMFTYu (weld of the B-M type) grades under the following conditions: I_w = 120–140 A, U_a = 22–24 V, $v_w \approx 18$ m/h (for welding of the root bead); and I_w = = 160–180 A, U_a = 26–28 V, $v_w \approx$ 13–14 m/h (for making the next weld layers, thus providing cooling of the HAZ metal at a rate of $w_{6/5} \approx$ 20–23 °C/s). Chemical composition of the investigated steel and weld metal of the joints welded by using the above welding consumables is given in Table 1.

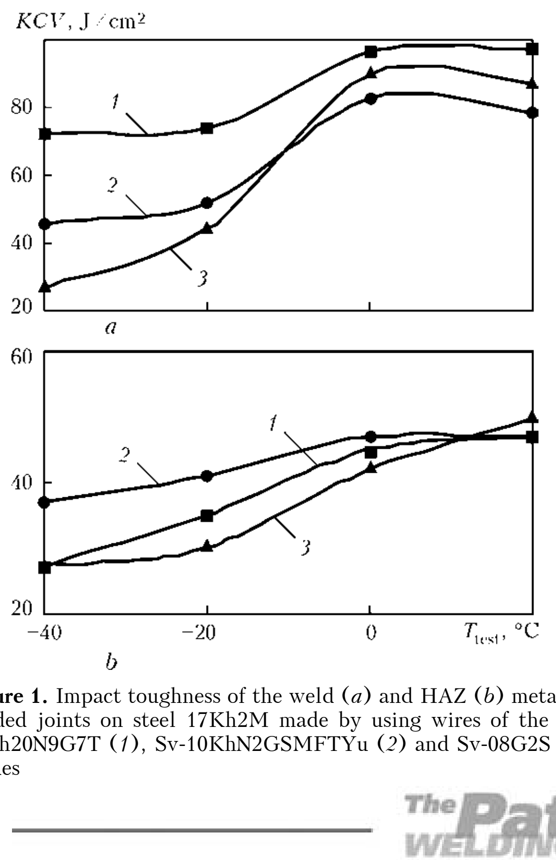

Figure 1. Impact toughness of the weld (*a*) and HAZ (*b*) metal of welded joints on steel 17Kh2M made by using wires of the Sv-08Kh20N9G7T (*1*), Sv-10KhN2GSMFTYu (*2*) and Sv-08G2S (*3*) grades

Specimens for mechanical tensile and impact bend tests (type II according to GOST 1497–84) were cut in the transverse direction relative to the weld axis. An annular groove 2 mm wide and 0.5 mm deep was made in them to localise the place of fracture (weld or HAZ). A notch in the impact specimens (type IX according to GOST 9454–78) was also made along the weld and HAZ axis.

As proved by the results of mechanical tests, welds of the B-M type made by using welding wire of the Sv-10KhN2GSMFTYu grade are characterised by the highest tensile strength value ($\sigma_t \approx$ 950 MPa). The lower values of this property were fixed in the welded joints with welds of the F-P ($\sigma_t \approx$ 860 MPa) and A-F ($\sigma_t \approx$ 750 MPa) types.

Results of impact bend tests of the specimens at test temperature T_{test} from +20 to −40 °C show that metal of all the welds investigated has impact toughness values that meet requirements imposed on steel 17Kh2M ($KCV \geq 27$ J/cm^2) (Figure 1). The values of KCV of the weld metal decrease with decrease of T_{test}. The most pronounced decrease in impact toughness takes place in the weld metal of the F-B type at T_{test} = −40 °C (from KCV^{+20} = 90–116 to KCV^{-40} = = 34–47 J/cm^2). The weld metal of the A-F type is characterised by the highest cold resistance (KCV^{-40} = = 78–83 J/cm^2). The values of impact toughness of such welds vary insignificantly with decrease in the test temperature. The welds of the B-M type have sufficiently high values of cold resistance as well.

Composition of the deposited metal also affects mechanical properties of the HAZ metal of the investigated welded joints. While in the joints with the B-M and F-P type welds they differ just insignificantly ($\sigma_t \approx$ 950–1000 MPa), tensile strength of the HAZ metal of the joints with the A-F type welds decreases to $\sigma_t \approx 820$ MPa. Also, there are differences in cold resistance of the HAZ metal of the welded joints with the welds of different alloying compositions. The joints with the B-M type welds have the highest values of impact toughness at the negative temperature. These values are much lower in the joints with the F-P and A-F type welds. A marked decrease in the impact toughness values of the HAZ metal of such joints begins already at $T_{test} = -20$ °C.

As seen from the results of mechanical tests, properties of the weld and HAZ metal of the welded joints on steel 17Kh2M depend on the composition of the deposited metal. Hence, they are related to peculiarities of the structures forming in them.

Structural-phase and concentration changes, a character of distribution and density of dislocations in the weld and HAZ metal were studied in detail by the integrated investigation method, which comprises optical metallography, analytic scanning electron microscopy (SEM-515 of the «Philips» Company, the Netherlands) and microdiffraction transmission electron microscopy (JEM-200CX of the JEOL Company, Japan). This made it possible to generate experimental information at different structural levels — from macro (grain) to micro (dislocation) level. This approach allows differential estimation of the contribution of individual structural-phase factors and parameters (phase composition, grain D_g and subgrain d_s sizes, dislocation density ρ, size of phase precipitate particles d_p and distance between them λ_p, etc.) to changes in the total (integrated) values of mechanical properties of the weld and HAZ metal, i.e. strength (proof stress $\sigma_{0.2}$ and tensile strength σ_t), brittle fracture resistance K_{IC}, distribution of localised strain ε_l and local internal stresses τ_{in} acting as internal stress raisers, which may be potential sources of fracture of the welded joints under certain conditions.

The following was established as a result of investigations of structural-phase components (pearlite P, ferrite F, upper bainite B_{up}, lower bainite B_{low}, and martensite M), grain size D_g and volume content V_c of these phases forming in the weld metal and in different HAZ regions during the welding process, as well as corresponding changes in microhardness HV.

Weld metal of the welded joints produced by using wire Sv-08G2S under the investigated cooling conditions consisted of coarse-grained (D_g = 50–100 μm) and dramatically graded (ΔD_g — more than 2–3 times) F and P structures with microhardness HV 1920–2100 MPa (Figures 2, *a* and 3) in the presence of the clearly defined orientation of columnar crystalline grains (h_{cr} = 40–100 μm) along the fusion

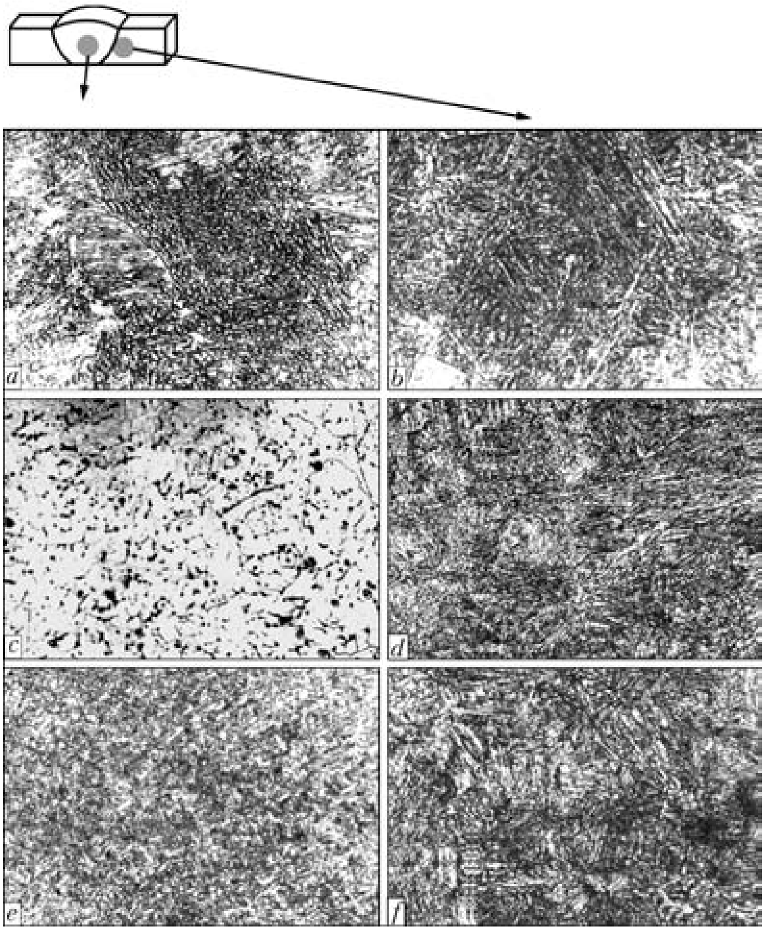

Figure 2. Microstructures (×1000) of metal of the welds (*a*, *c*, *e*) and coarse-grained regions (region I of HAZ) of welded joints on steel 17Kh2M (*b*, *d*, *f*) produced by using welding wires Sv-08G2S (*a*, *b*), Sv-08Kh20N9G7T (*c*, *d*) and Sv-10KhN2GSMFTYu (*e*, *f*) at $w_{6/5}$ = 20 °C/s

Table 2. Average values of structural parameters of welded joints on steel 17Kh2M produced by using welding wires of different grades

Investigated region	Structure	V_c, %	D_g, μm	d_s, μm	λ_p, μm	ρ, cm^{-2}	
						Local	Total
Sv-08G2S							
Weld	F	40	100 μm (h_{cr})	1.7	–	$1\cdot10^9$	$6\cdot10^9$–$2\cdot10^{10}$
	P	60		≤ 1.0	–	$(3–5)\cdot10^{10}$	
Region I of HAZ	F	7	5.5	1.7	–	$2\cdot10^9$	$(5–6)\cdot10^{10}$
	B_{up}	50	77	0.5	0.30	$(1.0–1.3)\cdot10^{11}$	
	B_{low}	43	42	0.45	0.10	$(6–7)\cdot10^{10}$	
Sv-08Kh20N9G7T							
Weld	A-F	100	20	2.0–5.0	–	$(3–4)\cdot(10^9–10^{10})$	$(3–4)\cdot(10^9–10^{10})$
Region I of HAZ	F	5	3	1.8	–	$2\cdot10^9$	$5\cdot10^{10}$
	B_{up}	40	60	0.45	0.27	$(8–9)\cdot10^{10}$	
	B_{low}	55	38	0.4	0.08	$(5–6)\cdot10^{10}$	
Sv-10KhN2GSMFTYu							
Weld	B_{up}	20	30	0.46	0.30	$8\cdot10^{10}$–$1\cdot10^{11}$	$(4–5)\cdot10^{10}$
	B_{low}	30	30	0.3	0.02	$5\cdot10^{10}$–$1\cdot10^{11}$	
	M	50	–	1.0	–	$1\cdot10^{11}$	
Region I of HAZ	F	4	2	1.5	–	$3\cdot10^9$	$(6–7)\cdot10^{10}$
	B_{up}	30	52	0.35	0.10	$(1–3)\cdot10^{11}$	
	B_{low}	45	30	0.2	0.06	$5\cdot10^{10}$–$1.1\cdot10^{11}$	
	M	21	–	0.88	–	$1\cdot10^{11}$	

line on the weld side. HAZ of such joints is also characterised by formation of a considerable volume content of coarse-grained ($D_g \approx 20$–80 μm) B_{up} structures, i.e. $V_{B_{up}} \sim 50$ and 25 %, at a substantially lower volume content of B_{low} (approximately 15 % lower) and presence of ferrite fringes ($V_{f.f} \approx 7$ %) (Figures 2, *b* and 3, and Table 2).

At a similar cooling rate the weld metal of the welded joints made by using wire Sv-08Kh20N9G7T has an equiaxed, more uniform in grain size and two-phase fine-grained ($D_g \approx 20$ μm) A-F structure (Figure 2, *c*) with a volume content of F equal to about 1.3–1.5 %. The following structural changes take place in the HAZ metal of such joints, compared to the welded joints with the F-P type welds. With a general refinement of the structure (by 10–30 %), especially in the coarse-grained and normalised regions, and at a 4–10 % increase in microhardness, there is a change in phase composition of structural components of metal in all the HAZ regions: region I is characterised by increase (1.3 times) in the volume content of B_{low} (approximately to 55 %) and decrease in that of B_{up} (to 40 %), and region II is characterised by increase in the volume content of the ferrite component (to 30 %).

Formation of the M structure takes place in the coarse-grained region of the welded joints on steel 17Kh2M produced by using wire Sv-10KhN2GSMFTYu, compared to the welded joints with the F-P type welds. The volume content of this structure changes comparatively uniformly, approximately from 50 to 20 % (in transition from the weld to HAZ metal). Also, a substantial decrease in the volume content of B_{up}, approximately by 40 %, takes place in this case, the ferrite component being absent (Figure 2, *e*, *f*, and Table 2). In addition, we should note a substantial (1.2–1.5 times) refinement of the structure (B_{up} — approximately to 30–50 μm, and B_{low} — to 20–30 μm).

Analysis of the concentration changes in the investigated welded joints, and first of all of the composition of main chemical elements (chromium, nickel and manganese), showed that the most abrupt gradients of the content of chromium (from 2 to 11 wt.%), nickel (from 3 to 6 wt.%) and manganese (from 0.5 to 4 wt.%) occur near the fusion line in the welded joints produced by using welding wire Sv-08Kh20N9G7T (weld of the A-F type). In the welded joints with the F-P and B-M type welds the gradient of the concentration changes in the welding zone is not in excess of 1.5 %.

Results of transmission electron microscopic examinations of fine structure, which give an idea of the type of the forming structures, variations in density and distribution of dislocations in different structural components (in the bulk of grains, along structural

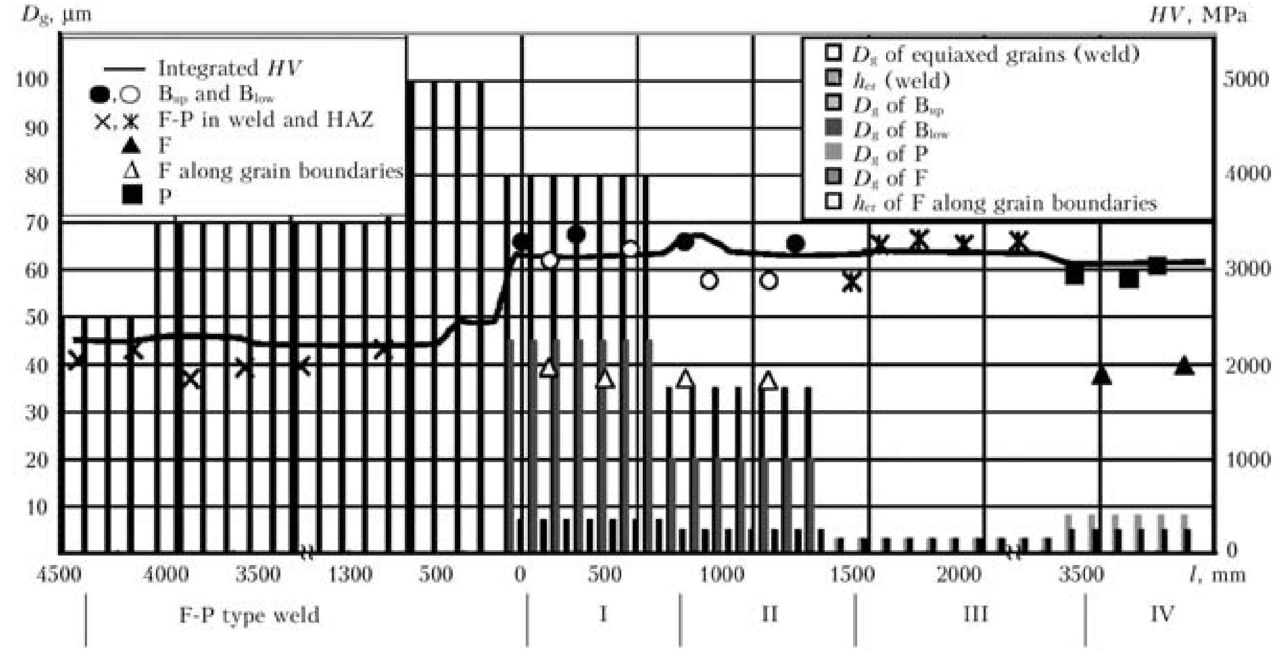

Figure 3. Variation in microhardness HV and grain size of structural-phase components in the weld metal and all HAZ regions of the welded joint on steel 17Kh2M produced by using wire Sv-08G2S: I–IV — HAZ regions: I — overheated (coarse-grained) region; II — refined (normalised) region; III — incompletely refined region; IV — recrystallised region; l — distance from the fusion line

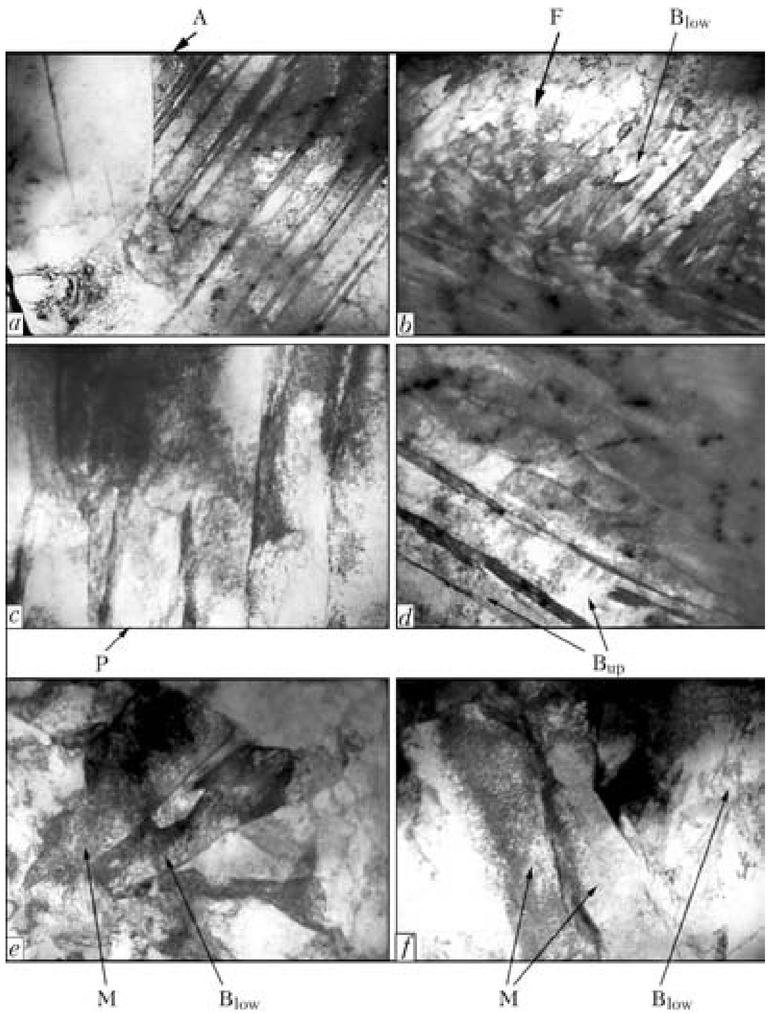

Figure 4. Fine structure of metal of the welds (a, c, e) and coarse-grained regions (region I of HAZ) of welded joints on steel 17Kh2M (b, d, f) produced by using welding wires Sv-08Kh20N9G7T (a, b), Sv-08G2S (c, d) and Sv-10KhN2GSMFTYu (e, f) (a — ×10,000; b, c, e, f — ×15,000; d — ×20,000)

boundaries) showed the following. The most uniform intragranular distribution of dislocations at their low density ($\rho \sim (3–4)\cdot(10^9–10^{10})$ cm^{-2}) is characteristic of the structure of the A-F type weld metal (Figure 4, *a*). With transition from the weld to HAZ the dislocation density increases to some extent both in the internal volumes of B grains ($\rho \sim 5\cdot10^{10}$ cm^{-2}) and along their boundaries, especially in B_{up}, where the values of this indicator amount to $\rho \approx (8–9)\cdot10^{10}$ cm^{-2} (Figure 4, *b*, and Table 2).

Compared to the joints produced by using wire Sv-08Kh20N9G7T (the A-F type weld), the welded joints with the F-P type welds feature some general increase in the dislocation density both in the weld metal (Figure 4, *c*) (1.5–2 times) and in HAZ (1.2 times) (Table 2). Like in the previous case, the structural zones characterised mainly by formation of the dislocation clusters are the extended intergranular boundaries of B_{up}. The dislocation density in such clusters amounts approximately to $(1.0–1.3)\cdot10^{11}$ cm^{-2} (Figure 4, *d*).

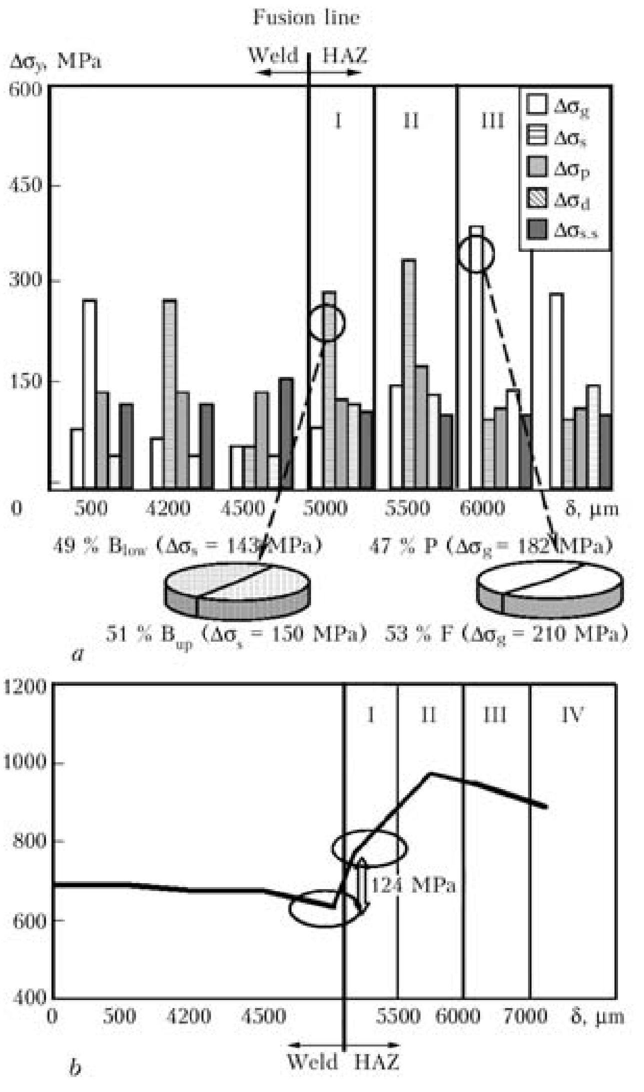

Figure 5. Bar and pie charts (*a*) reflecting differential contribution of individual structural parameters (grain and subgrain size, dislocation density, phase precipitates) to total (integrated) value of σ_y (*b*) in the weld metal and all HAZ regions in welding of steel 17Kh2M by using wire Sv-08G2S: $\Delta\sigma_d$ — dislocation strengthening; $\Delta\sigma_{s.s}$ — strengthening of solid solution by alloying elements; see the text for the rest of the designations

Compared to the welds of the F-P type, the welded joints with the B-M type welds are characterised by even higher values of the intragranular density of dislocations at their comparatively uniform distribution both in the HAZ regions (up to $\rho \sim 7\cdot10^{10}$ cm^{-2}) and in the weld metal ($\rho \sim 5\cdot10^{10}$ cm^{-2}), as well as by increase in the dislocation density along the grain boundaries, i.e. B_{up}, where $\rho \approx 3\cdot10^{11}$ cm^{-2} (Table 2, and Figure 4, *e*, *f*).

Therefore, comparison of the structural state of the weld metal in the investigated welded joints showed that wire Sv-10KhN2GSMFTYu used as a filler metal to produce welds of the B-M type provides the highest increase in the volume content of B_{low} (approximately by 30–35 %) and M (about 20–50 %) in the deposited metal, decrease (1.3–1.7 times) in the content of B_{up}, uniform growth of microhardness in all the HAZ regions, general refinement of structure and substructure, and rise in the density of dislocations with their comparatively uniform distribution. Noteworthy is a fundamental difference in formation of the dislocation clusters in the B_{up} and B_{low} structures (for B_{up} these are extended zones with a rather high dislocation density, and for B_{low} — short dislocation clusters with closed internal substructure).

The experimental data base generated as a result of investigations at all structural levels (from macro to micro) allowed analytical estimations of the most significant mechanical and service properties of the welded joints. For instance, the estimates obtained by using the Archard equation that includes the known Hall–Petch, Orowan and other dependencies [7–16] made it possible to determine the differential contribution of specific structural components (phase composition, alloying, grain and subgrain sizes, dislocation density, size, distribution and volume content of phase precipitates etc.) to a total (integrated) change in such strength characteristic as yield stress [17–21].

It follows from the results of experimental studies and analytical estimations (Figure 5) that in the welded joints produced by using wire Sv-08G2S the total (integrated) value of strengthening, $\Sigma\sigma_{0.2}$, of the weld metal is provided primarily by the carbide phase effect, substructure and increase of the dislocation density. In the welded joints with the A-F type welds their strengthening is related mainly to the growth of solid solution and grain strengthening caused by grain refinement. This is accompanied by decrease in the contribution of the substructural and dislocation components. As to the HAZ metal, strengthening in the overheated region grows (compared to the weld metal) for both types of the joints approximately 1.2–1.5 times, which is related to increase in the content of the bainite component. In addition, strengthening of the HAZ metal in the joints with the A-F type welds is caused by formation of the carbide phases, development of the substructure and growth of the dislocation density, which is associated with formation of the bainite phases in this region (especially B_{low}).

Transition from the weld to HAZ in the welded joints produced by using wire Sv-10KhN2GSMFTYu is characterised by a smoother change in the total level of strengthening, $\Sigma\sigma_{0.2}$, both near the fusion line on the side of the weld and in all the HAZ regions. The highest contribution to strengthening is made by refinement (dispersion) of the substructure ($\Delta\sigma_s \sim$ ~ 355 MPa) and carbide phase particles ($\Delta\sigma_p \sim$ ~ 183 MPa) in the B_{low} grains.

Therefore, comparison of the strengthening effect of the structures forming in metal of the investigated welds of the F-P → A-F → B-M transition system indicated the presence of the structural factors that are most significant in the level of the effect, i.e. B_{low}.

The strengthening contribution of B_{low} ($\Delta\sigma_{B_{low}}$) due to its external and internal components (sizes of grains $\Delta\sigma_g$ and subgrains $\Delta\sigma_s$, and of carbide phase particles $\Delta\sigma_p$) to the total (integrated) strength values $\Sigma\sigma_{0.2}$ of the welded joints is as follows: $\Delta\sigma_{B_{low}} \approx 287$ MPa for F-P, $\Delta\sigma_{B_{low}} \approx 395$ MPa for A-F, and $\Delta\sigma_{B_{low}} \approx 438$ MPa for B-M. As seen, the contribution of B_{low} grows with transition from the F-P type weld to the A-F type and B-M type welds.

The role of the structural factors also shows up in a change of structural strength of the welded joints with the F-P, A-F and B-M type welds, i.e. in a combination of values of yield stress σ_t and stress intensity factor K_{IC} (Figure 6). The given values of the stress intensity factor were determined from the Krafft dependence [22]: $K_{IC} = (2E\sigma_t\delta_t)^{-1/2}$, where E is the Young modulus, is assumed to be equal to $\Sigma\sigma_{0.2}$,

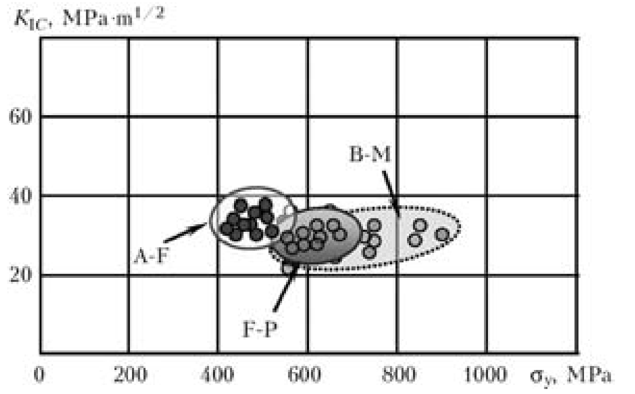

Figure 6. Regions of structural strength of the welded joint on steel 17Kh2M produced by using wires Sv-08G2S (F-P type welds), Sv-08Kh20N9G7T (A-F type welds) and Sv-10KhN2GSMFTYu (B-M type welds)

and σ_t is the critical crack opening displacement determined from the data of fractographic analysis of fractures and substructure parameters [18, 20]. It was established that the value of K_{IC} of the weld metal of the welded joints produced by using wire Sv-08Kh20N9G7T was somewhat higher, compared to the F-P and B-M type welds. It was caused by a substantial decrease in grain size, formation of a clearly defined substructure and uniform distribution of dislocations. The lower values of K_{IC} of the F-P and B-M type welds are attributable to a general increase and non-uniform distribution of the dislocation density, as well as to growth of the volume content of structures with extended cementite phase precipitates. Meanwhile, it should be noted that the welded joints with the B-M type welds are characterised by a high level of strength without any substantial decrease in the K_{IC} values (Figure 6), this being indicative of a good

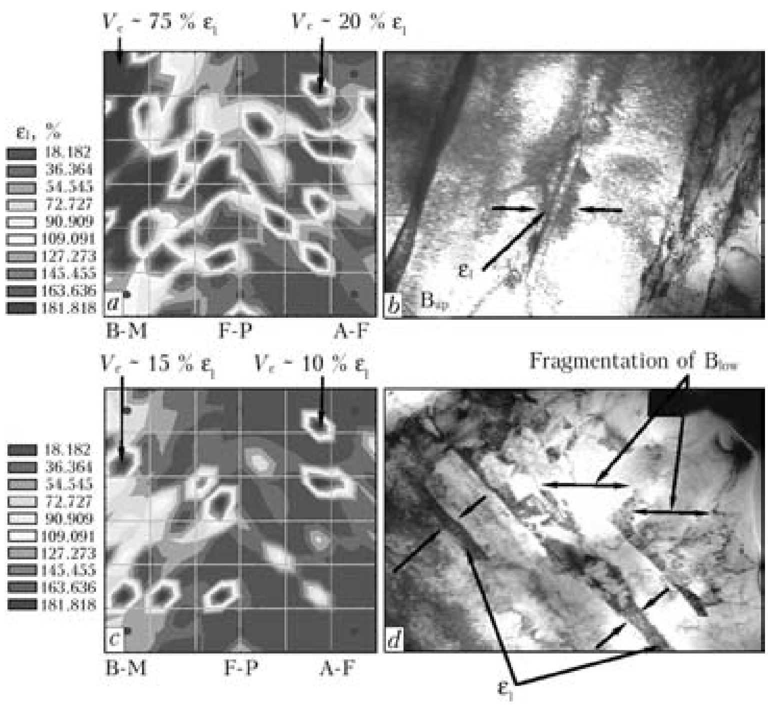

Figure 7. Diagrams (×20,000) of distribution of the zones of localisation of strains in B_{up} (*a*, *b*) and B_{low} (*c*, *d*) of different types of the weld metal

combination of strength and toughness characteristics of the welded joints.

The next step in structural-analytical investigation of the effect on properties of the welded joints by structural parameters was revealing a real picture of interrelation between the structural factors and distribution and intensity of the zones of localisation of strain ε_l and internal stresses τ_{in} in the weld and HAZ metal of the given joints. The required experimental information for analysis of this effect was obtained from examination of fine (dislocation) structure, density and size of structural-phase components in different regions of the joints. Analytical estimations of this type of the clusters were made by using the Conrad and Stroh relationships [23, 24] (respectively, $\varepsilon_l = \alpha_1 \rho b S$ and $\tau_{in} = Gbh\rho/\pi(1-\nu)$, where $\alpha_1 = 1.4$ is the coefficient that relates tensile strain to shear strain; ρ is the dislocation density; b is the Burgers vector; S is the average distance of movement of dislocations during loading, which practically corresponds to the substructure parameters; G is the shear modulus; $h = 2\cdot10^{-5}$ cm is the foil thickness; and ν is the Poisson's ratio).

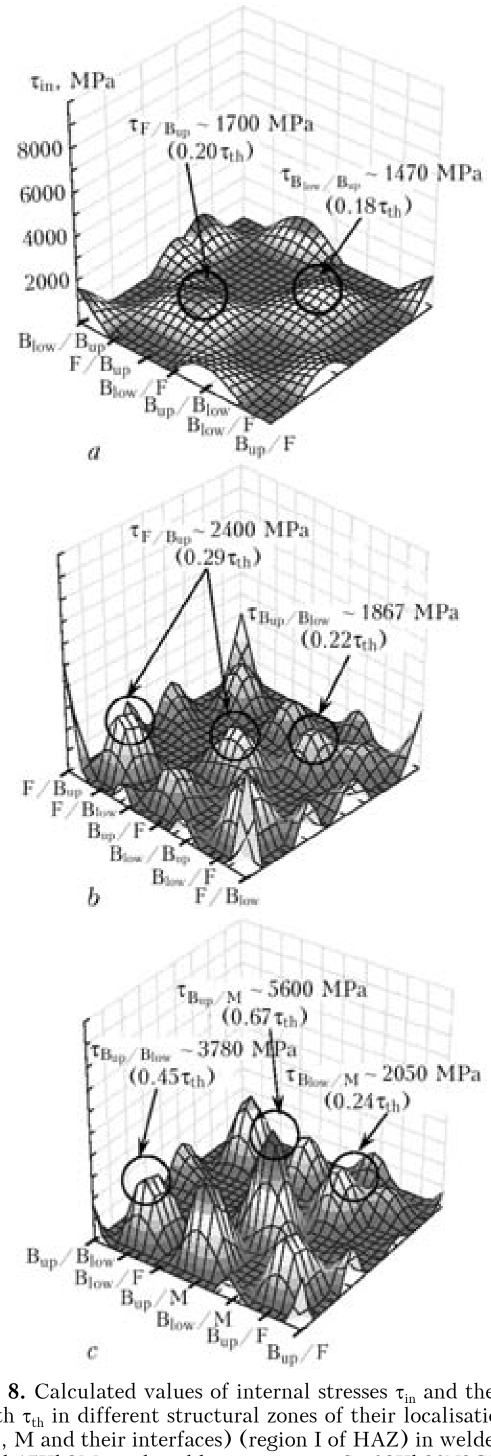

Figure 8. Calculated values of internal stresses τ_{in} and theoretical strength τ_{th} in different structural zones of their localisation (B_{up}, B_{low}, F, M and their interfaces) (region I of HAZ) in welded joints on steel 17Kh2M produced by using wires Sv-08Kh20N9G7T (A-F type welds) (*a*), Sv-08G2S (F-P type welds) (*b*) and Sv-10KhN2GSMFTYu (B-M type welds) (*c*)

The diagrams of distribution of strain localisation zones for the most significant structures of B_{up} and B_{low} in the investigated welded joints show that the most intensive localisation field of ε_l (V_c ~ 75 %) forms in the B_{up} structures of the HAZ metal of the welded joints with the B-M type welds (Figure 7, *a*, *b*), whereas the most uniform field (in intensity and distribution area) is characteristic of the zones of formation of B_{low} (Figure 7, *c*, *d*).

Results of comparison of the estimated τ_{in} values with the value of theoretical strength τ_{th} of the material (Figure 8) showed the following. A lower general level of local internal stresses distributed in the overheated region of the HAZ metal forms in the welded joints produced by using wire Sv-08Kh20N9G7T (τ_{in} = 1500–1700 MPa), which is approximately $(0.18-0.20)\tau_{th}$ (Figure 8, *a*). Increase in the τ_{in} values approximately 1.3–1.4 times is characteristic of the joints with the F-P type welds (Figure 8, *b*). The highest τ_{in} values (about 3800–5600 MPa) corresponding to $(0.45-0.67)\tau_{th}$, which are relatively uniformly distributed in metal of the corresponding HAZ region, are characteristic of the B-M type welds (Figure 8, *c*).

The following was established concerning the character of distribution of τ_{in} in different types of the structures. The longest (about up to 8–10 μm long) and most intensive dislocation clusters, i.e. internal stress raisers (τ_{in} ~ 5600 MPa) form in the B_{up} structures (along the intergranular cementite layers), which are potential sources of brittle fracture. At the same time, uniform distribution of the local dislocation clusters, decrease in their size and closed character in the bulk of grains correspond to B_{low}. In formation of this type of the structures this leads to wider possibilities for occurrence of plastic relaxation of stresses under conditions of the growing external loads due to connection to conventional (dislocation) and rotational mechanisms of their relaxation. This should be taken into account in development of the technological process for welding of high-strength steels, which must promote formation of primarily the B_{low} structures in the weld and HAZ metal, this being particularly important for welded structures operating under low-temperature conditions.

CONCLUSIONS

1. Integrated investigations at all structural levels of the processes of formation of welded joints under actual welding conditions established the effect of specific structural-phase changes during austenitic transformations on strength, ductility and character of localisation of strains and internal stresses, i.e. the factors that influence crack resistance of the welded joints.

2. It was determined that transition from the F-P type welds to the A-F type welds and then to the B-M type ones in the welded joints is accompanied by increase in the content of the B_{low} structures, refinement of the structure and substructure at the absence of abrupt gradients in grain size, as well as a more uniform distribution of the dislocation density in the bulk of grains.

3. It was proved by analytical estimation of differential contribution of the specific structural-phase parameters to the total (integrated) level of strength that increase in strength $\sigma_{0.2}$ of the joints with the B-M type welds is provided by the highest contribution to strengthening of the structures of B_{low} by its components (substructure and carbide phases). Lower values of the strength level in the joints with the A-F and F-P type welds are related to a considerable degree to formation of the coarse-grained and size-graded structures, as well as to a higher volume content of B_{up}.

4. The uniform distribution of local internal stresses τ_{in} and zones of localisation of strains ε_l with decrease in values of these parameters (approximately to $(0.18–0.20)\tau_{th}$) occurs in the welded joints with the A-F type welds. Increase in the τ_{in} value to $(0.22–0.67)\tau_{th}$ is characteristic of the welded joints with the F-P and B-M type welds.

5. The longest and most intensive dislocation clusters, i.e. internal stress raisers, which are potential sources of brittle fracture, form in the B_{up} structures. The uniform distribution of the local dislocation clusters, which is characteristic of the B_{low} structures, decrease in their size and closed character must promote realisation of plastic mechanisms of relaxation of internal stresses.

1. Paton, B.E., Medovar, B.I. (1962) On improvement of quality of steels and alloys for critical welded structures. *Avtomatich. Svarka*, **11**, 1–7.
2. Hrivnak, I., Pitrunova, M., Zayats, Ya. (1983) Measurement and calculation of maximal hardness of near-weld zone of structural steel joints. In: *Pap. of 2nd Symp. of CMEA on Application of Mathematical Methods in Study of Weldability* (Sofia, 1983), Pt 2, 213–221.
3. Bessyo, K., Ito, Y. (1968) Weldability formula of high strength steels related to heat-affected zone cracking. *IIW Doc. IX-576–68*.
4. Shorshorov, M.Kh., Belov, V.V. (1972) *Phase transformations and properties of steel in welding*. Moscow: Nauka.
5. Makarov, E.L. (1981) *Cold cracks in welding of alloy steels*. Moscow: Mashinostroenie.
6. Gorynin, I.V. (1980) *Weldable hull high-strength steels and their application*. Kiev: Naukova Dumka.
7. Suzuki, H. (1967) About yield strength of polycrystalline metals and alloys. In: *Structure and mechanical properties of metals*. Moscow: Metallurgiya.
8. Ashby, I.F. (1972) On Orowan stress. In: *Physics of strength and plasticity*. Moscow: Metallurgiya.
9. Goldshtejn, M.I., Litvinov, V.S., Bronfin, B.M. (1986) *Physics of metals of high-strength alloys*. Moscow: Metallurgiya.
10. Conrad, H. (1973) Model of strain hardening for explanation of grain size effect on stress of flow of metals. In: *Ultrafine grain in metals*: Call. of pap. Ed. by L.K. Gordienko. Moscow: Metallurgiya.
11. Armstrong, R.V. (1973) Strength properties of metals with ultrafine grain. In: *Ibid.*
12. Petch, N.J. (1953) The cleavage strength of polycrystalline. *J. Iron and Steel Inst.*, 173(**1**), 25–28.
13. Orowan, E. (1954) *Dislocation in metals*. New York: AIME.
14. Ashby, M.F. (1983) Mechanisms of deformation and fracture. *Adv. Appl. Mech.*, **23**, 118–177.
15. Kelly, A., Nickolson, R. (1966) *Precipitation hardening*. Moscow: Metallurgiya.
16. Ebelling, R., Ashby, M.F. (1966) Yielding and flow of two phase copper alloys. *Phil. Mag.*, 13(**7**), 805–809.
17. Markashova, L.I., Grigorenko, T.A., Poznyakov, V.D. et al. (2009) Influence of thermal cycles of welding and external loading on structural-phase variations and properties of joints of 17Kh2M steel. *The Paton Welding J.*, **7**, 18–25.
18. Markashova, L.I., Grigorenko, G.M., Arsenyuk, V.V. et al. (2002) Criterion of estimation of mechanical properties of dissimilar material joints. In: *Proc. of Int. Conf. on Mathematical Modeling and Information Technologies in Welding and Related Processes* (16–20 Sept. 2002, Katsiveli, Crimea, Ukraine). Kiev: PWI, 107–113.
19. Markashova, L.I., Grigorenko, G.M., Arsenyuk, V.V. et al. (2004) Structural approach to evaluation of mechanical properties in HAZ of steel and alloy joints. In: *Proc. of 2nd Int. Conf. on Mathematical Modeling and Information Technologies in Welding and Related Processes* (13–17 Sept. 2004, Katsiveli, Crimea, Ukraine). Kiev: PWI, 174–179.
20. Markashova, L.I., Grigorenko, G.M., Poznyakov, V.D. et al. (2009) Structural factors determining the properties of strength, ductility and fracture of welded joints. In: *Proc. of 4th Int. Conf. on Mathematical Modeling and Information Technologies in Welding and Related Processes* (27–30 May 2008, Katsiveli, Crimea, Ukraine). Kiev: PWI, 87–94.
21. Markashova, L.I., Grigorenko, G.M., Poznyakov, V.D. et al. (2009) Structural criterion of evaluation of strength, ductility and crack resistance of metals, alloys, composite materials and their welded joints. In: *Proc. of 4th Int. Conf. on Fracture Mechanics of Materials and Strength of Structures* (June 2009, Lviv). Lviv: G.V. Karpenko FMI, 447–451.
22. Romaniv, O.N. (1979) *Fracture toughness of structural steels*. Moscow: Metallurgiya.
23. Koneva, N.A., Lychagin, D.V., Teplyakova, L.A. et al. (1986) *Theoretical and experimental study of disclinations*. Leningrad: LFTI.
24. Conrad, H. (1963) Effect of grain size on the lower yield and flow stress of iron and steel. *Acta Met.*, **11**, 75–77.

APPLICATION OF NANOSTRUCTURED INTERLAYERS IN JOINTS OF DIFFICULT-TO-WELD ALUMINIUM-BASE MATERIALS (Review)

D.A. ISHCHENKO
E.O. Paton Electric Welding Institute, NASU, Kiev, Ukraine

The paper deals with the technologies of application of nanostructured interlayers in the form of foils or coatings to improve making permanent joints of difficult-to-weld aluminium-base materials in the processes of diffusion and resistance welding, and well as welding with heating due to exothermal reaction of self-propagating high-temperature synthesis.

Keywords: *diffusion welding, resistance welding, self-propagating high-temperature synthesis, aluminium alloys, nanostructure, fillers, interlayers, coatings, foils, powders, plastic deformation, exothermal reaction*

Aluminium and aluminium alloys come second after steel in terms of production and application. Owing to a unique combination of a complex of physico-mechanical, corrosion, and technological properties, aluminium-based alloys are successfully applied in different industries and in construction. Scope of aluminium alloy application in military equipment, in automotive, railway and water transportation, electrical engineering, in manufacture of cryogenic and chemical apparatuses, in agricultural and food machinery construction is considerable. In addition, high-strength aluminium alloys are the main structural material in flying vehicles, including aerospace engineering products (up to 80 % of volume by weight). Wider acceptance of such materials in manufacture of critical products is promoted by intensive current studies of weldability and development of effective measures on improvement of strength and reliability of welded joints, in particular, to prevent hot cracking and pores in welds.

In order to improve the processes of solid-state welding and the properties of permanent joints of difficult-to-weld materials, as well as alloys of different alloying systems, an effective technology was developed of application of nanostructured interlayers between the surfaces of items to be welded. Such interlayers are single- or multilayer coatings, foils or mixtures of ultradispersed powders. In diffusion welding with application of such materials high-strength welded joints with a dispersed microstructure are produced. Plastic deformation is localized in a thin interlayer that allows welding to be performed with application of modes with lower pressure, duration and temperature, i.e. the initial structure of welded materials is preserved.

Self-propagating high-temperature synthesis (SHS) of intermetallic compounds, applied for pressure welding, consists in gas-free combustion of metals (charge components) in the gap between the materials being welded. This process is activated when ultradispersed film or powder interlayers, consisting of metals capable of entering into an instant exothermal reaction, are used as charge. SHS technology provides sound formation of joints owing to a high degree of heating localization in the welding zone.

Process of resistance welding with application of nanostructured interlayers is also improved, owing to shortening of welding time and increased localization of heating with prevention of material softening.

The purpose of this review is analysis of current developments of the methods of solid-phase permanent joining of materials based on aluminium-alloys with application of nanostructured interlayers in the form of foils or coatings, as well as with application of ultradispersed fillers, that provide improvement of the dispersed structure of the permanent joint zone with high strength properties.

Producing permanent joints with application of nanostructured interlayers in explosion welding. Pre-clad plates are often used as initial blanks in manufacture of laminated plates from high-strength aluminium alloys, and their initial thickness in the pack can vary significantly, depending on the final plate thickness and required ratio of the layers, thus affecting the quality of layer joining and being manifested in instability of properties at static and dynamic testing. In [1] a comparative assessment is made of the quality of the joint made by explosion welding, at cladding of high-strength alloys of Al–Zn–Mg system (Σ Mg + Zn $\geq$ 9 %). It is shown that both strength and impact toughness of the joint increase with increase of the relative deformation rate ε at cladding. The most intensive growth of strength at increase of deformation rate up to 50 % and then a smoother increase up to values equal to the strength of AD1 interlayer are observed (Figure 1). Impact toughness reaches maximum values at higher deformation rates (ε = 80 %), being a characteristic more sensitive to defects of oxide film type. Heat treatment has a more significant influence on the joint quality, particularly, on the ductile properties (Figure 2). At increase of quenching temperature and soaking time, the joint impact toughness decreases. Fracture mode becomes more brittle, particularly after recrystallization annealing at 550 °C temperature and ε < 66 %. This influence decreases at increase of deformation rate.

SHS process for permanent joining of materials and producing intermetallic coatings. During metal joining using SHS, heating of the joint area occurs at the expense of an exothermal reaction in the charge, placed before welding between the surfaces to be joined [2]. SHS-product participates in formation of weld material to a greater or smaller degree. Distinction is made between two variants of the process realization. In the first case (SHS-brazing) the materials to be joined and charge layer placed into the gap between them are cold in the initial condition or uniformly preheated. Short-time local heating initiates a combustion wave in this layer that heats the surfaces being joined and melts the SHS product. After that the welding area is compressed, bringing the material surfaces as close as possible to each other and partially removing the SHS-product from the gap. In the second case (SHS-welding) electrically-conducting charge is used and the process is initiated at the expense of passing current through it and the materials being welded, the exothermal reaction running simultaneously in the entire volume of the charge.

In SHS-process the initiation temperature in thin bilayer films depends on the heating rate and ratio of each layer thicknesses. Gas-free combustion is realized at initiation temperatures which are by 300–350 °C lower than on powders (for instance, for Al/Fe and Al/Co it is in the range of 250–400 °C, and for Al/Ni it is 200–300 °C) [3]. SHS mechanism is similar to the process of explosive crystallization. At the initial stage, the solid-phase reactions arising on the contact surface of film condensates can be gas-free combustion. Reaction in thin films can be implemented also on powder surface, if the second reagent is in the liquid phase. High cooling rates after passing of SHS wave in two-layer films lead to stabilization of high-temperature and metastable phases.

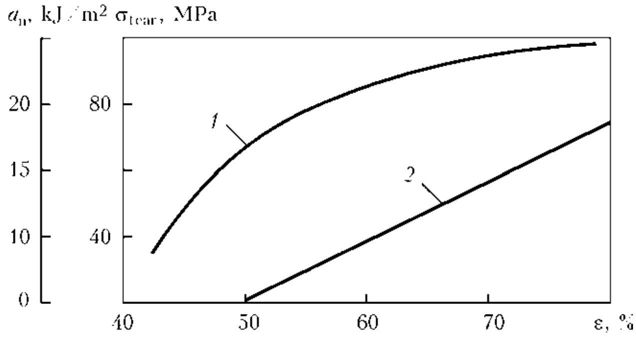

Figure 1. Dependence of the strength of layer adhesion, σ_{tear} (*1*) and impact toughness a_n (*2*) on the degree of deformation [1]

In the filed of permanent joining, the interest to multilayer foils based on elements forming intermetallics is also due to their application as fillers and as sources of local heating of metal at realization of SHS reaction (gas-free combustion) in the welding gap. In [4] evaluation of the intensity of heat evolution during SHS process in laminated Ni/Al foils placed between two copper foils being joined, was performed. It is shown that depending on chemical composition, thickness and initial microstructure characteristics of laminated foils, the intensity of heat evolution can vary in a broad range from 70 up to 400 W/cm^2. The velocity of propagation of gas-free combustion wave also depends on the thickness of component layers: at their reduction to the nanometric scale the velocity of propagation of SHS reaction wave through the foil can reach 10 m/s. The thermogram (Figure 3) shows that after initiation of SHS reaction the pack temperature quickly rises (in 0.1 s) up to the value dependent on the amount of the evolving heat, weight of sample and copper foil, which were selected so that heating of the entire pack did not exceed the copper melting temperature. This temperature, as a rule, was in the range of 500–700 °C.

Work [5] is devoted to investigation of the mechanisms of diffusion, formation and stability of new phase nuclei in the reactions corresponding to SHS in Ni–Al system. At comparison of the quantitative and qualitative change of phase composition for different content of aluminium particles (30 and 50 %) embed-

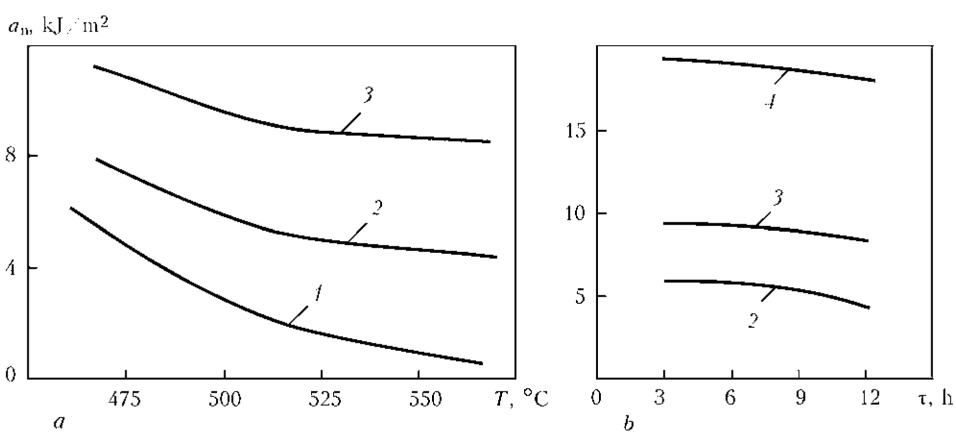

Figure 2. Dependence of joint impact toughness on quenching temperature (τ = 3 h) (*a*) and soaking time (*T* = 470 °C) (*b*) [1]: *1–4* — ε = 50, 60, 70 and 80 %, respectively

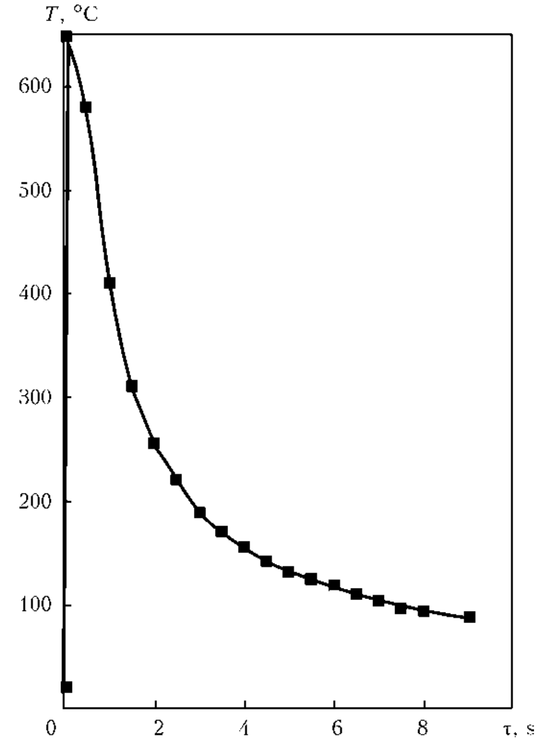

Figure 3. Thermograph of SHS reaction in a sample of Ni–Al system (61.2 wt.% Al) [4]

ded into the nickel matrix, prevalence of Ni_3Al phase for 30 % Al and 50 % NiAl is demonstrated. The rate of dissolution of embedded aluminium particles in the first case, when the system was heated pulse-like in an incremental series of successive time intervals, and the final material structure was memorized, is lower after the quenching process, than in the second case, when the system dynamic structure, which was obtained at pulsed heating was memorized, and it was again heated pulselike during a new time interval.

In [6–8] the micro- and nanostructures of multilayer films, obtained by the method of magnetron sputtering and consisting of alternating layers of titanium and aluminium in a broad range of layer thickness values, were studied. Microscopic features of propagation of gas-free combustion waves in them are considered. In the process of gas-free combustion in multilayer films of Al–Ti system the most probable mechanism of self-propagating reaction is aluminium diffusion into β-Ti at the temperature close to that of transition of α-Ti into β-Ti. SHS results in formation of intermetallic compounds of titanium and aluminium, which are highly textured poreless polycrystalline materials, which have two boundary systems normal to each other: between the layers and intergranular. Reagent layers are solid and rather even, and their mixing along the boundaries is slight (Figure 4). Columnar grains are oriented normal to the foil plane. They become almost indiscernible with decrease of layer thickness. However, the granular structure is preserved, and sometimes becomes more pronounced (Figure 5). As the coefficient of aluminium diffusion in titanium is quite small, intergranular boundaries can be the paths for anomalously fast diffusion, as they are oriented parallel to the diffusion flow. Compared to combustion of powder mixtures, «spreading» of SHS wave in the foil is more uniform On the other hand, the intergranular boundaries can slow down the heat flow directed from the hot products to the unburnt part of the sample, i.e. along the foil.

Work [9] describes the modes of phase transformations at heterogeneous reaction of gas-free combustion in multilayer nanofilms of Al–Ti system. It is shown that interaction of elements runs as a following sequence: disordering of titanium crystalline structure with simultaneous increase of interplanar spaces and saturation of solid titanium by aluminuim atoms; ordering of the crystalline lattice with formation of α-Ti based solid solution and parallel formation of $TiAl_3$ phase; ordering of mixed titanium and aluminium atoms into the crystalline structure of the final product of TiAl alloy. In the combustion mode all the process stages run almost instantaneously — in less than 0.04 s. At application of both the modes inheritance

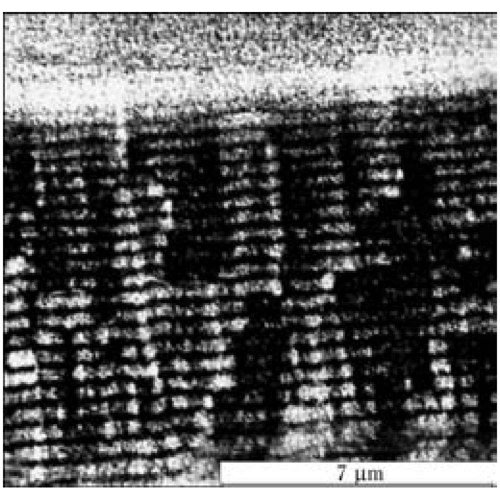

Figure 4. Microstructure of multilayer Al/Ti films as a result of SHS (scanning electron microscopy) [8]

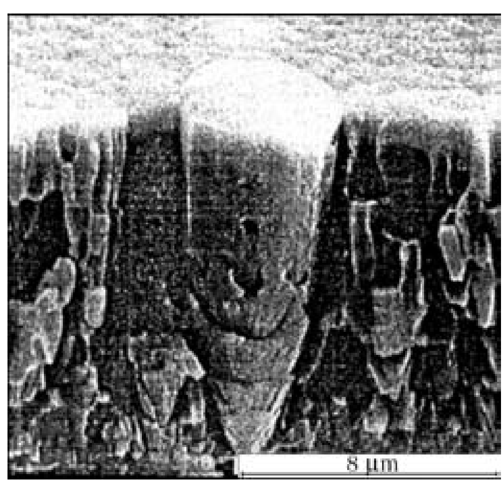

Figure 5. Microstructure of Al/Ti film fracture at 95 nm layer thickness [8]

of initial layer texture by the intermediate and final phases occurs.

In [10–12] the advantages of combining the SHS-process and mechanical impact at joining ultradispersed materials from AlNi and AlTi intermetallics are considered. Duration and mode of mechanical activation at dispersion in powder mixtures of nickel with aluminium and titanium with aluminuim, influence the process characteristics and composition of gas-free combustion products. Combustion for these compositions proceeds in a microheterogeneous mode, and heating rate is determined by the time of heating of the composite particles. In the case of thermal explosion mode, where combustion cannot be stopped immediately after reaching the inflammability limit, it can be slowed down at the expense of different duration of combustion after ignition, by changing the heating rate and using coarse nickel powder as in situ heat source. This indirect method successfully simulates the operation of wave hardening that is applicable only to the mode of plane wave propagation.

Resistance welding. Work [13] gives the results of investigation of the features of joint formation by resistance welding technology using Al/Ni and Al/Cu nanostructured foils as inserts between the parts of AD0, 1460 and AMg6 aluminium alloys to be joined. Such a technology is characterized by highly-concentrated heat evolution in the butt that reduces the welding time and prevents metal softening. When foil consisting of layers of aluminium and nickel is used, additional heat evolves in the contact zone that is due to running of exothermal reaction between the metals which is accompanied by formation of intermetallic phases. Development of an exothermal reaction depends on the heating rate in welding. With increase of the latter, the amount of flash increases under the impact of the compression force. Heating rate of 500–800 °C/s is optimum for producing sound joints. Foil fragments preserve their laminated structure, i.e. aluminium and nickel reaction runs locally (Figure 6). Application of aluminium-copper nanostructured foils allows a marked lowering of welding temperature (by 100–150 °C) owing to running of the process of formation of Al_2Cu eutectic in the foil. This is particularly important in welding thermally unstable aluminium alloys.

Proceeding from investigations of the mechanism of joint zone formation, authors of [14] developed methods to produce by resistance spot welding sound joints from steel and AMg6 and AMts aluminium alloys, using bimetal steel–aluminium plates, which were made by rolling or explosion welding. Here it is shown that in manufacture of the inserts, preference should be given to explosion welding, as it allows producing a sound joint with self-cleaning of the surface during slanting collision of sheet blanks. Using a bimetal transition piece, resistance spot welding of AMg6 alloy to St3 steel was performed. Regularities of the processes of melting, solidification, interdiffusion and chemical interaction of the components, as well as their change with increase of temperature and pressure allow determination of the optimum welding modes and producing a strong joint of the bimetal and base material.

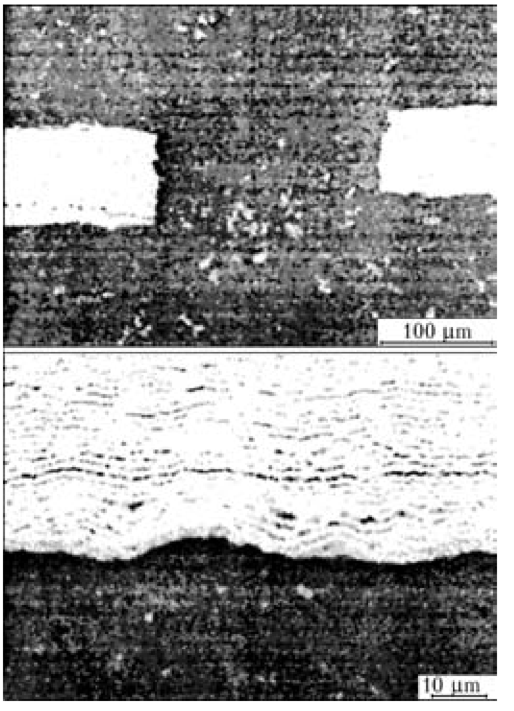

Figure 6. Fragments of Al/Ni foil in the weld metal [13]

Methods to produce nanostructured foils and coatings. Alongside the welding process parameters and postweld treatment, quality of joints made using nanostructured foils and coatings is also influenced by chemical and phase composition, size of ultradispersed particles and thickness of nanostructured foils or coatings. Therefore, features of the processes of their manufacture are also important. Nanostructured foils and coatings are made by the following methods: hardening by melt spinning [15–20]; detonation deposition [21, 22]; condensation [23]; deposition after thermal [24], magnetron [25], vacuum-arc [26] spraying; ion implantation [27, 28]; and electroplating.

CONCLUSION

The published results given above are indicative of a high efficiency of application of nanostructured interlayers for joining difficult-to-weld aluminium alloys. Such interlayers can be elementary or multilayer coatings, foils or mixtures of ultradispersed powders. The produced welded joints are high-strength, with a dispersed microstructure.

Under the conditions of diffusion welding with application of foils or coatings with an ultradispersed structure, plastic deformation is localized in a thin interlayer. This allows applying smaller compression force and accelerating the process of welding without heating, thus promoting preservation of the initial structure of welded materials.

SHS is characterized by high-temperature phase formations in the contact zone at anomalously fast reaction and diffusion. Here sound weld formation is ensured at comparatively soft temperature modes, owing to a high decree of heating localization in the welding zone.

Application of nanostructured multilayer foils in resistance welding causes an additional highly concentrated heat evolution in the joint zone. This is promoted by a local exothermal reaction between the interlayer metals, initiated by electric current, that allows preserving the structure and strength properties of the base material.

1. Shlensky, A.G. (2008) Examination of joint quality in cladding of Al–Zn–Mg system alloys. *Tekhnologiya Mashinostroeniya*, **8**, 20–23.
2. Klubovich, V.V., Kulak, M.M., Samoletov, V.G. (2005) Producing permanent joints of materials using SHS. In: *Welding and related technologies*: Transact. Minsk.
3. Myagkov, V.G., Zhigalov, V.S., Bykova, L.E. et al. (1998) Self-propagating high-temperature synthesis and solid-phase reactions in two-layer thin films. *Zhurnal Tekhnich. Fiziki*, 68 (**10**), 58–62.
4. Shishkin, A.E., Rogovchenko, D.S., Ustinov, A.I. (2009) Evaluation of heat evolution intensity in quick-propagating high-temperature synthesis in Ni/Al multilayer foils. *Metallofizika i Nov. Tekhnologii*, 31(**9**), 1179–1188.
5. Denisova, N.F., Starostenkov, M.D., Kholodova, N.B. (2005) Study of formation and stability of new phase nuclei in reactions corresponding to SHS in Ni–Al system. In: *Proc. of 9th Int. Sci.-Techn. Conf. on Composites in National Economy* (Barnaul, Nov. 2005). Barnaul: AltGTU, 100–105.
6. Rogachev, A.S., Grigoryan, A.E., Illarionova, E.V. et al. (2004) Gas-free burning of bimetallic Ti/Al nanofilms. *Fizika Goreniya i Vzryva*, 40(**2**), 45–51.
7. Grigoryan, A.E., Elistratov, N.G., Kovalev, D.Yu. et al. (2001) Autowave propagation of exothermic reactions in thin multilayer films of Ti–Al system. *Doklady RAN*, 381(**3**), 368–372.
8. Grigoryan, A.E., Illarionova, E.V., Loginov, B.A. et al. (2006) Structural peculiarities of thin multilayer Ti/Al films for self-propagating high-temperature synthesis. *Izvestiya Vuzov. Tsvet. Metallurgiya*, **5**, 31–36.
9. Rogachev, A.S., Gashon, Zh.K., Grigoryan, A.E. et al. (2006) Formation of crystalline structure of products during heterogeneous reaction in multilayer bimetallic nanosystems. *Izvestiya RAN. Physics Series*, 70(**4**), 609–611.
10. Grigorieva, T.F., Korchagin, M.A., Barinova, A.P. et al. (2000) Self-propagating high-temperature synthesis and mechanical fusion in producing monophase highly-refined intermetallics. *Materialovedenie*, **5**, 49–53.
11. Biswas, A., Roy, S.K. (2004) Comparison between the microstructural evolution of two modes of SHS of NiAl: key to a common reaction mechanism. *Acta Mater*., 52(**2**), 257–270.
12. Shkodich, N.F., Kochetov, N.A., Sachkova, N.V. (2006) On the influence of mechanical activation on SHS compositions of Ni–Al and Ti–Al. *Izvestiya Vuzov. Tsvet. Metallurgiya*, **5**, 44–50.
13. Kuchuk-Yatsenko, V.S., Shvets, V.I., Sakhatsky, A.G. et al. (2007) Specifics of resistance welding of aluminium alloys with nanostructural aluminium-nickel and aluminium-copper foils. *Svarochn. Proizvodstvo*, **9**, 12–14.
14. Kovalevsky, V.N., Demchenko, E.B., Lopatko, I.G. (2006) Application of nanocoatings in pressure welding of dissimilar materials. *Svarka i Rodstv. Tekhnologii*, Issue 8, 84–87.
15. Shpak, A.P., Majboroda, V.P., Kunitsky, Yu.A. et al. (2004) Nanolayered fragments in aluminium alloys. *Nanosistemy, Nanomaterialy, Nanotekhnologii*, 2(**2**), 681–687.
16. Neumerzhitskaya, E.Yu., Shepelevich, V.G. (2005) Structure, properties and thermal stability of rapidly-solidified foils of aluminium alloy with chromium, nickel and manganese. *Perspect. Materialy*, **4**, 69–73.
17. Karpets, M.V., Firstov, S.O., Kulak, L.D. (2006) Specifics of phase formation in quickly-hardened Al–Fe–Cr alloys in the presence of quasicrystals. *Fizyka i Khimiya Tv. Tila*, 7(**1**), 147–151.
18. Gutko, E.S., Shepelevich, V.G. (2005) Investigation of rapidly-solidified foils of binary and ternary aluminium-base alloys containing zinc and magnesium. *Fizika i Khimiya Obrab. Materialov*, **4**, 81–85.
19. Tashlykova-Bushkevich, I.I., Shepelevich, V.G. (2000) Elemental layer-by-layer analysis of component distribution in the volume of rapidly-solidified aluminium low alloys. *Ibid*., **4**, 99–105.
20. Tashlykova-Bushkevich, I.I., Gutko, E.S., Shepelevich, V.G. et al. (2008) Structural and phase analysis of rapidly-solidified Al–Fe alloys. *Poverkhnost. Rentg., Sinkhr. i Nejtronnye Issledovaniya*, **4**, 69–75.
21. Oliker, V.E., Sirovatka, V.L., Timofeeva, I.I. et al. (2005) Influence of properties of titanium aluminides and detonation spraying conditions on phase and structure formation of coatings. *Poroshk. Metallurgiya*, **9**/**10**, 74–84.
22. Romankov, S.E., Kaloshkin, S.D., Pustov, L.Yu. (2006) Synthesis of titanium-aluminide coatings by the method of mechanical fusion and subsequent annealing on the surface of titanium and aluminium. *Fizika Metallov i Metallovedenie*, 101(**1**), 65–73.
23. Perekrestov, V.I., Kosminskaya, Yu.A., Kravchenko, S.N. (2003) Principles of structure formation of condensates of low-supersaturated Cu, Ti, Al and Cr vapors. *Metallofizika i Nov. Tekhnologii*, 25(**6**), 725–735.
24. Buzhenets, E.I., Majboroda, V.P., Shpak, A.P. et al. (2004) Structural peculiarities of quasi-crystalline coatings of $Al_{63}Cu_{25}Fe_{12}$ alloy. *Nanosistemy, Nanomaterialy, Nanotekhnologii*, 2(**4**), 1323–1329.
25. Hampshire, J., Kelly, P.J., Teer, D.G. (2003) Tribological properties of co-deposited aluminium-titanium alloy coatings. In: *Proc. of 30th Int. Conf. on Metallurgical Coatings and Thin Films* (Apr. 28–May 2, 2003, San Diego, Calif.), 392–398.
26. Budilov, V., Kireev, R., Kamalov, Z. (2004) Intermetallic products formed by joint cold cathode vacuum arc sputtering of titanium and aluminium. In: *Proc. of 11th Int. Conf. on Rapidly Quenched and Metastable Materials* (Oxford, 25–30 Aug. 2002), 656–660.
27. Kurzina, I.A., Bozhko, I.A., Kalashnikov, M.P. et al. (2005) Formation of surface layers containing intermetallic compounds of Ni–Al and Ti–Al systems at high-intensity ion implantation. *Perspekt. Materialy*, **1**, 13–23.
28. Kurzina, I.A., Bozhko, I.A., Kalashnikov, M.P. et al. (2004) High-intensity implantation of aluminium ions into titanium. *Metallofizika i Nov. Tekhnologii*, 26(**12**), 1645–1660.

FORMATION OF NARROW-GAP WELDED JOINTS ON TITANIUM USING THE CONTROLLING MAGNETIC FIELD

V.Yu. BELOUS and **S.V. AKHONIN**
E.O. Paton Electric Welding Institute, NASU, Kiev, Ukraine

The mechanism of formation of welded joints in a narrow groove under the external effect of the controlling magnetic field is suggested. Dependence of the argon plasma flow rate and gas-dynamic pressure of the arc on the weld pool surface upon the welding process parameters and tungsten electrode geometry was established by the experimental-calculation method.

Keywords: *TIG welding, titanium, magnetic control of the arc, narrow gap, formation of joints*

TIG welding of titanium in argon atmosphere is a widely applied method for joining parts with a thickness of up to 100 mm. As a rule, the more than 16 mm thick joints are produced by multilayer filler-wire welding with groove preparation. The multilayer U-groove welding method is of low productivity and cost effectiveness, the heat-affected zone in this case being quite big.

The narrow-gap TIG argon-arc welding method has received wide acceptance lately for fabrication of thick structures. Compared to U-groove welding, this method allows decreasing the volume of the deposited metal, reducing the consumption of labour for preparation of edges of the parts welded, and substantially increasing the productivity of welding.

However, for successful implementation of the narrow-gap welding process it is necessary to overcome certain difficulties, the main one being ensuring a reliable fusion of vertical side walls of the groove. With traditional TIG welding the major portion of the heat energy of the arc is consumed for penetration of the narrow groove bottom or repeated penetration of the previous-pass weld metal. Therefore, to ensure the reliable fusion of the vertical walls of the narrow groove it is necessary to provide redistribution of heat input into the welded joint, which can be achieved by mechanically moving the tungsten electrode [1] or affecting the arc by the external magnetic field [2].

The E.O. Paton Electric Welding Institute developed the technology for narrow-gap TIG welding by using the controlling magnetic field, which makes it possible to redistribute the heat energy of the arc within the preset limits between the bottom wall of the groove, vertical side walls and molten weld pool. According to this technology, welding is performed with a tungsten electrode lowered into the groove and with a protective nozzle located over the weld edges, this reducing the groove width to 10–11 mm. Magnetic core of the electromagnet is combined with a filler wire feed guide, and is placed in the groove ahead of the tungsten electrode. The electromagnet induces the magnetic field, the force lines of which within the arc zone are directed mostly along the welding line. The value of magnetic induction within the arc zone amounts to 12 mT. This field is transverse with respect to the arc, and its direction changes into the opposite at a certain frequency.

The purpose of this study was to investigate the mechanisms of formation of joints by narrow-gap TIG welding using the controlling magnetic field. The authors suggest the following mechanism of formation of the narrow-gap TIG welded joints using the external controlling magnetic field. Interaction of the external controlling reversible magnetic field generated by the electromagnet with the arc current induces Lorentz force F_a, which deflects the arc and leads to displacement of the anode spot in a direction of action of this force:

$$\vec{F}_a = \vec{j}\,\vec{B}, \tag{1}$$

where $\vec{j}$ is the density of the arc current, A/m^2; and $\vec{B}$ is the magnetic induction, T.

Redistribution of the welding arc energy input into the metal welded and fusion of vertical walls of the groove in the base metal during narrow-gap welding are provided by the alternating deflection of the arc to the side walls of the groove under the effect of Lorenz force F_a (Figure 1). The key parameters of the controlling magnetic field for narrow-gap welding are values of the component of magnetic induction along the welding direction, B_x, transverse component of magnetic induction, B_y, and frequency of reversing of the magnetic field, w.

At the initial time moment, when the arc is at the centre of the magnetic core, magnetic induction in a direction of axis y is equal to zero, i.e. $B_y = 0$. Hence, the arc is affected only by component F_x of the Lorentz force in a plane normal to the weld axis. Deflection of the arc to the extreme position generates additional component F_y of the Lorentz force, the direction of which depends on the direction of component B_y (Figure 2). Under the effect of F_y, the anode spot is

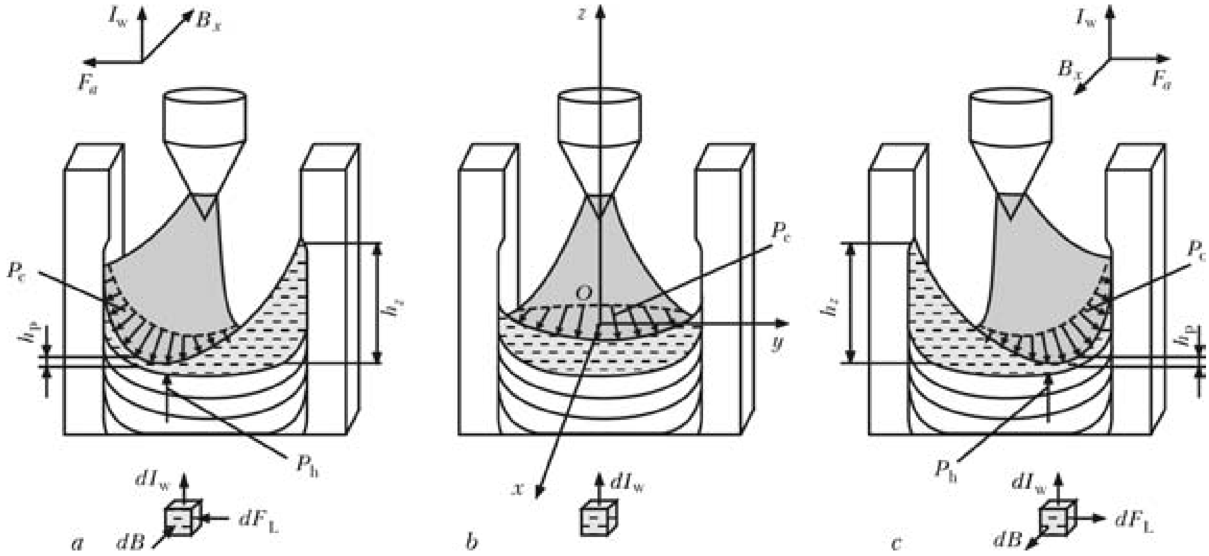

Figure 1. Schematic of fusion of side walls of the groove and location of the welding arc in extreme (*a*, *c*) and intermediate (*b*) positions

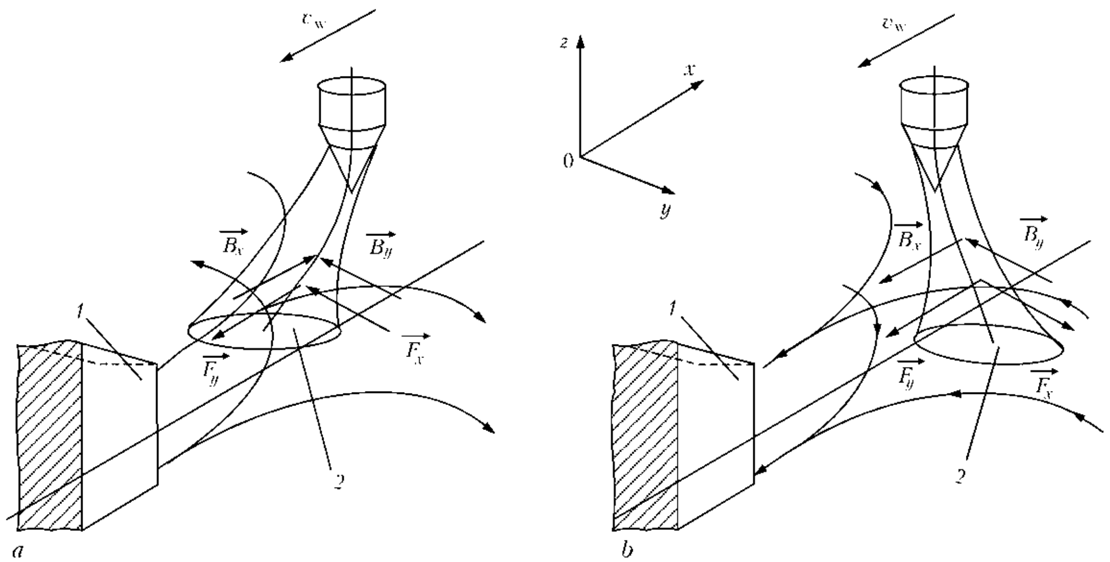

Figure 2. Direction of magnetic induction and forces affecting the arc in narrow-gap welding at the extreme left (*a*) and right (*b*) positions of the arc: *1* — magnetic core; *2* — anode spot; $\vec{B}_x$ and $\vec{B}_y$ — components of magnetic induction in planes zOx and zOy, respectively; $\vec{F}_x$ and $\vec{F}_y$ — components of the Lorentz force generated by interaction of components $\vec{B}_x$ and $\vec{B}_y$; v_w — welding speed

moved along the welding direction to the head part of the weld pool.

The force of pressure of the arc column plasma, P_c (see Figure 1) causes the weld pool surface to sag, thus pushing off the molten metal from the wall fused and head part of the weld pool to its tailing part and the opposite wall of the groove. As a result, thickness of the molten metal layer under the arc decreases, and thickness of the molten metal layer, h_z, in the tailing part of the weld pool increases. Lorentz force F_L generated due to interaction of the current in the weld pool and external controlling magnetic field, and the force of hydrostatic pressure of the molten pool metal, P_h, prevent the liquid interlayer thickness from decreasing. With alternating deflection of the arc to the side walls of the groove the molten metal flows over from the walls fused by the arc (Figure 3, *a*), this resulting in excitation of transverse oscillations of the molten pool metal. Disappearance of the molten metal interlayer under the arc may cause lacks of fusion in the form of cavities that are not filled with molten metal and undercuts (Figure 3, *b*). Investigations on estimation of variations in values of the above forces during narrow-gap welding were carried out to analyse their effect on the behaviour of the molten metal.

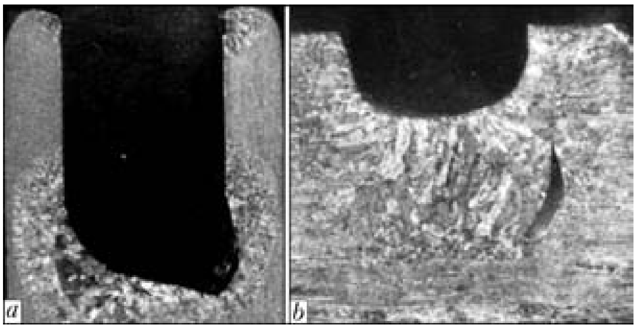

Figure 3. Transverse macrosections of solidified welds: *a* — shape of free surface of the weld pool; *b* — lack of fusion formed as a result of disappearance of liquid interlayer

Figure 4. Photos (light filter IKS-5) of the 5 mm diameter flat-tip electrode with a tip width of 1 (*a*), 2 (*b*) and 5 (*c*) mm, and the arc gap in narrow-gap welding at I_w = 400 A

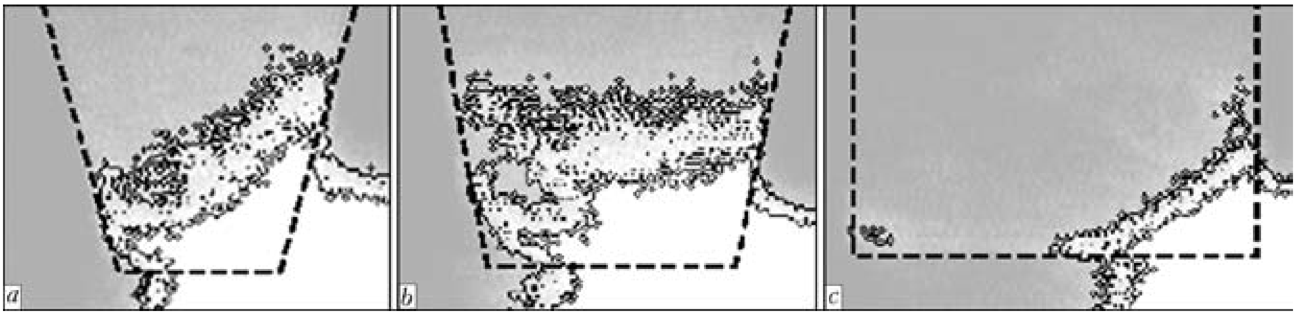

Figure 5. Images of the arc column near cathode in narrow-gap welding at I_w = 400 A after computer processing: *a*–*c* — see Figure 4

Lorenz force F_L induced in the weld pool by the magnetic field can be estimated from the following formula:

$$F_L = (I_w B_x) h_p, \tag{2}$$

where h_p is the depth of the molten metal interlayer under the arc in the weld pool (see Figure 1).

As proved by experimental studies, the depth of the weld pool within the arc affected zone during narrow-gap welding decreases from 2 to 1 mm with increase in values of the transverse component of magnetic induction B_x from 2.5 to 12.0 mT and longitudinal component $B_z \leq 4.0$ mT [3]. In this case the value of Lorenz force F_L is not in excess of $5 \cdot 10^{-3}$ N.

The force of pressure of the arc column plasma, P_c, can be estimated by determining geometric parameters of the arc. Assuming that the arc in narrow-gap welding of titanium has the shape of a cone with a height equal to arc length l_a and radii of the arc column near cathode R_{cath} and near anode R_{an}, respectively, of the upper and lower bases of the cone, it is possible to estimate the rate of the gas-dynamic plasma flow and total force of pressure of the arc column on the weld pool surface.

Distribution of plasma flow rate v_z was determined by the procedure suggested in study [4]. The total force of pressure of the arc column plasma on the weld pool surface was determined from the formula for a conical model of the welding arc [5]:

$$F_c = \mu_0 I_w^2/(4\pi) \ln (R_{an}/R_{cath}), \tag{3}$$

where μ_0 is the magnetic permeability.

Geometric parameters of the welding arc near cathode were estimated by filming the real arc process (Figure 4) followed by computer processing of the resulting images (Figure 5). Diameter of the arc near anode was determined by the divided anode procedure [6].

Tungsten electrodes with a rod diameter of 5 mm, having a cone-shaped (Figure 6, *a*) or flat (Figure 6, *b*) tip, can be used for narrow-gap welding of titanium with the magnetically controlled arc. An electrode with the flat tip is located during welding with its wide side across the weld axis. The flat-tip tungsten electrodes are advantageous in that they allow regulating displacement of the cathode spot in alternating deflection of the arc under the effect of the external magnetic field and, hence, within the certain limits, as well as heating of the tungsten electrode edge. Also, they allow changing geometric parameters of the arc

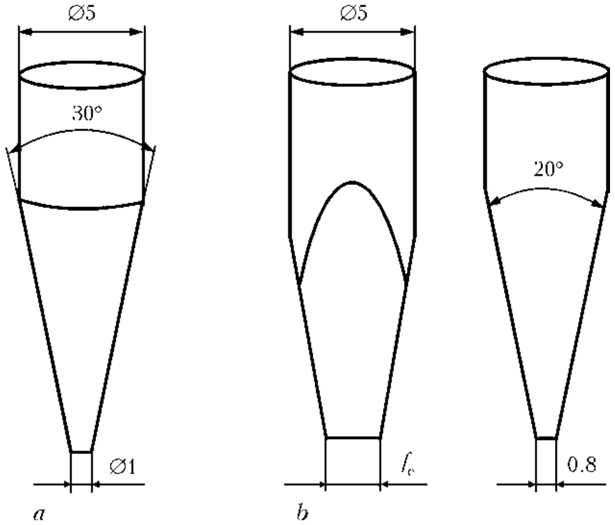

Figure 6. Types and sizes of tungsten electrodes used for narrow-gap welding of titanium, having cone-shaped (*a*) and flat (*b*) tips

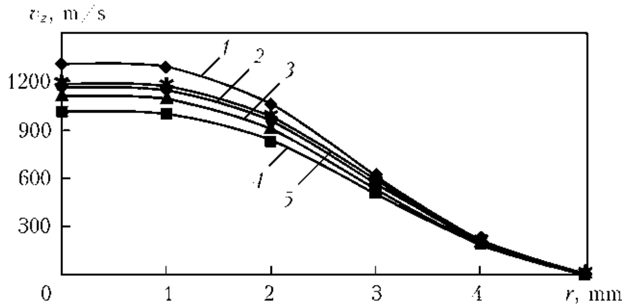

Figure 7. Distribution of plasma flow rate v_z near anode at width of the tip of the flat-tip electrode f_e equal to 1.0 (*1*), 2.5 (*2*), 2.0 (*3*), 2.5 (*4*) and 5.0 (*5*) mm: r — distance from the anode centre

discharge by selecting only one parameter — electrode tip width f_e.

Results of calculation of distribution of the plasma flow rate are shown in Figure 7, and those of the total force affecting the weld pool surface are shown in Figure 8. Analysis of the results indicated that the use of the cone-shaped tungsten electrode in narrow-gap welding at I_w = 400 A provides the maximal plasma flow rate and maximal pressure of the arc column on the weld pool surface, $P_c \approx 2.5 \cdot 10^{-2}$ N. When using an electrode with flat tip f_e = 1.0 mm wide, pressure of the arc column plasma is $P_c \approx 2.4 \cdot 10^{-2}$ N. The use of an electrode with flat tip f_e = 2.5 mm wide provides the largest diameter of the arc column near cathode and minimal plasma flow rate with the minimal pressure of the arc. Increasing the tip width to more than 3.0 mm leads to decrease in diameter of the arc column near cathode, as well as increase in both plasma flow rate and arc pressure on the weld pool surface. Decrease in diameter of the arc column, in the opinion of the authors, is related to lower heating of tungsten electrodes with a tip more than 3.0 mm wide.

The analysis conducted allows a conclusion that in narrow-gap welding the force of pressure of the arc plasma is much in excess of Lorentz force F_L. That is why the pressure of the arc plasma is balanced in the main by the force of hydrostatic pressure of the molten pool metal. Therefore, the main cause of formation of lacks of fusion and undercuts in narrow-gap welding is increase in pressure of the arc column plasma. It is well-known that the pressure of the arc on the molten metal can be decreased by decreasing the welding current. However, this will lead to decrease in productivity of the welding process. The arc pressure on the molten metal can also be decreased by changing geometric parameters of the arc. In particular, the use of the flat-tip tungsten electrodes in narrow-gap welding allows reducing the rate of the gas-dynamic plasma flow and arc pressure on the weld pool surface.

Comparison of the results of calculation of the arc plasma pressure with the results of investigation of transverse macrosections of the welds shows that no undercuts and lacks of fusion will form in the welds providing that the arc plasma pressure does not exceed $2 \cdot 10^{-2}$ N. Therefore, to reduce the probability of formation of defects in the form of lacks of fusion and

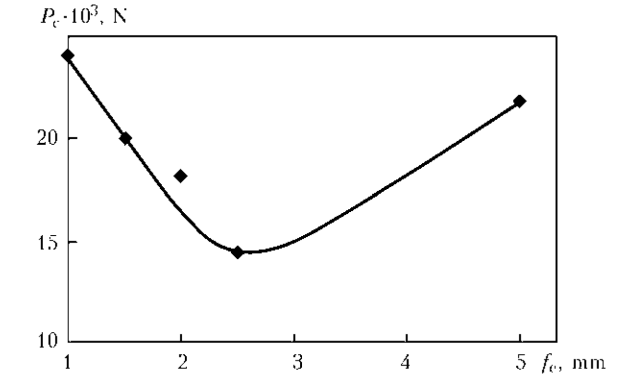

Figure 8. Dependence of total pressure of the arc column plasma P_c on width of the tip of the flat-tip electrode f_e in narrow-gap welding at I_w = 400 A and l_a = 5 mm

undercuts in the welds, in narrow-gap welding with the controlling magnetic field it is necessary to use tungsten electrodes with a special shape of the tip that provides decreased values of the arc pressure on the weld pool surface.

CONCLUSIONS

1. The mechanism of formation of a welded joint in the narrow groove under the effect of the external controlling magnetic field was suggested. According to this mechanism the vertical walls of the groove are fused due to the heat of the anode spot that is moved in turns to the opposite side walls with reversing of the magnetic field, thus pushing off the molten metal to the vertical walls and tailing part of the weld pool due to the effect of the force of gas-dynamic pressure of the arc plasma.

2. Dependence of the argon plasma flow rate and gas-dynamic arc pressure on the weld pool surface in narrow-gap welding with the magnetically controlled arc on the welding process parameters and width of the tip of the flat-tip tungsten electrodes was proved by the experimental-calculation method.

3. It was shown that the use of tungsten electrodes with the tip of an increased width allows decreasing the total value of the force of pressure of the arc column plasma on the weld pool surface, thus preventing formation of the lack of fusion type defects in the welds.

1. Hori, K., Haneda, M. (1999) Narrow-gap arc welding. *J. JWS*, **3**, 41–62.
2. Paton, B.E., Zamkov, V.N., Prilutsky, V.P. (1996) Narrow-groove welding proves its worth on thick titanium. *Welding J.*, **4**, 37–41.
3. Belous, V.Yu., Akhonin, S.V. (2007) Influence of controlling magnetic field parameters on weld formation in narrow-gap argon-arc welding of titanium alloys. *The Paton Welding J.*, **4**, 2–5.
4. Voropaj, N.M., Krivtsun, I.V. (1978) Gas-dynamic characteristics of plasma flows in welding arcs. *Magnit. Gidrodinamika*, **1**, 132–136.
5. Lenivkin, V.A., Dyurgerov, N.G., Sagirov, Kh.N. (1989) *Technological properties of welding arc in shielding gases*. Moscow: Mashinostroenie.
6. Topolyansky, P.A., Khristofis, B.O., Ermakov, S.A. et al. (2005) Relationship between the integral value of effective power of axisymmetric heat source on a segment and function of radial distribution of heat flow density. In: *Proc. of 6th Int. Pract. Conf.-Exhibition on Repair Technologies* (St.-Petersburg, 13–16 April 2004). St.-Petersburg: SPbGPU, 3–9.

DEPOSITION OF TITANIUM-BASED GRADED COATINGS BY LASER CLADDING

V.K. NARVA and **A.V. MARANTS**
National University of Science and Technology «MISIS», Moscow, Russian Federation

Investigation of the technology of laser cladding of a titanium substrate and analysis of the properties of graded materials of Ti–Si and Ti–NiCr systems were carried out. Cladding was performed in Trumpf DMD 505 laser system of 5 kW power. A graded change in coating properties was determined by scanning electron microscope, optical microscope and X-ray diffraction. Analysis of hardness variations through thickness of the deposited layers was carried out by *HV* method. The possibility of providing sound graded coatings in order to improve the titanium substrate properties was proved.

Keywords: *laser, laser cladding, graded coatings, titanium base, phase composition, structure, hardness*

Development and introduction of laser technologies today is a promising avenue of progress of science and technology. One of the advanced laser technologies — laser cladding — allows deposition of wear- and high temperature-resistant, thermally-stable, corrosion-resistant graded and composite coatings on part surfaces of a complex geometry [1]. It can be used also for reconditioning of worn surfaces of parts, deposition of protective coatings, and manufacture of 3D objects [2]. In laser cladding powder transportation into the laser impact zone is performed by shielding carrier gas. Material penetrating into the melt pool, which is formed in the subsurface layer by the laser beam, melts, partially mixes with it, and provides a high strength of adhesion of the deposited layer with the substrate. High cooling rates in laser cladding lead to formation of a unique structure and properties in the deposited material [3]. Owing to the fact that in laser cladding it is possible to mix various materials in the specified proportions, graded coatings of different composition are produced [2, 4].

The purpose of this work consisted in obtaining new experimental data on the influence of parameters of laser cladding mode on the structure and properties of coatings of titanium-based graded materials.

Graded coatings were produced on a titanium substrate from materials of Ti–Si and Ti–NiCr systems, which feature higher high-temperature resistance and thermal stability. For this purpose compositions of coating surface layers of Ti–Si (70/30 wt.%), and Ti–NiCr (70/30 wt.%) systems were selected. To reduce inner stresses between the titanium substrate and coating, three intermediate layers were made, thus allowing the difference between the values of the coefficient of thermal expansion (CTE) of the coating and substrate to be reduced, as well as producing a graded coating and highly-alloyed surface layer.

Compositions of coatings, both of Ti–Si and Ti–NiCr system were varied by addition of silicon in the amount from 12 to 30 wt.% with 6 % step. Thickness of each layer was varied from 0.6 up to 2.0 mm, depending on laser cladding mode parameters (Figure 1). Layers were deposited using dispersed powders of nichrome (49.7 wt.% Ni) with particle size d = 60–160 μm, titanium (d = 50–150 μm), and silicon (d = 50–150 μm). Schematic of laser cladding process is given in Figure 2 [5].

Main parameters of laser cladding process, strongly influencing the structure and properties of the cladding material, are powder feed rate (consumption), nozzle displacement speed and laser power. In order to determine their influence on cladding properties, the values of these parameters were varied in the following ranges: rate of powder feeding into the laser impact zone (speed of rotation of the disc injecting the powder) was 3000–5000 rpm, speed of nozzle displacement was 500–1000 mm/min. Laser power was 5 kW. Influence of laser cladding parameters was assessed using X-ray phase and microstructural analyses, electron microscopy, as well as layer-by-layer hardness determination. Microstructural studies were conducted in the optical and electron microscopes. X-ray phase analysis was performed at filming in K_{Cu}-radiation with 15.4 nm wave length, 2° step with 5 s exposure per point. Hardness variation by coating height was determined by *HV* method.

Light optical microscope was used for visual determination of the structural features (grain size, approximate assessment of phase content and their distribution) of graded coatings of Ti–Si and Ti–NiCr system.

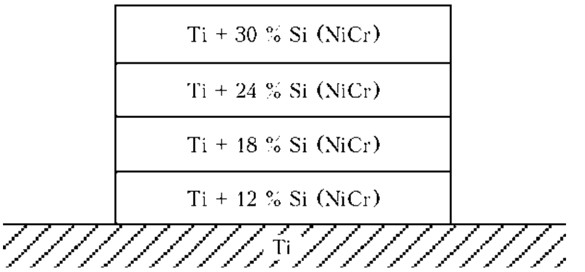

Figure 1. Schematic of the change of layer composition by height of deposit of Ti–Si and Ti–NiCr system coatings

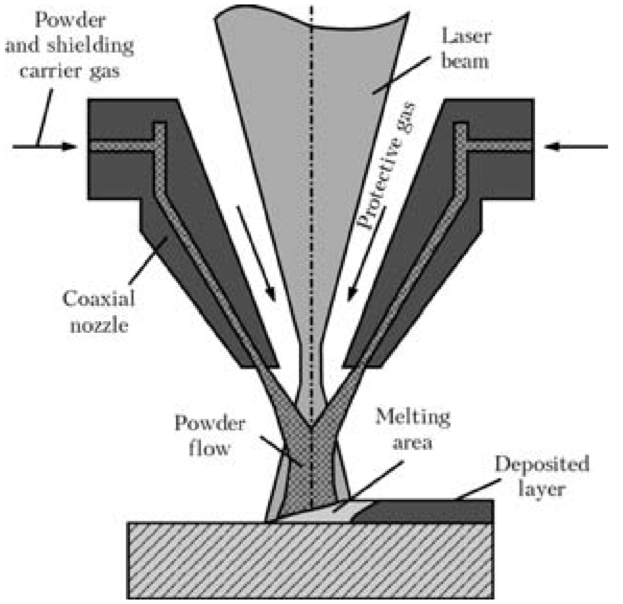

Figure 2. Schematic of laser cladding

Change of coating metal structure was studied by its height, as well as at variable parameters of laser cladding mode. At layer-by-layer analysis of metal structure of Ti–NiCr coating system it is seen that the grain size decreases from the lower to the subsurface layer (Figure 3), which is due to the thermal influence of the above-lying layers that promotes an increase of grain size of the lower-lying layers [6].

Main phases in the coating structure are β-(Ti–Cr) solid solution and $NiTi_2$ intermetallic. Weight fraction C of forming intermetallic components increases with increase of the content of NiCr(Si) alloying component (Figure 4).

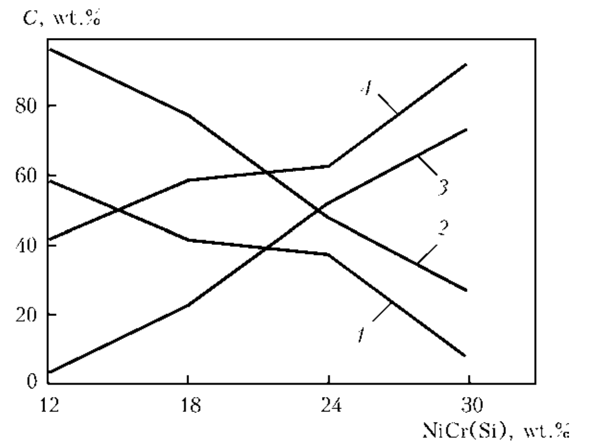

Figure 4. Influence of the content of NiCr(Si) alloying component on phase composition of materials of Ti–Si and Ti–NiCr systems: *1* — α-Ti; *2* — β-(Ti–Cr); *3* — $NiTi_2$; *4* — Ti_5Si_3

Change of variable parameters (powder feed rate v_f, and nozzle displacement speed v_n) has a considerable influence on coating metal structure. At increase of nozzle displacement speed or lowering of powder consumption, grain size is refined [7], which is attributable to increase of cooling rate in connection with decrease of layer thickness. At a high speed of nozzle displacement, unmolten titanium particles remain in the coating structure. X-ray spectral analysis confirmed their presence in the subsurface layer of the coating made at v_n = = 1000 mm/min, and v_f = 3000 rpm.

Alloy phase composition also depends on laser cladding parameters. Weight fraction of precipitating $NiTi_2$ intermetallic phase increases with increase of powder feed rate and decreases with increase of substrate displacement speed. This is connected with that

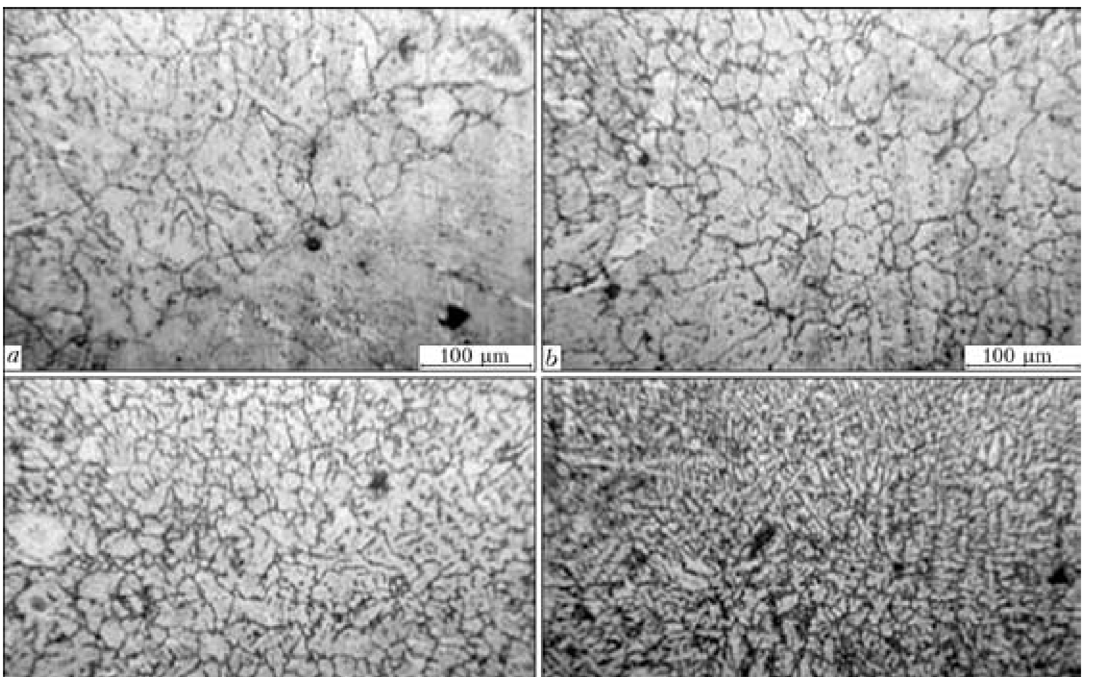

Figure 3. Microstructures of the deposit of Ti–NiCr system material from the substrate to the subsurface layer: *a* — first layer, 12 wt.% NiCr; *b* — second layer, 18 wt.% NiCr; *c* — third layer, 24 wt.% NiCr; *d* — fourth layer without NiCr

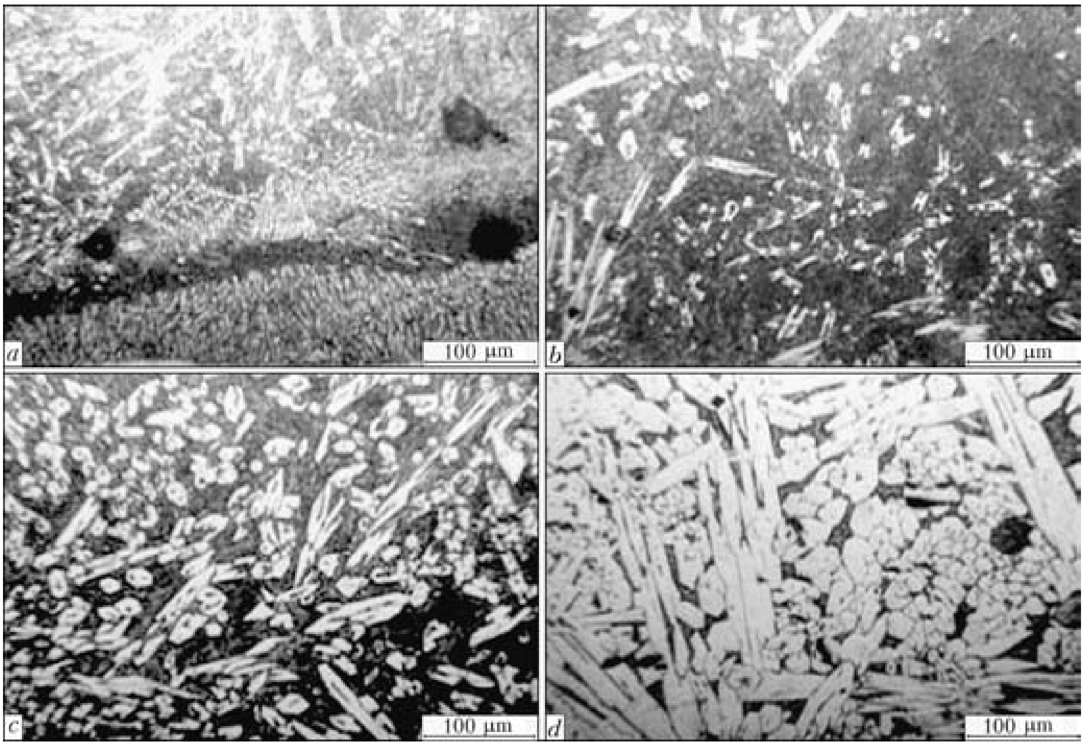

Figure 5. Microstructures of deposit of Ti–Si system material from the substrate to subsurface layer: *a* — first layer with 12 wt.% Si; *c* — second layer with 18 wt.% Si; *c* — third layer with 24 wt.% Si; *d* — fourth layer with 30 wt.% Si

increase of powder feed rate leads to increase of coating thickness and, hence, to its slower cooling. The longer the coating is cooling down, the closer is its phase composition to the equilibrium composition, and the greater the amount of intermetallic phase that is able to precipitate, whereas increase of nozzle displacement speed has a reverse influence.

At layer-by-layer analysis of the structure of Ti–Si system coating metal, an increase of the content of precipitating titanium silicide Ti_5Si_3 and alloying component content from the substrate to the coating was established (Figure 5), which is confirmed by the results of X-ray phase analysis (see Figure 4).

Proceeding from investigation results, the change of phase composition of Ti–Si system materials depending on the varied parameters leads to the conclusion that the content of precipitating titanium silicide Ti_5Si_3 rises with increase of powder feed rate and decreases with increase of nozzle displacement speed. This is related to the fact that increase of powder feed rate leads to an increase of coating thickness and, therefore, to its slower cooling. The longer the coating cools down, the closer will its phase composition be to the equilibrium one, and the greater the amount of titanium silicide that will have time to precipitate. Increase of the nozzle displacement speed leads to a reverse effect.

Change of coating hardness by the height of the deposited layers was studied, as well as the influence of laser cladding parameters on it [8]. Hardness rises continuously from the substrate to the coating surface layer in materials of both Ti–NiCr and Ti–Si systems, which is due to formation of solid solutions and presence of intermetallic and silicide phases in the coating.

Depending on the varied parameters of laser cladding mode, surface layer hardness in Ti–NiCr system coating changes only slightly and stays within instrument error (Figure 6). This leads to the conclusion that variation of the above parameters in a broad range does not affect the deposited coating hardness.

Ti–Si system materials are characterized by a dependence of hardness on laser cladding mode parameters. Surface layer hardness decreases with increase of nozzle displacement speed v_n and increases with increase of powder feed rate (Figure 6), as v_n increase leads to reduction of coating thickness, increase of cooling rate and reduction of weight fraction of Ti_5Si_3 titanium phase, which does not have enough time to

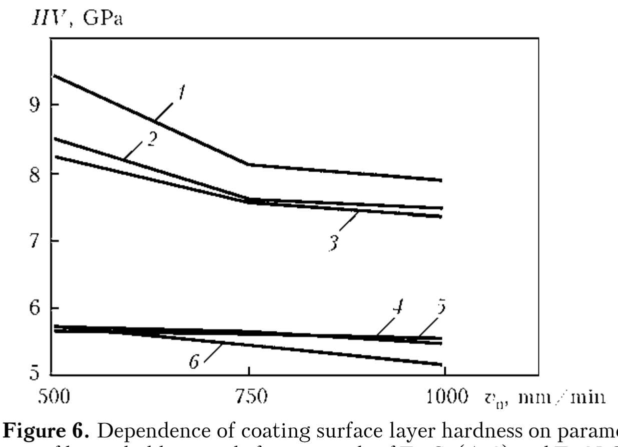

Figure 6. Dependence of coating surface layer hardness on parameters of laser cladding mode for materials of Ti–Si (*1–3*) and Ti–NiCr (*4–6*) systems: *1*, *6* — v_n = 6000; *2*, *5* — 4500; *3*, *4* — 3000 rpm

precipitate, that is confirmed by X-ray phase analysis. Powder feed rate has a similar influence.

CONCLUSIONS

1. Influence of parameters of laser cladding mode (powder feed rate and nozzle displacement speed) on the structure and properties of coatings from material of a graded composition of Ti–NiCr and Ti–Si systems was studied.

2. A refinement of grain size from coating lower layer (Ti–12 wt.% NiCr) to the surface layer (Ti–30 wt.% NiCr) with lowering of powder feed rate (at v_n = 3000–5000 rpm) and increase of nozzle displacement speed up to 500–1000 mm/min is established, as well as increase of intermetallic content from coating lower layer (Ti–12 wt.% NiCr or Si) to surface layer (Ti–30 wt.% NiCr or Si) with increase of powder feed rate and decrease of nozzle displacement speed.

3. An increase of coating layer hardness towards the surface layer is established, and the change of parameters of laser cladding process has only a minor influence on hardness of Ti–NiCr material layers.

4. In Ti–Si system materials surface layer hardness decreases with increase of nozzle displacement speed and increases with increase of powder feed rate.

5. Deposition of layers of Ti–NiCr and Ti–Si system materials by laser cladding can be recommended for improving the hardness and wear resistance of the titanium base.

1. Toyserkani, E., Khajepour, A., Corbin, S. (2005) *Laser cladding*. CRC Press.
2. Thivillon, L., Bertrand, Ph., Laget, B. et al. (2009) Potential of direct metal deposition technology for manufacturing thick functionally graded coatings and parts for reactor components. *J. Nucl. Mater.*, **385**, 236–241.
3. Nerovny, V.M. (2007) *Theory of welding processes*. Moscow: N.E. Baumana MGTU.
4. Ocelik, V., De Oliveira, U., De Boer, M. et al. (2007) Thick Co-based coating on cast iron by side laser cladding: Analysis of processing conditions and coating properties. *Surface and Coatings Techn.*, **201**, Issue 12, 5875–5883.
5. Yakovlev, A., Trunova, E., Grevey, D. et al. (2005) Laser-assisted direct manufacturing of functionally graded 3D objects. *Ibid.*, **190**, 15–24.
6. Gaard, A., Krakhmalev, P., Bergstrom, J. (2006) Microstructural characterization and wear behavior of (Fe, Ni)–TiC MMC prepared by DMLS. *J. Alloys and Compounds*, **421**, 166–171.
7. De Nascimento, A.M., Ocelik, V., Lerardi, M.C.F. et al. (2008) Wear resistance of WCp/duplex stainless steel metal matrix composite layers prepared by laser melt injection. *Surface and Coatings Techn.*, **202**, 4758–4765.
8. Thivillon, L., Novichenko, D., Bertrand, Ph. et al. (2009) Mechanical properties of parts manufactured by direct metal deposition technology. In: *Proc. of 5th Int. WLT-Conf. on Lasers in Manufacturing* (Muenich, 2009), 99–103.

ELECTRIC ARC SPRAYING OF CERMET AND METAL-GLASS COATINGS

A.A. KARPECHENKO

Admiral S.O. Makarov National Shipbuilding University, Nikolaev, Ukraine

Upgraded unit of the electric arc sprayer for deposition of composite coatings is described. The possibility of formation of cermet and metal-glass coatings is shown. Optimal spraying parameters are given. Wear resistance and strength of adhesion of the electric-arc metal-glass coatings are considered.

Keywords: *electric arc spraying, electric metallizator, spraying head, upgrading, cermet and metal-glass coatings, wear resistance, strength of adhesion, optimal parameters*

Composite materials and coatings, obtained using powder metallurgy methods, plasma, flame and detonation spraying [1–4], get wider application in the friction assemblies of different machines and mechanisms. However, process of obtaining of the composite materials by powder metallurgy is sufficiently power-consuming and requires significant power inputs [1, 2].

The cermet coatings, obtained by flame, plasma and detonation methods, are mainly used for strengthening and repair of worn surfaces of the parts, that allows increasing their life time several times [4, 5].

A method of coating deposition depends on requirements making to the coating properties. These requirements, on the one hand, are determined by composition of the material of coating and, on the other hand, by parameters of the process of its spraying and achievable values of heat and kinetic energy of the particles. Others criteria are costs of coating deposition, including cost of power input and consumables per unit of coating being sprayed.

Heat efficiency of a flame torch makes 0.8–0.9 in flame spraying, however, a level of effective application of heat of a jet for heating up of powder particles and their acceleration makes only 0.02–0.10 [6]. Higher level of the coating properties (adhesion strength, porosity) is achieved at supersonic flame spraying, however, process performance requires increased fuel consumption (gas, liquid fuel), that results in rise of the cost of coating unit. The flame spraying has limitations in spraying materials, related to temperature of combustion materials.

The coatings from all the materials, which do not decompose at heating to melting temperature, can be formed using plasma spraying. Heat efficiency of a plasmatron usually lies in the ranges from 0.55 to 0.70 depending on its structure and operation parameters [6]. Quantity of plasma jet heat consumption for heating and acceleration of particles makes 0.02–0.27 depending on a way of powder feeding in the jet [7].

The process of electric arc spraying of the coatings is based on a phenomenon of melting of a material by high amperage arc and dispersion of forming melt by compressed gas jet. Absence of the necessity to heat the high-speed particles of the coating up to melting stage during a short period of their movement in a jet volume provides the process of high-level of energy-saving. Index of thermal efficiency of the process achieves 0.7–0.9, that in combination with simplicity of the equipment provides its mass application. Comparative assessment of the costs for obtaining of the coatings by different thermal spraying methods shows that the electric arc coatings have 3–10 times below cost than others [7–13].

The electric arc spraying gained the highest distribution in deposition of corrosion-resistant coatings, mainly, from aluminum and zinc on different structures and constructions [13–16]. The electric arc coatings from different steels, bronze etc. are used as wear-resistant ones. Pseudoalloy coatings from steel and copper, copper and tin and other combinations [4, 10–13, 15, 16] are being perspective. One of the main disadvantages of this method is possibility of application only current conducting wire materials as spraying ones. Application of the flux-cored wires for obtaining cermet coatings allowed significantly widening a list of compositions of the electric arc coatings, that became a new stage of development of electric arc metallizing [10, 17].

The aim of the present paper was development of a method for formation of cermet and metal-glass coatings by electric arc spraying method using upgraded electric arc apparatus EM-14M. Upgrading of a cap of spraying head of EM-14M apparatus was carried out for obtaining the composite coatings by electric arc method. It allowed formation of the coatings with participation of flux-cored material by means of feeding it in a high-temperature zone of arc discharge.

Intensive injection of ambient air in the jet took place after flow of the compressed air jet from the nozzle. Thus, if spraying powder is supplied to the nozzle opening, located in the cap of spraying head, it will be drawn in the air jet flowing out of the nozzle opening. The air flow, shooting out from the nozzle opening, is turbulent, that promotes good mixing of the particles of spraying powder with the drops of molten metal and uniform distribution of the particles of spraying powder in the coating.

The upgrading of EM-14M apparatus lied in development of a unit for continuous feeding of powder material in the high-temperature zone of arc discharge (Figure 1) [18, 19]. Structural changes were made in the spraying head since feeding of powder material should be performed into the flow of metal molten particles. Additional bronze nozzle *7* with opening bigger than opening of the main nozzle is installed before bronze nozzle *9*. Main nozzle *9* comprises eight slots entering in the cavity between additional nozzle *7* and main nozzle *9*, positioned normal to the axis of gas flow. Nozzles *7* and *9* are embedded in fluoroplastic inserts *8* which being pressed to cap *5* with the help of shield screen *4*. Spraying powder from hopper *1* is supplied in dosing apparatus *2*. Powder due to injection at pressing on control arm *3* is supplied in the cavity between additional nozzle *7* and main nozzle *9*. Adapter *6* is designed for regulating zone of powder feeding. Powder, passing additional nozzle *7* and arc between the two wire-electrodes, mixing with the compressed air flow and molten particles of metal, is directed toward the surface being sprayed.

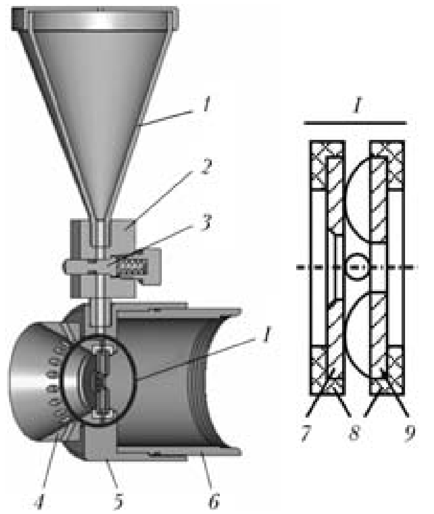

Figure 1. Scheme of upgraded cap of spraying head (designations see in the text)

The composite coatings with different concentration of powder particles in a sprayed layer can be obtained regulating powder supply with the help of dosing apparatus and rate of wire feed.

1.2 mm diameter seamless wire of Sv-08G2S-O grade and powders (40–80 μm particles of glass breakage of group A, ZrO_2, Al_2O_3) were used in the experiments.

«Remdetal» 026–7 machine was used for jet-abrasive machining of the substrate surface before deposition of the metal-glass and cermet coatings. Electrocorundum of 7B grade of abrasive grit 125 was used as an abrasive. The coatings of the following compositions were obtained as a result of spraying with upgraded apparatus EM-14M (Figure 2): Sv-08G2S-O–A-glass, Sv-08G2S-O–ZrO_2, Sv-08G2S-O–Al_2O_3.

Microhardometer PMT-3 was used for identification of phases in the coatings at indenter loading 50 g. An average microhardness of metal matrix from Sv-08G2S-O in all composite coatings made 1900 MPa

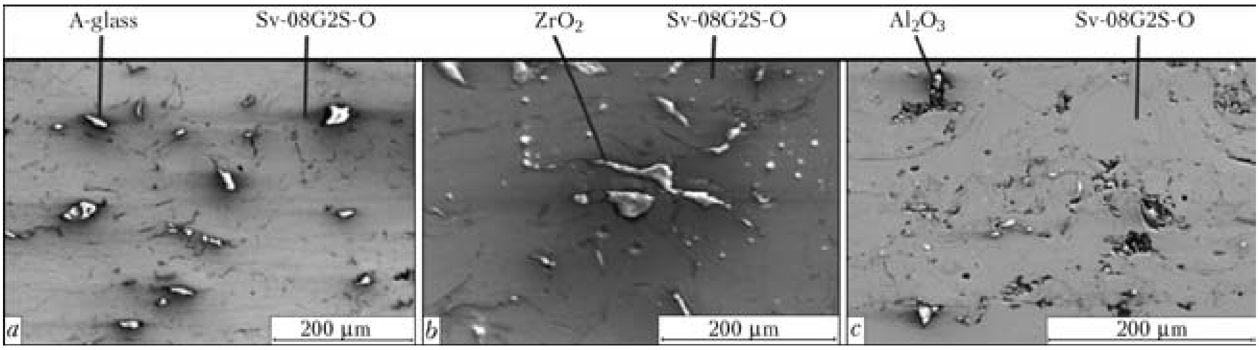

Figure 2. Microstructures of composite coatings: *a* — Sv-08G2S-O–A-glass; *b* — Sv-08G2S-O–ZrO_2; *c* — Sv-08G2C-O–Al_2O_3

and in fillers A-glass it was 5850, ZrO_2 — 12880 and Al_2O_3 — 16104 MPa.

Difficulties, related with spraying of the coatings of specified composition, appeared during development of a technological process of deposition of the metal-glass and cermet coatings. They lied in a complexity of experimental selection of parameters providing specified content of filler for obtaining optimal physical-mechanical properties.

The method of complete factorial experiment of 2^k type was selected for determination of the possibilities for regulation of content of the coatings from compositions Sv-08G2S-O–A-glass, Sv-08G2S-O–Al_2O_3 and Sv-08G2S-O–ZrO_2. A response surface (optimization parameter) is a content of the filler in coating Y. Current intensity X_1, powder consumption X_2 and pressure of compressed gas X_3 were selected as parameters determining the process of coating deposition.

Known techniques [20] were used for carrying out calculation of the coefficients of regression equation and verification of the conformity of built models. The following regression equations were obtained after mathematical processing of a design matrix at 5 % level of importance of polynomial coefficients:

$$Y + 5.56 = 0.07Y_1 + 0.134X_2 + 13.5X_3$$

for composition Sv-08G2S-O-A-glass;

$$Y + 7.62 = 0.007X_1 + 0.23X_2 + 11.41X_3$$

for composition Sv-08G2S-O–Al_2O_3, and

$$Y + 3.96 = 0.01X_1 + 0.28X_2 + 6.34X_3$$

for composition Sv-08G2S-O–ZrO_2.

It was determined as a result of analysis of regression equations that the first main factor, having influence on output parameters of the process, is current intensity. It increase rises a concentration of molten particles of metal in the jet and their enthalpy, that results in higher content of the filler in the coating. The second important factor is pressure of compressed gas. Intensity of powder injection in the high-temperature jet and speed of particles in it rise with pressure increase, that results in a rise of content of the filler in the coating. The third factor is powder consumption: the higher amount of it is supplied in the high-temperature jet, the higher amount of the filler will be in the coating.

Computer metallographic program MEGRAN [21] and stereometric methods of metallography were used for studying microstructure of the metal-glass and cermet coatings. Structural composition of the coatings was determined by volume using spot method [22]. The following upper limits of volume content of the fillers were determined as a result of computer metallographic analysis through regulating composition of the electric arc coatings, %: cerment Al_2O_3 — 9 and ZrO_2 — 12, metal-glass of A-glass — 18.

Tests on wear resistance and adhesion strength were carried out for determining optimal content of A-glass in the metal-glass coatings. Their wear resistance was determined on SMTs-2 fraction machine by roller–block scheme under following conditions: circumferential speed 0.8 m/s, specific pressure 5 MPa, consumption of oil of M-10-DM grade under conditions of limited lubrication made 30 drops per minute,

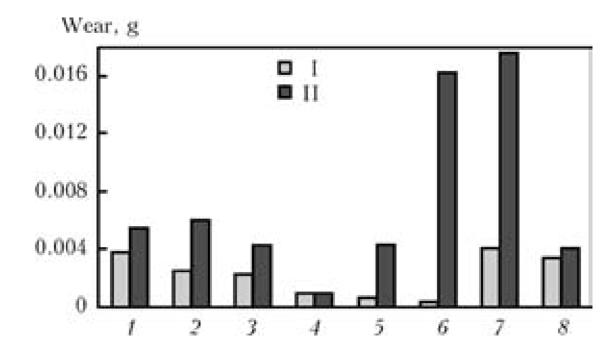

Figure 3. Histogram for results of determination of wear resistance by roller (II)–block (I) scheme: *1* — Sv-08G2S; *2* — 5 % A-glass; *3* — 8; *4* — 11; *5* — 14; *6* — 17; *7* — Br.AZh 9-4 (*HRC* 20–23); *8* — Br.AZh 9-4 (*HRC* 39–41)

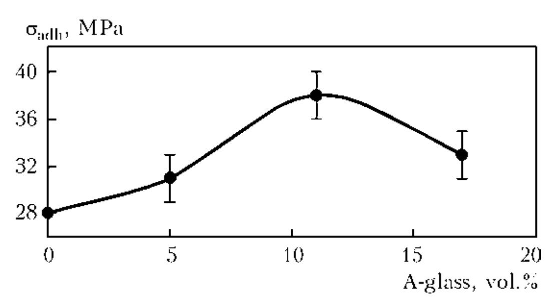

Figure 4. Dependence of adhesion strength on content of A-glass in the coating

traversed path after run-in 10 km. Wear was measured by mass loss.

Composite metal-glass coatings were deposited on the blocks. The rollers were manufactured from steel 45 after *HRC* 30–32 heat treatment. The wear of Br.AZh 9-4 bronze before and after heat treatment under similar conditions was determined for comparison of wear resistance of the metal-glass coatings with bronze.

Analysis of results of wear resistance investigation of the coatings with content of glass phase from 5 up to 17 vol.% (Figure 3) showed that the coating with 17 vol.% of glass phase has 13.5 times less wear than Br.AZh 9-4 grade bronze after heat treatment (*HRC* 39–41), but at that disastrous wear of the roller is observed. Optimal wear resistance has a pair with the metal-glass coating: content of glass phase 11 vol.% at total wear 5.6 times less than in the pair with unfilled coating from Sv-08G2S-O, and 4.5 times less than in bronze one (*HRC* 39–41).

Adhesion strength of the coating with the base (Figure 4), determined by method of «pin pulling» on tensile-test machine UMM-5, rises with increase of A-glass content in the coating and then reduces. Increase of the adhesion strength, probably, related to the fact that the infused particles of A-glass in the coating, colliding with surface of the base, additionally activate it due to their high kinetic energy and fragment form, and colliding with already fixed plastic metal particles introduce them into surface microirregularities of the base and further layers. Reduction of the adhesion strength connected with the following increase of content of the glass phase as a result of which actual zone of contact of the metal particles with the base is reduced.

Results of experiments on determination of wear resistance and adhesion strength allowed making a conclusion that optimal content of the glass phase in the metal-glass coatings makes from 8 up to 14 vol.%. At that, such coatings have maximum wear resistance and adhesion strength with the base.

Optimal parameters for deposition of the metal-glass coating, providing content of the glass phase from 8 up to 14 vol.%, are calculated based on obtained regression equation and as follows: current intensity 100 A, voltage 30 V, pressure of compressed gas 0.5 MPa, powder consumption 25 g/min, spraying distance 100 mm.

It is well-known that optimal content of the oxides, providing high wear resistance of Me + ZrO_2, Me + + Al_2O_3 compositions, makes 5–10 % [1]. Thus, the electric arc cerment coatings, filled with ZrO_2 and Al_2O_3 and deposited by upgraded apparatus EM-14M, are perspective for providing high wear resistance of friction pairs.

Thus, upgraded electric arc sprayer EM-14M allowed obtaining the cerment and metal-glass coatings through introduction of powder-filler in the high-temperature zone due to injection between the main and additional nozzles. Optimal parameters were set for spraying of the metal-glass coatings, providing their maximum wear resistance and adhesion strength.

1. Fedorchenko, I.M., Frantsevich, I.N., Radomyselsky, I.D. et al. (1985) *Powder metallurgy. Materials, technology, properties, fields of application*: Refer. book. Kiev: Naukova Dumka.
2. Terkhunov, A.G., Chernovol, V.I., Tiunov, V.M. et al. (1983) *Combined metal-polymeric coatings and materials*. Kiev: Tekhnika.
3. Khrolenok, V.V., Yarkovich, A.M., Nikitena, A.S. (2002) Repair of machine parts by deposition of composite coating. *Svarshchik*, **5**, 8–11.
4. Isakaev, E.Kh., Mordynsky, V.B. (2009) Wear-resistant coatings of parts of submerged centrifugal pumps. *Svarochn. Proizvodstvo*, **6**, 40–45.
5. Petrov, S.V., Korzhik, V.N., Gorban, V.F. et al. (2008) Plasma coatings of piston-cylinder group of locomotive diesels. *Ibid*., **4**, 35–43.
6. Borisov, Yu.S., Kharlamov, Yu.A., Sidorenko, S.L. et al. (1987) *Thermal coatings from powder materials*. Kiev: Naukova Dumka.
7. Korobov, Yu.S. (2005) Efficiency of application of activated arc metallization for deposition of protective coatings. *Svarochn. Proizvodstvo*, **2**, 47–49.
8. Dubovoj, A.N., Karpechenko, A.A. (2007) Study of feasibility of composite coating spraying by electric arc method. *Zbirnyk Nauk. Prats NUK*, 416(**5**), 66–70.
9. Kazimirenko, Yu.A., Karpechenko, A.A. (2009) Formation of electric arc coatings filled with hollow glass microspheres. *Ibid*., 424(**1**), 81–86.
10. Pashchenko, V.N., Fen, E.K. (2005) Repair of transport technics by electric arc metallization. *Svarshchik*, **3**, 16–18.
11. Petrov, S.V. (2004) Thermal coatings for solution of problems of railway transport. *Ibid*., **5**, 10–19.
12. Sergeev, V.V., Spiridonov, Yu.L., Farakhshin, I.I. (2004) Repair of crankshafts of domestic and foreign diesel engines by electric arc metallization. *Svarochn. Proizvodstvo*, **2**, 44–46.
13. Sonin, V.I. (1973) *Thermal spraying of materials in machine-building*. Moscow: Mashinostroenie.
14. Demianov, I.A., Murashov, A.P., Borisov, Yu.S. et al. (2005) Application of electric arc metallization for anticorrosive protection of TV tower in Kiev. *Svarshchik*, **3**, 19–21.
15. Kats, N.V., Antoshin, E.V., Vadivasov, D.G. et al. (1966) *Spraying metallization*. Moscow: Mashinostroenie.
16. Hasui, A. (1975) *Spraying technique*. Moscow: Mashinostroenie.
17. Pokhmursky, V.I., Student, M.M., Pokhmurska, G.V. et al. (2005) *Electric arc repair and protective coatings*. Lviv: H.V. Karpenko FMI.
18. Dubovij, O.M., Karpechenko, A.A., Shumov, S.M. *Device for electric arc spraying*. Pat. 83603 Ukraine. Appl. 25.06.2007. Publ. 25.07.2008.
19. Dubovij, O.M., Karpechenko, A.A., Shumov, S.M. *Device for electric arc spraying*. Pat. 30382 Ukraine for utility model. Appl. 29.10.2007. Publ. 25.02.2008.
20. Adler, Yu.P., Markova, E.V., Granovsky, Yu.V. (1976) *Planning of experiment in search of optimal conditions*. Moscow: Nauka.
21. Ivlev, A.I., Kazimirenko, Yu.O., Komarov, M.Yu. et al. (2005) Application of computer metallography in special disciplines. In: *Proc. of All-Ukrainian Sci.-Method. Conf. on Problems of Comprehensive Computer Training in the Higher School* (Mykolaiv, 2005).
22. Saltykov, S.A. (1976) *Stereometric metallography*. Moscow: Metallurgiya.

TECHNOLOGICAL CAPABILITIES FOR IMPROVEMENT OF RELIABILITY OF WELDED JOINTS ON ALUMINIUM-LITHIUM ALLOYS

T.M. LABUR
E.O. Paton Electric Welding Institute, NASU, Kiev, Ukraine

Technological capabilities for increasing strength and fracture toughness of welded joints on aluminium-lithium alloys are considered in terms of ensuring the reliability and safe operation of structures. It is shown that the use of low heat input in welding and new modified welding wires with a decreased content of harmful impurities provides a sufficient level of mechanical properties in all structural zones of the welded joint.

Keywords: *arc welding, aluminium-lithium alloys, welded joints, aerospace engineering, strength properties, fracture resistance, product reliability, technological operations*

Metal scientists, technologists and designers for a long time tried to create all-welded structures for aerospace engineering instead of the regular built-up-riveted structures. This predetermines the urgent need to develop high-strength readily weldable aluminium alloys with a high specific strength. Development of structures with extensive application of various assembly-welded and monolithic elements was also required, namely press panels, wing spars and connector profiles, and large-sized sheet stampings for parts of the wing and fuselage.

Solving these tasks was made possible by appearance of a new class of high-strength lithium-containing aluminium alloys: Al–Li–Mg (1420, 1421, 1423, 1424) and Al–Li–Cu (1450, 1451, 1460, 1461, 1463, 1464, 1468) with the ultimate strength of 400–420 and 500–550 MPa, respectively, which are readily welded by various welding processes [1–8]. This was promoted by a unique combination of properties, characteristic for aluminium-lithum alloys, namely high values of strength and modulus of elasticity at a low specific weight that distinguishes them from the traditional aluminium alloys. A comparatively low rate of fatigue crack growth in the alloys, high values of the critical coefficient of stress intensity, low-cycle fatigue life, resistance to stress corrosion cracking, layer and intercrystalline corrosion, allow including them into the class of the most promising materials for development of samples of new equipment with improved tactico-technical parameters.

These features of aluminium-lithium alloys were used in development of an all-welded aluminium airplane, where pressurized load-carrying tank compartments of a frame structure were applied [3–6]. However, manufacturing and operation revealed individual short-comings both of the structure proper and of 1420 alloy, in particular, its low ductility, which were later on leveled out by adding rare-earth metals to the alloy composition, development of a new technology of melting and pouring, as well as application of rational design of specific parts and components.

High specific strength and increased modulus of elasticity of aluminium-lithium alloys allow reducing the structure weight by 8 –15 %. New design solutions provided a reduction of the quantity of reinforcing elements and sealing materials that reduces the weight by another 12 %. Such an effect of aluminium-lithium alloy application in aerospace engineering products allowed an essential improvement of technico-economic characteristics of the product that is quite important to reduce fuel costs and improve flight characteristics [2].

The objective of this work is generalization of the published investigation results on the influence of thermal cycle of welding on the structure and properties of joints of aluminium-lithium alloys and substantiation of technological methods of improvement of welded structure reliability in operation.

By now the technological difficulties of producing sound welded joints which are related to metal softening, formation of a heterogeneous structure in different regions, as well as internal defects such as pores and oxide films, have been overcome [3]. Results of investigation of the features of formation of welded joints on aluminium-lithium alloys in fusion welding were the basis for development of ingenious welding technologies, application of which provides tighth welds with high values of physico-mechanical properties [3, 7, 8]. Strength of arc-welded joints is equal to 75–85 % of base metal strength level. Application of electron beam welding allows making joints of the strength close to base metal. In this case, the length of the HAZ is essentially reduced compared to arc-welded joints. Improvement of properties is noted not only in the weld metal, but also in the joint weakest zone — on the boundary of its fusion with the base metal that is due to formation of a fine-crystalline structure in the weld. Nonetheless, it was found [9] that metal overheating during welding leads to lowering of the level of critical coefficient of stress intensity to a greater degree, particularly in the zone of alloys, compared to the traditional alloys of Al–Mg–Mn and Al–Cu–Mn alloying systems (Figure 1, *a*, *c*). Development of embrittlement of aluminium-lithium alloys in the heating zone increases the probability of crack initiation in the joint in service. The problem of protection of welded structures from premature failure, which is one of the most urgent for the national economy, is closely related to cost issues. Metal loses at failure amount to billions of hryvnias per year [1]. In this connection development of new products for aerospace engineering should take into account the influence of technological factors of welding on the features of structure formation in different zones of aluminium-lithium alloy joints, and causes leading to metal embrittlement. Development and realization of a package of measures will allow increase of the level of strength and fracture toughness of welded joints and improvement of their performance under diverse operating conditions.

Formation of conditions for accelerated initiation and propagation of a crack near brittle phase inclusions is due to characteristic partial melting of structural components that arises in aluminium alloys under the influence of non-equilibrium solidus temperature in welding. Formation in intergranular space of extended brittle regions from oversaturated and intermetallic phases hindering plastic deformation of metal, is associated with its long-time soaking at high temperatures (673–773 K) that accompany the welding process. The latter leads both to intensive development of structural heterogeneities, and distribution of alloying elements and impurities contained in various zones of welded joints, and to their segregation along grain boundaries. With increase of volume fraction of such regions in the welded joint structure, an increase of the level of stress concentration is noted, that is indicated by formation of flat sections of the relief along the boundaries of crystallites and grains in the fractures of broken samples [10–15]. This is accompanied by lowering of fracture resistance characteristics: nominal breaking stress σ_{br} from 340 to 265 MPa, critical coefficient of stress intensity K_C from 29.5 to 21.5 MPa$\sqrt{m}$, critical crack opening displacement δ_C from 0.14 up to 0.03 mm, initiation energy J_C and

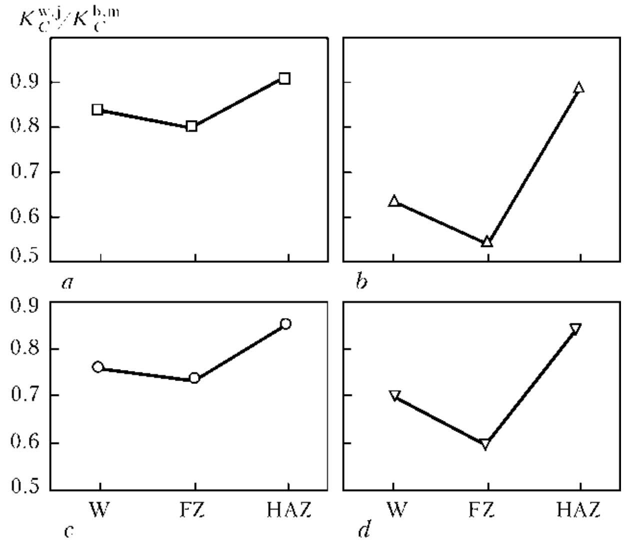

Figure 1. Comparison of crack resistance $K_C^{w.j}$ of different zones of welded joints of aluminium-lithium alloys made by conventional nonconsumable-electrode arc welding and base metal $K_C^{b.m}$: *a* — Al–Mg–Mn; *b* — Al–Li–Mg; *c* — Al–Cu–Mn; *d* — Al–Li–Cu

specific work of crack propagation (SWCP) from 5.8 and 7.5 to 2.5 and 3.8 J/cm^2 [14].

Increase of stress concentration as a result of the presence of geometrical or mechanical notch, including a fatigue crack, reduces by 40–55 % the value of the coefficient of stress intensity K_C, determining the fracture conditions [10]. Range of scatter of the values of this fracture resistance index varies depending on the radius of stress raiser sharpness and stress-strain state of welded joint structural zones. In the weld metal it is 10 %, and in the fusion and heat-affected zones — 20–25 %, that differs essentially from Al–Mg and Al–Cu system alloys without lithium. Non-uniform influence of the stress raiser on K_C fracture toughness value in the zones of welded joints is due to varying amounts of lithium-enriched phases, precipitating along the boundaries of weld crystallites and base metal grains during welding heat impact. This is particularly pronounced in samples of joints, in which the notch tip is combined with the weld to base metal fusion line (Figure 2). The found dependence is related to the features of formation of the structure of this joint zone under the conditions of metal solidification after heating in welding. In arc welding processes thickened grain boundaries, pres-

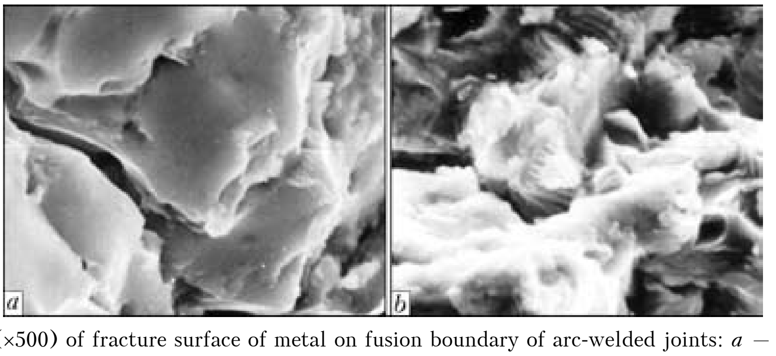

Figure 2. Microstructures (×500) of fracture surface of metal on fusion boundary of arc-welded joints: *a* — 1421 alloy; *b* — 1460

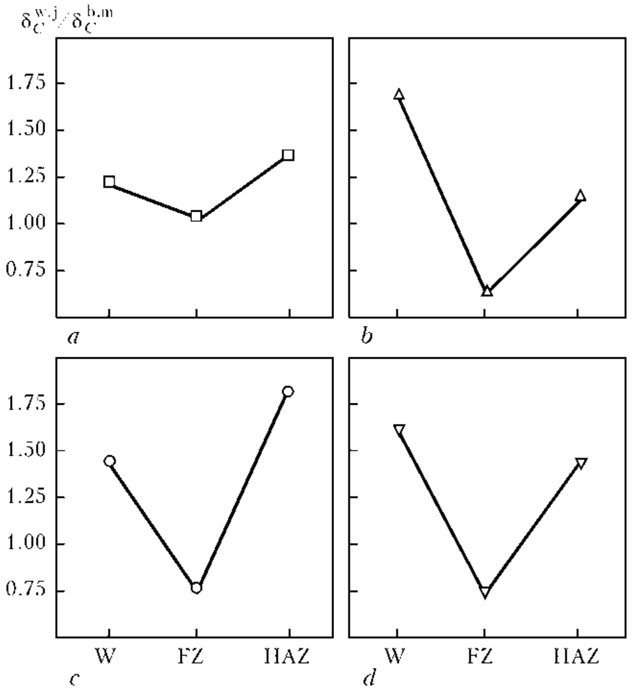

Figure 3. Comparison of the value of critical crack opening displacement $\delta_C^{w.j}$ in different zones of welded joints of aluminium-lithium alloys and base metal $\delta_C^{b.m}$: *a* — Al–Mg–Mn; *b* — Al–Li–Mg; *c* — Al–Cu–Mn; *d* — Al–Li–Cu

ence of their triple junctions and a considerable amount of partially melted phases are found in the fusion zone structure. Increased density of secondary phase precipitates and coarsening of intermetallic phase inclusions in the HAZ metal lead to formation of regions of unfavourable structure in the form of individual clusters or frame following the grain boundaries. In electron beam welding a predominantly polyhedral structure with rare inclusions of partially-melted phases is found [9].

Dimensions and position of phase inclusions in the intergranular space, particularly on the boundary of weld fusion with the base metal, influence stress concentration and volume fraction of brittle regions, i.e. conditions of crack initiation in welded joints of aluminium-lithium alloys. Presence of such structural sections along the grain boundaries, alongside the shear bands forming during semi-finished product manufacturing, limits plastic deformation and promotes an increase of the stress-strain state in welded joints. Shear bands, being the areas softened by deformation localization, as though predetermine the brittle mode of crack initiation in the HAZ metal in the regions of contact of the slip band with the boundary of the crystallite or grain. Total action of applied stresses and local stress concentration in the vicinity of the phases and shear bands cause intensive crack initiation both across the body, and along the boundary of contact with the matrix (see Figure 2).

Values of crack initiation energy (*J*-integral) of aluminium-lithium alloys 1421, 1460 and their welded joints

Alloy	Studied zone	*J*-integral, J/cm^2
1421 (Al–Li–Mg)	BML	3.6–4.4
	BMT	2.5–3.8
	W	4.9–6.8
	FZ	1.5–2.9
	HAZ	2.8–3.6
1460 (Al–Li–Cu)	BML	4.0–5.6
	BMT	2.5–3.8
	W	5.2–6.7
	FZ	2.9–3.4
	HAZ	4.2–5.7

Note. BML and BMT — base metal of longitudinal and transverse orientation relative to rolling direction, respectively; W — weld metal; FZ — fusion boundary metal; HAZ — HAZ metal at 5 mm distance.

A similar dependence of fracture resistance on structure condition in welded joint zones is also traceable by a characteristic change of critical crack opening displacement δ_C and its initiation energy (J-integral). As is seen from Figure 3 and the Table, the line of weld fusion with the base metal features minimum values of fracture resistance compared to other structural zones of the welded joint that should be taken into account in design of critical products. K_C and δ_C values for this joint zones are equal to 23 MPa$\sqrt{\text{m}}$ and 0.004 mm, respectively. J_C and SWCP values, reflecting the features and nature of crack initiation and propagation, depend on chemical composition of alloys being welded. In 1421 alloy (with magnesium), they are equal to 3.1 and 4.5 J/cm^2, respectively, and copper-containing alloy 1460 has higher values of J_C (4.0 J/cm^2) and SWCP (6.2 J/cm^2). Established regularities of the change of properties of aluminium-lithium alloy joints are indicative of a strong influence of structural state of the boundaries of weld crystallites and base metal grains in the welding heating zone on the strength of adhesion of the matrix with phase precipitates determining the metal susceptibility to brittle fracture.

Presence of stress raisers in welded joint metal is particularly hazardous for difficult conditions of structure operation, when the action of turbulent air flow results in a change of the loading pattern or deformation rate, while increase of the flight altitude leads to a temperature change. The above service factors lead to an additional loss of metal ductile properties in the structure, although the joint strength can increase up to 400–420 MPa here, as a result of strain or low-temperature hardening [11–15]. Degree of lowering of ductility and fracture toughness depends on the volume fraction of brittle local regions formed in the intergranular space at heating, and level of working stress. Reaching a critical value, they lead to crack initiation under the operation conditions and determine the subsequent nature of its propagation (in keeping with Griffith theory [1]).

Increased susceptibility of aluminium-lithium alloy joints to embrittlement is attributable to a high degree of their alloying compared to other high-strength base alloys of Al–Mg–Mn and Al–Cu–Mn alloying systems that results in an excess amount of phases forming in the intergranular space. Their presence and dimensions prevent relaxation of alloy stresses during plastic deformation that leads to stress accumulation and formation of an unfavourable dislocation structure of complanar type near the phases, revealed after sample fracture at testing. Brittle fracture in this case occurs as a result of running of even though intensive, yet highly localized plastic flow that may run at a very low level of shear stresses, and may lead to development of powerful and hazardous dislocation clusters creating the conditions for crack initiation [1]. This feature of aluminium-lithium alloys is attributed to lithium susceptibility to plane slipping during its redistribution along the grain boundaries that results in ductility lowering. Lowering of lithium content in the alloy (to 1.7–1.9 wt.%) promotes 1.5 times increase of such a ductility characteristic as relative elongation [2].

Procceding from experimental studies [9] it was found that favourable thermophysical conditions of welding are provided by processes featuring minimum heat input: pulsed arc $(10–13)\cdot10^5$ J/m) or electron beam $(1.2–1.4)\cdot10^5$ J/m) welding that allows 4 and 10 times reduction of the extent of the regions, respectively, in which brittle intecrystalline interlayers are present in the welds and inergranular interlayers in the HAZ metal, as well as microvoids in the fusion zone. Such a state of welded joint structure provides an improvement of metal resistance to crack initiation. Value of σ_{br} parameter in individual zones of the joints in this case rises by 70–100 MPa, and that of K_C – by 20–25 %. Improvement of metal quality leads to an increase of properties not only in the weld metal, but also in the weakest zone of welded joints: on the boundary of joint fusion with the base metal. Reduction of metal sensitivity to stress raisers creates prerequisites for ensuring reliabile performance of welded parts and components from aluminium-lithium alloys in fabrication of load-carrying panels, compartments and fuselage structure as a whole. Replacement of riveted overlap joints by butt joints allows reducing the number of transverse welds by application of extended blanks.

Application of modes of two-step annealing with intermediate deformation of up to 3 % also has a positive influence on the level of physico-mechanical properties of aluminium-lithium alloys [15]. Such a technological operation ensures formation of a favourable alloy structure that has an influence on the level of fracture resistance characteristics. Introduction of straightening after quenching suppresses the process of brittle phase coarsening, accelerating dissolution of strengthening phase δ, and somewhat reduces its dimensions, thus increasing the value of fracture toughness parameter K_C by 10 %.

Improvement of reliability parameters is achieved also by optimization of weld metal composition by addition of scandium in the range of 0.4 to 0.6 % to filler wire composition [16–18]. Here, not only the susceptibility of aluminium-lithium alloys to hot cracking is decreased, but also high fracture toughness values are ensured: σ_{br} = 310–320 MPa, K_C = 25–28 MPa$\sqrt{\mathrm{m}}$, σ_C = 0.05–0.07 mm, J_C = 4–6 J/cm^2, SWCP = 8–10 J/cm^2. Level of weld metal strength rises by 20 %, and relative elongation is equal to 7 %. This is promoted by formation of fine-crystalline and subgrain structure of welds due to complete dimensional-structural similarity of dispersed particles of scandium aluminide Al_3Sc with the matrix [3]. Scandium presence in the base metal decelerates the recrystallization processes, running in welding of aluminium alloys that reduces the length of the softening zone. The noted effect is very important for fabrication of welded structures of aerospace engineering. It allows lowering the strictness of specifying the temperature-time conditions of welding, limiting the aluminium-lithium alloy susceptibility to softening, as the HAZ extent depends not only on the welding process, but also on the alloy composition. As shown by investigations [9–12], the action of welding heating on the strength and toughness of welded joint metal is manifested to a smaller degree in alloys containing magnesium as the main alloying component than in alloys with copper. This is due to stronger ability of magnesium, compared to copper additive, to accelerate the processes of precipitation of strengthening phase δ′, and thus increasing their density in the metal bulk [1]. It should be noted that alloys of 1460 type, alloyed with copper, perform satisfactorily at cryogenic temperatures in contact with liquid oxygen, hydrogen and helium [12]. Strength and ductility characteristics of the alloys and their welded joints here rise with temperature lowering. Such a feature of the alloys allows them to be used in welded structures of space flying vehicle fuel tank of a complex geometry with provision of high service properties of welded joints and their leak-tightness. Use of an alloy of 1460 type in the structure of the tank of US Delta rocket allowed the tank weight to be reduced from 2259 to 1430 pounds [13]. Improvement of welded joint reliability is further promoted by reduction of volume fraction of intermetallic phases in the alloy structure, which contain impurities of alkali and alkali-earth elements (sodium, calcium, barium and potassium). Even thousandths of a percent of these elements in the alloy composition have an adverse effect on welded joint properties as a result of lowering of melting temperature of the phases precipitating along the grain boundaries, making them hazardous for fracture development. Being at the grain boundaries, they, because of their high chemical activity relative to aluminium, reduce the metal surface energy on the inner free surfaces, for instance, on the edges of present microcracks, and thus increase the metal susceptibility to embrittlement and crack propagation [19, 20]. Here, the level of ductility and fracture toughness characteristics decreases by 30–40 %, whereas no deterioration of strength is noted. Limitation of the quantity of impurities in the alloy composition to 0.01 % reduces the adverse influence of boundaries of crystallites and grains on the processes of crack initiation, increases the quantity of tough regions of fracture relief, thus increasing level of σ_{br} by 20 % and K_C level by 40 % at δ_C = 0.05 mm, J_C = 4 J/cm^2, SWCP = 5.2 J/cm^2. Maximum effect is achieved only at uniform distribution of intermetallic phases in the metal volume. Mode of joint fracture in the fusion zone changes from intercrystalline to transcrystalline.

Generalizing the results of investigations of welded joints of aluminium-lithium alloys [1, 2, 9, 10, 18–20], it can be stated that the condition of grain boundaries in structural zones forming under the influence of thermal cycle of welding, determines the level of physico-mechanical properties and mode of joint fracture. Condition of grain boundaries depends on the quantity of alloying elements and impurities, presence of phase clusters located along the rolling line, in the initial metal. Adverse influence of welding is manifested only in the case of development of extended regions of the weld and HAZ with an unfavourable structure forming during metal heating with a high heat input. To prevent such a phenomenon in aluminium-lithium alloy welding, it is necessary to strictly specify the heat input, using pulsed arc welding modes or electron beam (laser) welding, which are characterized by a high concentration of applied heat. In this case welded joints have the necessary values of strength and fracture toughness that is important for aerospace engineering products in operation under extreme conditions, including a wide temperature range (20–500 K). As a result, alongside reduction of product weight, also the task of provision of good adaptability of the structure to fabrication, as well as reliable failure-safe operation during an extended operation period, is solved. This is confirmed by the available cases of application of aluminium-lithium alloys and their welded joints in the structure of load-carrying sheaths of aircraft, helicopters and rocket fuel tanks for reusable space vehicles [3–6].

1. Fridlyander, I.N., Chuistov, K.V., Berezina, F.L. et al. (1992) *Aluminium-lithium alloys, structure and properties*. Kiev: Naukova Dumka.
2. Fridlyander, I.N., Beletsky, V.M., Krivov, G.A. (2000) Aluminium alloys in aircraft structures. *Tekhnolog. Sistemy*, **1**, 5–17.
3. Krivov, G.A., Ryabov, V.R., Ishchenko, A.Ya. et al. (1998) *Welding in aircraft construction*. Ed. by B.E. Paton. Kiev: MIIVTs.
4. Imamura, Ts. (1991) Application of light metals for construction of aircraft. *Keikinzoku*, 41(**9**), 623–634.
5. Ishchenko, A.Ya., Labur, T.M., Lozovskaya, A.V. (1995) Aluminium-lithium alloys for welded structures of aerospace engineering. *Avtomatich. Svarka*, **2**, 41–44.
6. Ovchinnikov, V.V., Drits, A.M., Krymova, T.V. (1997) Technological specifics of manufacturing of aircraft welded structures from aluminium-lithium alloy 1460. *Svarochn. Proizvodstvo*, **12**, 26–29.
7. Barabokhin, N.S., Bushuev, Yu.G., Shulgina, E.V. et al. (1999) Technological specifics of welding of high-strength aluminium alloy 1460. *Ibid*., **11**, 12–14.
8. Birk, R.K., Dajkus, D.P., Fridlyander, I.N. et al. (2001) Aluminium-lithium alloy 1441 as a promising material for fuselage. *Metallovedenie i Termich. Obrab. Metallov*, **8**, 7–10.
9. Labur, T.M., Bondarev, Andr. A., Lozovskaya, A.V. (2001) Influence of welding process on fracture resistance of joints of aluminium-lithium alloys 1420 and 1460. *The Paton Welding J*., **7**, 11–15.
10. Ishchenko, A.Ya., Labur, T.M., Lozovskaya, A.V. (2001) Can aluminium-lithium alloys be used in welded constructions for cryogenic engineering? *Welding in the World*, 45(**9/10**), 26–29.
11. Kojima, Y. (1989) Aluminium-lithium alloys. *Welding of Light Metals*, 39(**1**), 67–80.
12. Labur, T.M. (2001) Influence of cryogenic conditions on the properties of welded joints of aluminium-lithium alloys. *Welding in the World*, 45(**9/10**), 30–32.
13. *www*.Aviation Week @ Space Technology
14. Labur, T.M. (1994) Change of resistance to fracture of 01421 alloy welded joints in high-temperature heating conditions. *Avtomatich. Svarka*, **12**, 8–11.
15. Elagin, V.I., Orozov, A.I., Shcheglova, N.M. et al. (1996) Examination of effect of LTMT conditions on properties of 1571, 1430, 1441 alloys. *Tekhnologiya Lyog. Splavov*, **5**, 40–43.
16. Labur, T.M., Ilyushenko, R.V. (1992) Effect of scandium additives in filler wire in welding of aluminium alloy 1420. *Avtomatich. Svarka*, **11/12**, 53–54.
17. Labur, T.M., Ilyushenko, R.V. (1993) Effect of scandium on fracture resistance characteristics of 1420 and 1421 alloy welded joints. *Tekhnologiya Lyog. Splavov*, **12**, 37–41.
18. Labur, T.M. (1996) Investigation of efficiency of weld metal strengthening by scandium in welding of aluminium-lithium alloy 1420. *Avtomatich. Svarka*, **7**, 17–19.
19. Grushko, O.E., Sheveleva, L.M. (1994) Impurities of alkaline- and alkaline-earth metals in aluminium-lithium alloy 1420. *Tsvet. Metally*, **4**, 48–51.
20. Labur, T.M. (1998) Effect of impurity elements on fracture resistance. *Avtomatich. Svarka*, **6**, 40–43.

INFLUENCE OF SURFACE STRENGTHENING AND ARGON-ARC TREATMENT ON FATIGUE OF WELDED JOINTS OF STRUCTURES OF METALLURGICAL PRODUCTION

E.V. KOLOMIJTSEV[1] and **A.N. SERENKO**[2]
[1]PJSC «Ilyich Iron & Steel Works», Mariupol, Ukraine
[2]Priazovsky State Technical University, Mariupol, Ukraine

The results of fatigue tests of the T-joints on low-alloy steels are given and methods for extending the life and increasing the strength of welded joints (surface deformation by using a ball-rod strengthening device and argon-arc treatment) are described. It is shown that the optimal method is surface strengthening of the weld and near-weld zone. Treatment of crane beams and rocker bars of well cranes «Slabbing-1150» at the «Ilyich Iron & Steel Works» by this method provided a 15 times increase in their cyclic fatigue life.

Keywords: *welded structures, crane beams, welded joints, surface strengthening, argon-arc treatment, residual stresses, stress concentration, fatigue strength, life*

The experience of service of heavy-loaded welded structures (crane beams, balance beams of well cranes, etc.) at the «Ilyich Iron & Steel Works» shows that not static but fatigue strength is of critical importance for their accident-free operation.

Damageability and fracture of crane beams and elements of load-carrying cranes depend on many factors: design, technological, service. Crane beams are subjected to different force influences, the main of which are loads from rolls of cranes in vertical and horizontal planes, transmitted to rail of a beam. It results in formation of alternate stresses, distributing very unequally in designed sections, in welded joints of beams. The characteristic damages in crane beams observed during experience of operation are the following:

- cracks formation along the line of fusion of fillet welds connecting a web with upper flange (the most typical and dangerous damage). The length of a crack in the moment of its removal is 400–500 mm and in some cases is 2–3 m;
- violation of continuity and fracture of diaphragms;
- crack in the places of fastening crane beams to the pillars;
- damage of coupling along the crane beams.

To find the most efficient method of increasing fatigue strength and life of welded joints of crane beams the cheap and simple variant of comparative fatigue tests of models of crane beams is necessary as far as full simulation of all factors causing their damage is complicated and expensive.

The fatigue tests were carried out on specimens modeling joining of a flange with a web (T-joint) at alternating flat bending with a constant amplitude of deformation (rigid loading).

During manufacture of crane beams the webs and flanges are cut of rolled flanges of a required thickness. The longitudinal axes of flanges and web during preparation coincide with direction of rolling. The next welding of a flange with a web, performed by fillet welds, has also direction along the rolling which was considered during development of scheme of cutting sheets into blanks for manufacture of welded specimens.

T-joint specimen (Figure 1, *a*) simulates the joining of a flange with a web of crane beams of storage of ore and concentrates of agglomeration factory of «Ilyich Iron & Steel Works». The width of specimen

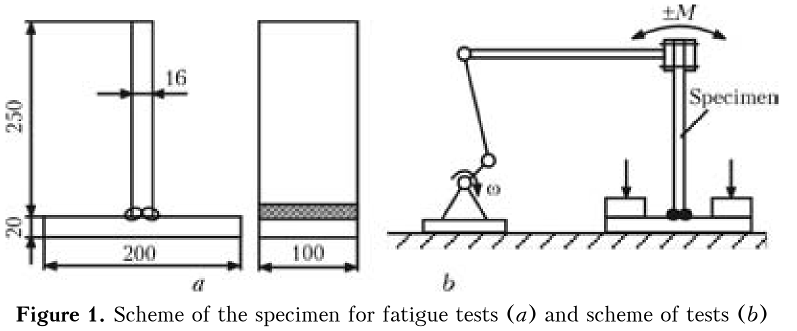

Figure 1. Scheme of the specimen for fatigue tests (*a*) and scheme of tests (*b*)

(100 mm) was selected with the purpose to obtain longitudinal residual stresses in it, approximately equal to residual stresses forming in the zones of beam welds. The surface of flanges and webs of beams and, respectively, specimens were not subjected to post-rolling treatment. The specimens were manufactured of hot-rolled steel 09G2S (σ_y = 350 MPa, σ_t = = 500 MPa).

The assembly and welding of specimens were performed in a jig allowing decrease of angular deformations of flanges using their fastening by screw clamps.

The flange welds of blanks (five specimens in the blank) of 500 mm length were performed by the automatic gravity position welding using tractor ADF-1001 with welding wire Sv-08A of 4 mm diameter under flux AN-348A in the following conditions: I_w = = 700–750 A; U_a = 36–37 V; v_w = 21 m/h; electrode stickout h = 40 mm; direct current of reversed polarity. In capacity of a power source the thyristor rectifier VDU-1201 was applied.

The beginning and end of flange welds were performed on additional tabs. The second weld was produced after cooling of a blank, heated in the process of producing the first weld.

The produced blanks were divided into three series: initial position after welding; fusion of transition zone from a weld to base metal in the argon atmosphere; surface plastic deformation of transition zone of a weld to the base metal.

After welding or appropriate treatment of near-weld zone the blank was cut into specimens using mechanical method. The cutting was carried out without water cooling under a soft condition, which did not cause heating of specimens higher than 50 °C and, consequently, did not lead to relaxation of residual stresses. Then, the specimens were subjected to mechanical treatment of edges.

It is known that life of welded joints at alternate loads can be increased using different methods [1–6]:

• before welding by selection of rational welding consumables, welding conditions and other;

• during welding by regulation of thermodeformational cycle of welding and conditions of crystallization;

• after welding by improving the surface properties of metal and setting of compressive stresses in it by mechanical, heat, ultrasonic and other types of treatment.

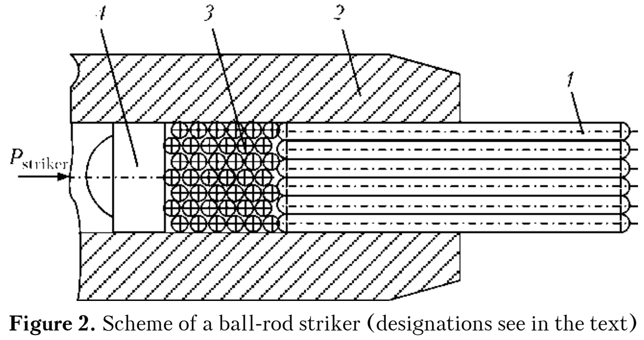

Figure 2. Scheme of a ball-rod striker (designations see in the text)

As far as methods, preceding and accompanying welding, are more perfected, the attempt has been made in the present work to evaluate the possibilities of technological methods of treatment of welded joints taking into account the results obtained earlier [3–6].

One of the most recognized methods to increase cyclic strength of welded structures is surface plastic treatment [2–6]. A ball-rod strengthener was used having a number of advantages as compared to other types [7]. The tool consists of two basic units: pneumatic hammer KMP-24 and ball-rod striker (Figure 2). Pneumatic hammer is a source of shock pulses, and design of a striker allows performing transmission of pulses through the system of bodies to freely floating rods *1* and maintaining them in working and non-working conditions in a striker body *2*. For uniform transmission of shock to all the rods, the intermediate layer of balls *3* of 2.0–2.5 mm diameter is used. The correlation of diameters of balls to diameter of rods was selected within the range of 0.6–0.8. The shock pulse is transmitted to the balls through the head *4*. A layer of balls performs function of a quasiliquid and allows conducting plastic treatment of weld surface and transition zones without missings. The speed of treatment using ball-rod strengthener was 6–8 m/h. The pressing force of working tool to strengthened surface varies in the limits of 80–120 N.

The surface plastic treatment by ball-rod strikers results in the following processes: strengthening (cold-working) of surface layers of weld metal and near-weld zone; setting of favorable compressive residual stresses in them; decrease of stress concentration in transition zone of a weld to the base metal due to increase of transition radius. The specific microrelief of a cold-worked surface is formed by multiple overlapping and intersection of single traces (dents) from rounded ends of the rods.

The depth of a cold-worked layer, intensity and character of distribution of residual stresses across the thickness of the layer a was determined according to the methods of the works [6, 8]. The investigations were conducted on 16 × 20 × 300 mm flat specimens of steel 09G2S under the conditions mentioned above. Figure 3 shows that the depth of a cold-worked layer and depth of spreading the compressive stresses reach 3 mm and maximal compressive stresses are close to the yield strength for the steel 09G2S.

Another method offered for testing on elements simulating the work of upper flange of crane beams was fusion of place of transition of a weld to the base metal by the arc in argon [2, 3] which finds its application in machine and ship building.

The fatigue tests were carried out in the machine with a crank mechanism at symmetric cycle of loading. The bending at constant deformation was carried out in the plane perpendicular to a vertical web of the

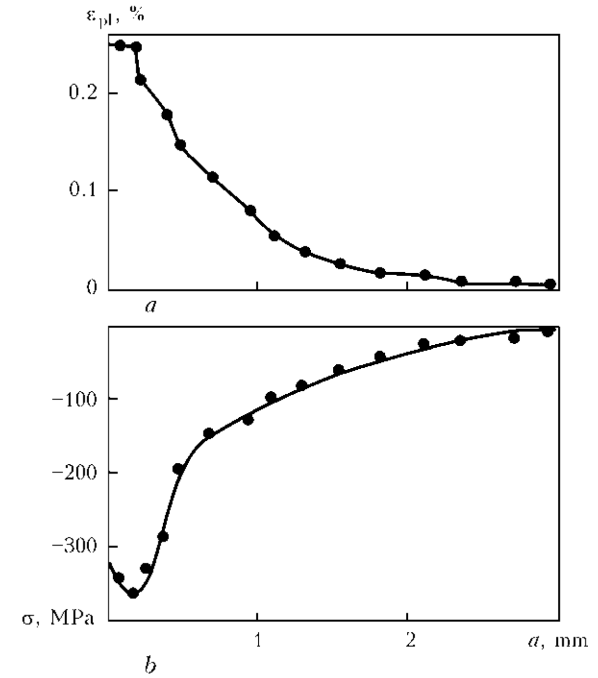

Figure 3. Distribution of plastic deformations (*a*) and residual stresses (*b*) across the section of the specimen strengthened by pneumatic hammer with a ball-rod striker

specimen (see Figure 1, *b*). The tests were carried out on the base of $3\cdot10^6$ cycles at 13 Hz loading frequency. The results of tests are given in Figure 4.

The fatigue strength of a T-joint at initial state after welding was changed from 200 MPa at $50\cdot10^3$ cycles up to 70 MPa at $3\cdot10^6$ cycles (Figure 4, curve *1*).

The argon-arc treatment of the place of transition of a weld to the base metal (Figure 4, curve *2*) increased the fatigue strength from 70 up to 100 MPa (1.4 times), the life was 2.5–3 times increased (at equal levels of loading — 140 and 200 MPa). The increase of fatigue limit and life is mainly achieved by increase of radius of transition from weld to base metal which results in decrease of stress concentration.

The surface plastic deformation using ball-rod strengthener increased fatigue strength up to 140 MPa, i.e. 2 times (Figure 4, curve *3*). The life of a T-joint after setting of compressive stresses increased 8–10 times.

The specimens in initial state after welding were fractured in the place of transition from a weld to the base metal (web) (Figure 5, *a*) which coincides with the data of works [1, 2, et al.]. After argon arc treatment a crack was formed in the place of transition of fused weld metal to the web (Figure 5, *b*). The fatigue strength and life are mainly increased due to increase of radius of transition, at least some increase of microhardness in HAZ metal (from *HV* 188–195 up to *HV* 210–214) was observed.

After treatment using ball-rod strengthener the specimens were fractured as a rule beyond the borders of the treated area (Figure 5, *c*), i.e. along the base metal.

The increase of fatigue strength of welded elements occurs as a result of setting of compressive stresses in the surface layers where grains are refined and their orientation changes, the hardness of grains practically does not change. The increase of limit of endurance 2 times and fatigue life 8–10 times and possibility to conduct this type of treatment in any spatial position under working conditions allow recommending it for treatment of critical welded structures of metallurgical enterprises.

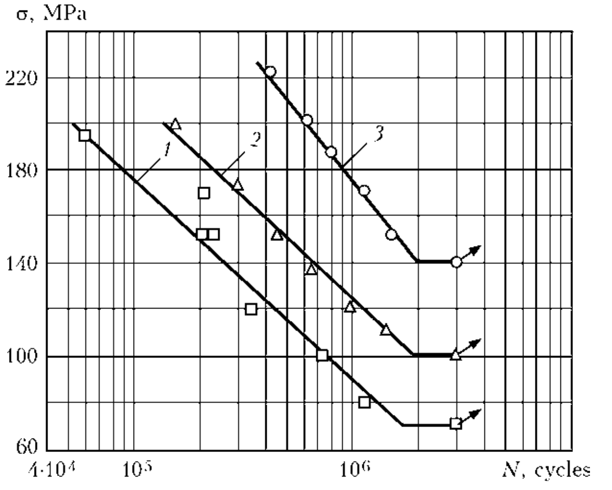

Figure 4. Results of fatigue tests of welded specimens: *1* — initial state (after welding); *2* — argon-arc treatment of transition zone of a weld to the base metal; *3* — strengthening of the same zone using pneumatic hammer with ball-rod striker

The industrial application of technology of a ball-rod strengthening was tested at pilot batch of six crane beams (Figure 6, *a*) of storage of ore and concentrates of agglomeration factory of «Ilyich Iron & Steel Works». The formation of fatigue cracks in welded joints of beams is connected with a risk of their transition to brittle fracture, therefore the service of these structures require constant inspection and relatively costs. The pilot batch of strengthened beams has been operating without formation of fatigue cracks already more than ten years.

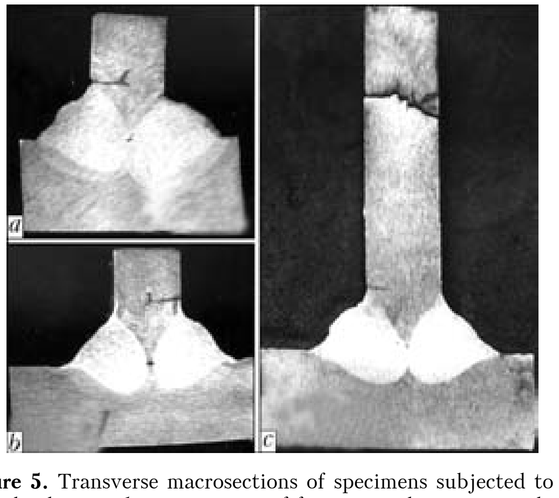

Figure 5. Transverse macrosections of specimens subjected to fatigue loading: *a*, *b* — initiation of fatigue cracks, respectively, in initial specimens (non-treated) and treated using remelting of transition zone by arc in argon; *c* — fracture of specimen along the base metal after strengthening of transition zone using pneumatic hammer with a ball-rod striker

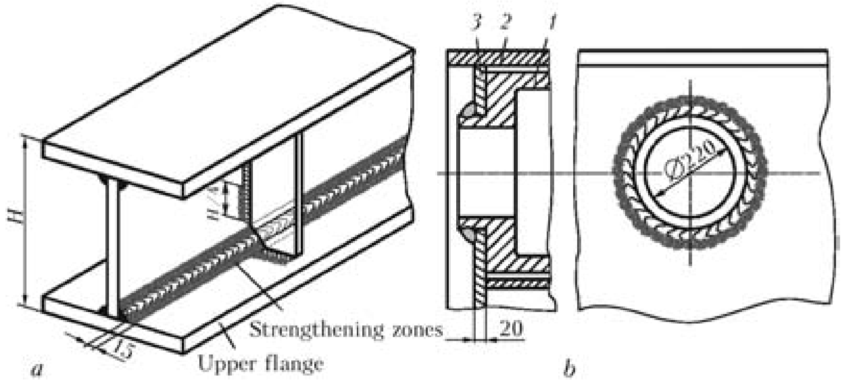

Figure 6. Strengthening zones of welded joints (darkened) of crane beams (*a*) and balance beam of well cranes (*b*): *1* — bushing; *2* — upper flange; *3* — web

Another critical welded structure subjected to cyclic loading and formation of fatigue fractures is a balance beam of well crane «Slabing-1150». It was found by the service of master mechanic together with authors that effect of alternating loads caused service life of a balance beam to be not more than three months before initiation of crack along the weld or HAZ metal at the distance of 5–10 mm from the fusion line in the zone of welding-on of a bushing to the body of a balance beam (Figure 6, *b*).

At the beginning of 2007, basing on the results represented in this article, two balance beams of well cranes were treated using a ball-rod strengthener. Nowadays the life of balance beams after such strengthening treatment reached 15-times increase. The operation of balance beams is continuing, thus proving high technical and economic efficiency of strengthening treatment using the ball-rod strengthener.

1. Trufyakov, V.I. (1973) *Fatigue of welded joints*. Kiev: Naukova Dumka.
2. Mikheev, P.P. (1981) *Methods of fatigue resistance improvement of steel structure welded joints*. Kiev: Znannya.
3. Asnis, A.E., Ivashchenko, G.A. (1985) *Increase in strength of welded structures*. Kiev: Naukova Dumka.
4. Olejnik, N.V., Kychin, V.P., Lugovsky, A.L. (1984) *Surface dynamic strengthening of machine parts*. Kiev: Tekhnika.
5. Kolomijtsev, E.V., Serenko, A.N. (1990) Effect of ultrasonic impact and laser treatment on fatigue resistance of welded joints in air and corrosion media. *Avtomatich. Svarka*, **11**, 13–15.
6. Kravtsov, T.G., Sevryukov, V.V. (2001) *Ultrasonic treatment of ship parts and welded structures*. Nikolaev: UGMTU.
7. Kolomijtsev, E.V., Serenko, O.M., Kirilchenko P.M. *Device for deformation strengthening of welded joints*. Pat. 30992 Ukraine for utility model. Publ. 25.03.2008.
8. Makhnenko, V.I., Kravtsov, T.G. (1986) Thickness of plastically deformed layer in ultrasonic impact treatment of surfaced products. *Avtomatich. Svarka*, **8**, 14–19.

LASER WELDING OF THIN-SHEET STAINLESS STEEL

V.D. SHELYAGIN[1], **A.G. LUKASHENKO**[1], **D.A. LUKASHENKO**[1], **A.V. BERNATSKY**[1], **V.P. GARASHCHUK**[2] and **V.I. LUTSENKO**[3]

[1]E.O. Paton Electric Welding Institute, NASU, Kiev, Ukraine
[2]National Technical University of Ukraine «Kiev Polytechnic Institute», Kiev, Ukraine
[3]SRIC ARMATOM Ltd., Kiev, Ukraine

Peculiarities of laser welding of the 0.15 and 0.20 mm thick austenitic stainless steel sheets were studied. It was shown that at a certain power of the laser beam the experimentally measured width of the weld could be satisfactorily described by the model of a linearly moving source in a homogeneous approximation. Increase in power of the laser beam results in formation of a hole on the surface being welded, through which part of the beam power goes away, thus leading to violation of correlations with the model. Based on the peculiarities revealed, a procedure is proposed for determination of optimal welding parameters to provide the maximal effective efficiency of the process.

Keywords: *laser welding, stainless steel, thin sheet, effective efficiency, quality criteria, weld width and shape, weld metal structure, strength*

Butt laser welding of thin (δ = 0.1–0.2 mm) stainless steel sheets is applied for manufacture of tubular billets to produce bellows. A prompt selection of optimal welding parameters is required under the small-scale production conditions because of a large number of different types of the billets.

Domestic and foreign literature comprises an insignificant amount of publications dedicated to estimation and effect of the laser welding parameters on properties of the butt joints on thin stainless steels, and disclosing methods for selection of optimal technological modes [1–6].

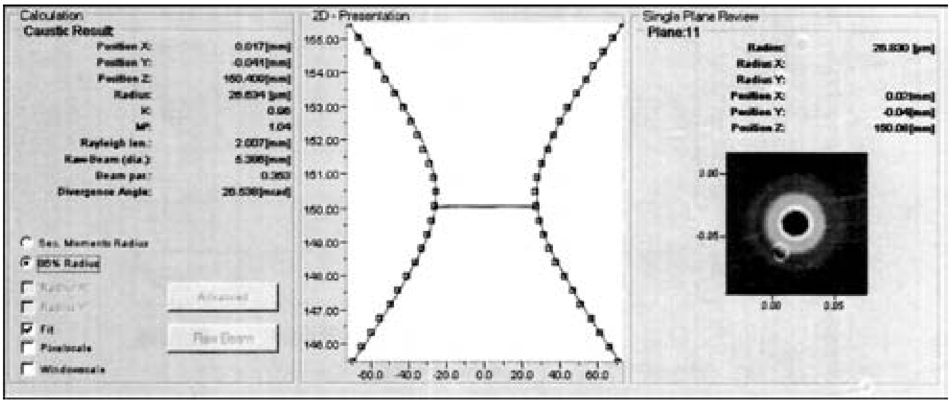

Figure 1. Characteristics of the beam of laser LS-01-B determined by using software «Primes Laser Quality Monitor»

The purpose of this study was to determine relationship between parameters of laser welding of thin-sheet stainless steel and quality criteria of the welded joints, as well as to develop a procedure for selection of the welding parameters in the manufacturing environment.

Experimental materials and equipment. Strips with δ = 0.15 and 0.20 mm, made from steels 12Kh18N10T and 1.4541 (according to DIN EN 10028-7:2000, the latter being a close analogue of steel 08Kh18N10T) were welded.

The samples were welded by using three-coordinate laser system ARMA-100M (manufacturer — E.O. Paton Electric Welding Institute) equipped with the 100 W single-mode ytterbium fiber laser of the LS-01-B type (manufacturer — Research and Production Company IRE-Polus, Fryazino, Russian Federation), the generating core of which had a diameter of 10 μm. Characteristics of the laser beam are shown in Figure 1 [7]. The laser radiation was focused on metal into a 40 μm diameter beam.

Helium (from the top of the welded joint) and argon (from below) were used as shielding gases. The following data on consumption of some shielding gases and their mixtures were obtained experimentally, m^3/s: He $(50-60)\cdot10^{-5}$, He + 50 % Ar $(45-55)\cdot10^{-5}$, and Ar $(15-20)\cdot10^{-5}$.

Both butt welded joints and penetration welds on a whole metal sheet were investigated. The sheets for butt welding were cut by sheet shears with electric drive MHSU 1000×2.0 (Schroeder Maschinenbau, Germany). The device in which the sheets to be welded were abutted provided minimal deplanation of edges.

Strength of the welded joints was tested by using tensile testing machine FP10/1. Width of the welds was measured in a region produced under the steady-state thermal conditions of welding by using small toolmaker's microscope MMI-2. Geometry of the weld and strength of the joint were chosen as key criteria of quality of the welded joints.

Main requirements to geometry of the weld on tubular billets of bellows were verticality of the fusion line and absence of rolls and sags. With these requirements it is possible to investigate only the relationship between the welding process parameters and width of the weld.

Effect of welding speed on weld (penetration) width. Samples of steel 12Kh18N10T with thickness of 0.15 mm were welded and penetrated at constant laser power P = 65 W, and those of steel 1.4541 with thickness of 0.15 and 0.20 mm were welded and penetrated at P = 55 and 60 W, respectively. Welding speed v_w was varied from 0.8 to 2.5 cm/s. Dependencies of the weld width and effective efficiency on the welding speed for the samples of the above steel grades are shown in Figure 2.

Curve *1* in Figure 2 (experimental data) shows variations in width of the welds on steel 12Kh18N10T with thickness of δ = 0.15 mm depending on the weld-

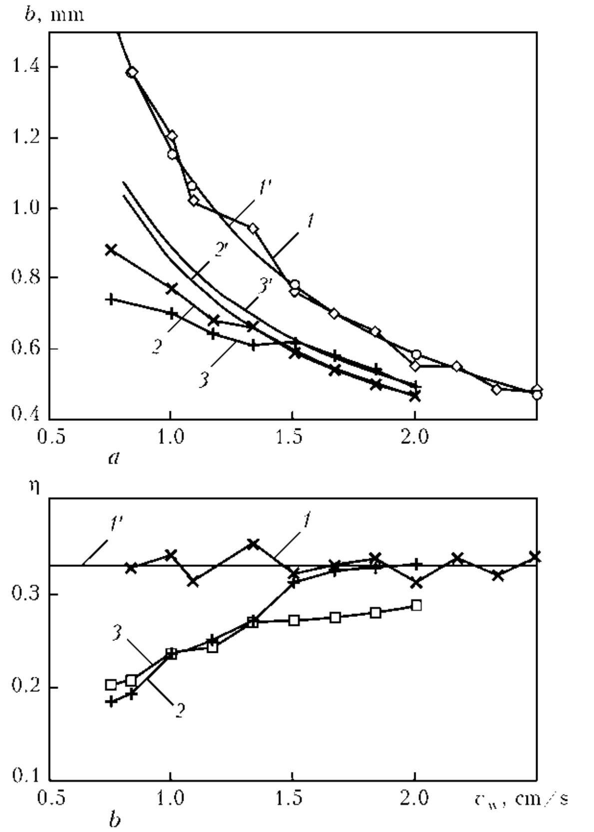

Figure 2. Dependence of weld width b (*a*) and effective efficiency η (*b*) on welding speed v_w in samples of steel 12Kh18N10T with δ = 0.15 mm (*1*, *1'*), and steel 1.4541 with δ = 0.15(*2*, *2'*) and δ = = 0.20 (*3*, *3'*) mm

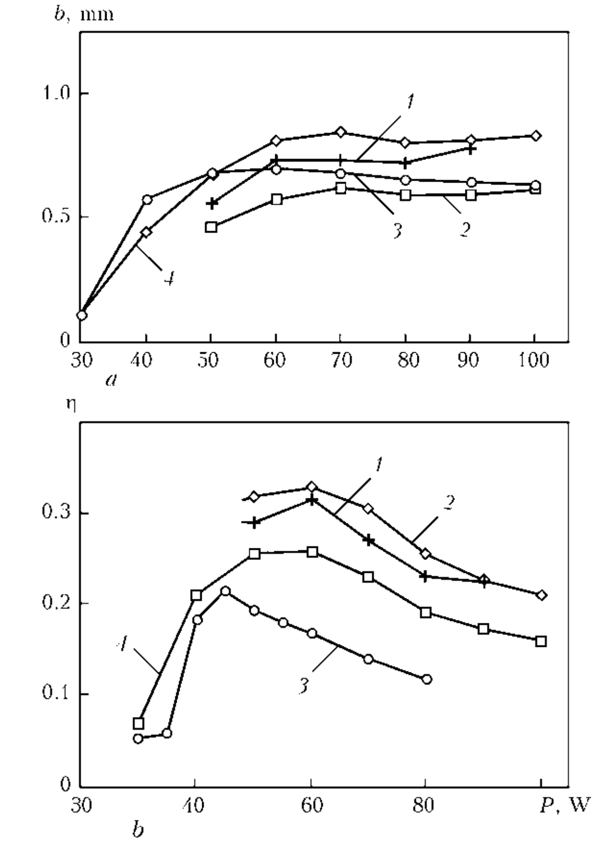

Figure 3. Dependence of weld width b (a) and effective efficiency η (b) on the beam power in samples of steel 12Kh18N10T with δ = = 0.15 mm at v_w = 1.5 (*1*) and 2.0 (*2*) cm/s, and steel 1.4541 with δ = 0.15 (*3*) and 0.20 (*4*) mm at v_w = 0.8 cm/s

ing speed, whereas curve *1′* was calculated by the least square method as $b = f(v_w)$. As seen from the Figure, all of the experimental points fit well the hyperbolic curve described by expression

$$b = 2.981 \cdot 10^{-3} + 1.163/v_w. \quad (1)$$

For steel 1.4541 the hyperbolic dependence takes place only at a high welding speed (compare curves *2*, *2′* and *3*, *3′* in Figure 2, *a*). Moreover, for the steel strip with δ = 0.20 mm this dependence holds at a somewhat lower speed than for the strip with δ = = 0.15 mm. At both values of the strip thickness and a low welding speed the weld width is smaller than it follows from the hyperbolic dependence determined from the experimental data at a high welding speed.

Dependence of weld width on laser radiation power. The experiments were carried out at constant welding speeds v_w = 0.8, 1.5 and 2.0 cm/s and at a power varied from 30 to 100 W. The results obtained are shown in Figure 3, *a*.

In the samples of steel 12Kh18N10T with δ = = 0.15 mm and at a welding speed of 1.5 and 2.0 cm/s the weld width grows with a power increased to 60 W (curves *1* and *2* in Figure 3, *a*), whereas the weld width hardly depends on it at higher values of P.

The samples of steel 1.4541 with δ = 0.15 and 0.20 mm were welded at welding speed v_w = 0.8 cm/s. At a power of 30 and 40 W the weld width was almost the same as in the samples of steel 12Kh18N10T with δ = 0.15 mm. The growth of the weld width slowed down with increase in the P values, and at $P \geq 60$ W the value of b remained almost unchanged (see curves *3* and *4* in Figure 3).

Strength characteristics of welded joints. The joints were made by using argon (from below of a welded joint) and helium (from the top) as shielding gases. The Table gives results of tensile tests of the welded joints. Comparison of these results shows that the strongest joints most fully meeting the specification requirements were produced at a laser beam power of 50–65 W and welding speed of 1.0 to 1.8 cm/s.

Metallographic examinations of weld metal. The samples of the 1.4541 steel strip (base metal had austenitic structure with precipitated carbonitrides) were examined. The samples were welded at laser beam power P = 40, 50, 60 and 70 W and v_w = 1 cm/s. The samples were etched by the electrolytic method in 20 % solution of chromic acid. Hardness was measured with LECO microhardness meter M-400 under a load of 0.98 N. The content of ferrite was determined by using ferrite meter «Ferritgehaltmesser 1,053» (Germany).

The following conclusions can be made based on the metallographic examinations of the said samples:

- at a laser beam power of 40–70 W and welding speed of 1 cm/s the fusion lines are located almost vertically, and there are no rolls and sags (Figure 4);
- columnar crystalline grains are located at the end of the cast zone, and equiaxed crystals are at the centre;
- hardness of the weld metal increases insignificantly (by 13–17 %) compared to the base metal (hardness of the base metal is *HV*01 156–165, hardness in the central part of the weld is *HV*01 176–193, and that in the heat-affected zone is *HV*01 165–181);
- content of the ferrite phase increases from 0 (in the base metal) to 0.15 vol.% (in the weld metal) with increase in the laser beam power.

Results and discussion. The model of a moving linear concentrated source in a homogeneous approximation with Gaussian distribution of the radiation intensity, at which the temperature at any point of a sheet is the same or thickness-averaged, was taken as a scheme for calculation of metal heating [8].

Comparison of practical results (see Figure 2) with the calculated ones showed that the speed values coincided in a certain range. Besides, maximal temperature T_{max}, which is achieved at distance y_0 from the weld axis, can be determined by the following expression [9]:

$$T_{max} = \frac{0.484q}{v_w c\gamma 2y_0}\left(1 - \frac{\beta y_0^2}{2a}\right)^2, \quad (2)$$

where q is the thermal power of the laser beam; $c\gamma$ is the volumetric heat capacity; β is the heat transfer coefficient; and a is the thermal diffusivity coefficient. At T_{max} equal to the melting point of the investigated steel, $2y_0 \equiv b$. As welding is performed at a high speed, it can be assumed that the surface heat transfer is negligible ($\beta = 0$). Then dependence of the weld width on the welding speed can be described by the hyperbolic dependence.

Approximation function (1) differs from dependence (2) in a free term. However, its value is so low that it can be neglected. Good agreement of dependencies (1) and (2) in some regions of the weld is indicative of low and stable heat losses taking place during dwelling of such a region at the melting point.

It is a common practice to characterise efficiency of the welding process by the value of effective efficiency η, which is usually determined by the calorimetry method. However, this method fails to give reliable results in welding of thin sheets with a low-power laser source. The calculated value of η can be used for qualitative estimation of the efficiency of the welding process. We use formula (2) to calculate the thermal power required for penetration of the sheet to a width whose values were determined experimentally. The ratio of the calculated value of the thermal power to the laser beam power gives us the value of the coefficient of utilisation of the laser beam power or effective efficiency η.

The following thermal-physical characteristics of stainless steel were used to calculate η: thermal conductivity coefficient $\lambda = 0.25$ W/(cm·K) (for high-alloy steels the values of λ grow with increase in temperature approximately up to 1100 K, above which the values of λ for different steel grades in the austenitic state are close to each other and do not exceed 0.25–0.33 W/(cm·K) [9], the lowest value of λ out of the probable ones was taken because of its increase at a low temperature); specific heat $c = 3.97$ J/(m^3·K) (0.46 kJ/(kg·K)); thermal diffusivity coefficient $a = 0.063$ cm^2/s; and melting point $T_{max} = 1673$ K [10]. Dependence of the coefficient of the effective efficiency on the welding speed and laser beam power is shown in Figures 2, *b* and 3, *b*, respectively.

According to expression (2), the weld width is directly proportional to the thermal power of a linear source. However, as evidenced by the experimental data, this dependence for steels 12Kh18N10T and 1.4541 holds only in the initial region of the curve (at a low power value), with increase in the power the weld width depends just insignificantly on P. For steel 1.4541 the weld width at a low welding speed is smaller than that following from the hyperbolic dependence (see Figure 2, *b*). It is shown in this Figure that in the regions of the hyperbolic dependence of the weld width on the welding speed the value of the calculated effective efficiency is constant and equal to $\eta = 0.33$ or close to it. In the regions where the experimental value of η deviates from the hyperbolic

Strength characteristics of welded joints produced at different welding parameters and using different shielding gases

Sample No.	P, W	v_w, cm/s	Tensile force F, MN	Elongation δ, %	Shielding gas
1	65	1.82	65.8	25.0	Helium
2	50	1.00	81.6	25.0	Same
3	60	1.25	86.7	28.0	»
4	65	1.67	45.0	12.5	Argon
5	50	1.00	57.3	16.3	Same
6	60	1.25	60.0	22.0	»
Base metal	–	–	63.6	32.4	–
Specification	–	–	≥54.0	≥20.0	–

dependence, $\eta < 0.33$, the higher the deviation, the lower being this value.

As seen from Figure 3, *b*, $\eta < 0.07$ at the lowest values of the power ($P < 40$ W), while with increase in power the effective efficiency grows to the values close to 0.33, and then decreases. The lowest values of η correspond to incomplete penetration of the sheet. The resulting $\eta = f(P)$ dependence can be explained as follows. The metal surface melts with increase in the beam power, the coefficient of absorption of laser radiation growing. This is followed by formation of a crater and keyhole, resulting in increase of the radiation absorption and effective efficiency. This mechanism works until the values of the beam power, at which the keyhole depth becomes equal to the sheet thickness, are achieved and until η amounts to the maximal value. Further increase in the beam power causes formation of a hole in the crater bottom, via which part of the laser radiation passes through the sheet transferring no energy to the metal edges. In this case the effective efficiency dramatically decreases. As in our case the diameter of the neck of the focused beam is approximately 0.04 mm, the calculated diameter of the linear source and temperature of its side surface should insignificantly depend on the power [11]. Growth of the laser radiation power

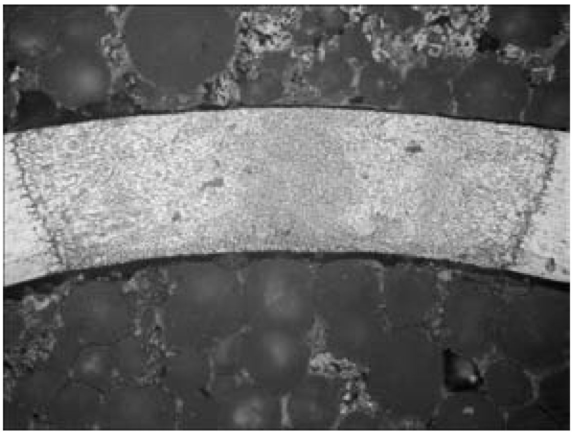

Figure 4. Macrosection (×200) of the joint on sheet steel 1.4541 with $\delta = 0.20$ mm welded at $v_w = 0.8$ cm/s and $P = 60$ W

Figure 5. Appearance of three-coordinate system of the ARMA-100M type for laser welding

leads to increase in the diameter of the hole formed inside the linear source and, hence, to the energy losses. With this the weld width is many times in excess of the diameter of the linear source and remains almost unchanged.

It can be concluded on the basis of estimates of the efficiency of the welding process that the technological parameters of welding can be selected from the maximal value of the effective efficiency.

Based on the above-said, formulate the procedure for determining the optimal technological parameters of laser welding of thin-sheet stainless steel billets: it is necessary to set the weld width required from the technological standpoint; experimentally determine dependence of the weld width on the welding speed, $b(v_w)$ at P = const; calculate the maximal value of the welding speed, $v_{w\,max}$, at which the rectangular weld geometry is provided; experimentally determine dependence $b(P)$ at $v_w = v_{w\,max}$; and find the inflection point, at which the value of the weld width, b, remains unchanged with further increase in laser radiation power P. The obtained values of the welding speed are optimal in terms of the maximal efficiency of the welding process.

This procedure was used for the development of the technology for laser welding of small batches of different-diameter longitudinal thin-walled stainless steel pipes intended for manufacture of bellows. The designed three-coordinate laser welding systems of the ARMA-100M type (Figure 5) were applied at Joint Stock Company «Kiev Central Design Bureau of Armature Engineering» (Kiev) and SRIC ARMATOM Ltd. (Kiev). Application of the developed procedure together with the ingenious technological fixture allowed achieving the monthly productivity of one such system equal to 5000 tubular billets for the manufacture of bellows. The bellows (Figure 6) were certified according to the OIT (Certification of Equipment, Products and Technologies for Nuclear Plants, Radiation Sources and Storage Facilities) certification system to correspondence to the requirements of the Russian codes, as well as other regulation documents that set requirements to ensuring safety in the field of utilisation of atomic energy in the Russian Federation.

Figure 6. Samples of multilayer bellows manufactured by laser welding of tubular billets of steel 1.4541 with δ = 0.15 mm

The products manufactured are used in different types of stop valves operating in increased-pressure pipelines and under constant high- and low-frequency vibrations, and in locking assemblies requiring precise adjustment of position of a locking element.

CONCLUSIONS

1. As experimentally established, the sound welded joints meeting the corresponding specification requirements can be provided at a laser beam power of 50–65 W, welding speed of about 1 cm/s, and helium (from the top) and argon (from below) used as shielding gases.

2. The procedure was developed for determination of optimal technological parameters to provide the maximal efficiency of the welding process under production conditions.

1. (1974) *Technology for fusion electric welding of metals and alloys*. Ed. by B.E. Paton. Moscow: Mashinostroenie.
2. *http*://www.thefabricator.com/article/tubepipeproduction/laser-welding-of-stainless-pressure-tubes
3. *http*://www.medicaldevice-network.com/features/feature81029/
4. Daurelio, G., Memola Capece Minutolo, F., Curcio, F. et al. (2003) On the welding of austenitic/ferritic stainless steels by a high power diode laser. In: *Proc. of 12th Int. Sci. Conf. on Achievements in Mechanical & Materials Engineering* (7–10 Dec. 2003, Gliwice), 187–190.
5. Nobuyuki, A. (2005) Microwelding of thin stainless steel foil with a direct diode laser. *Transact. of JWRI*, 34(**1**), 19–23.
6. Stasovsky, Yu.N. (2008) Scientific bases of resource-saving technologies for manufacturing small-size precision pipes as applied to minicompanies using thin-wall welded billets. *Suchasni Problemy Metallurgii*, **11**, 377–384.
7. (2009) *YLR-100-AC*: Ytterbium fiber laser. IPG Laser GmbH.
8. Rykalin, N.N. (1951) *Calculations of thermal processes in welding*. Moscow: Mashgiz.
9. Grigoriants, A.G., Shiganov, I.N., Misyurov, A.I. (2006) *Technological processes of laser treatment*: Manual for institutes of higher education. Moscow: N.E. Baumana MGTU.
10. Averin, V.G., Aronzon, B.A., Babaev, N.S. et al. (1976) *Tables of physical values*: Refer. Book. Ed. by I.K. Kikoin. Moscow: Atomizdat.
11. Vedenov, A.A., Gladush, G.G. (1985) *Physical processes in laser treatment of materials*. Moscow: Energoatomizdat.

METHOD FOR ESTIMATION OF WELDING PROPERTIES OF POWER SOURCES FOR ARC WELDING

N.V. SHEVCHENKO[1], **I.O. SKACHKOV**[1] and **V.E. PONOMAREV**[2]
[1]National Technical University of Ukraine «Kiev Polytechnic Institute», Kiev, Ukraine
[2]Federal University, Uberlandia, Brazil

Method for in-process monitoring of welding properties of power sources by their electric parameters using fuzzy logic algorithms was developed. Criteria for estimation of each indicator and an algorithm for obtaining a general estimate are proposed.

Keywords: *arc welding, power source, welding properties, method for estimation, fuzzy logic algorithms*

There is a necessity to monitor welding properties of the power sources during their production and process of operation. Today, the power sources are to fulfill the requirements of DSTU 60974–1 [1], in which a method for monitoring of welding properties is not indicated. Many enterprises still use the recommendations of GOST 25616 [2] which are based on indirect estimation of the power sources for manual arc and CO_2 welding by expert methods. Two high-qualified welders are recruited to perform that in accordance with the standard.

Differential method of monitoring is used for arc welding power sources in accordance with given standard and the following indicators of welding properties are estimated: initial arc ignition, stability of welding process, metal spattering, quality of weld formation and arc elasticity.

The indicator of welding properties of the power sources for CO_2 welding is estimated by reliability of establishing of welding process, metal loss and quality of weld formation.

There are methods based on simple calculations by overall indicator for objective decision-making which take into account contribution of each indicator [3–5]. Their disadvantage is caused by influence of human factor.

There is a possibility to determine parameters of all specified indicators on results of registration of energy parameters of the welding process, namely, welding current and voltage, without human assistance. Application of artificial intelligence systems, i.e. fuzzy logic algorithms, is one of the variants for solving the problems of influence of the human factor on estimation results.

Estimation of each quality indicator lies in referring it to one of the sets: «fulfill the requirements» or «do not fulfill the requirements». The fuzzy logic system allows estimating to which set a value of quality indicator refers as well as level of its membership in this set. For this, membership function $\mu A: X \to$ $\to [0, 1]$ is used. It for each element x puts in correspondence figure $\mu A(x)$ from [0, 1] interval, where 0, 1 are the lowest and the highest level of membership of element in subset, respectively.

In general, a mechanism of logical conclusion (Figure 1) includes four stages [6]:

- introduction of fuzziness. Membership functions, determined on input variables, are applied to their true values for determining a degree of prerequisite validity of each rule;
- logic conclusion. Obtained value of validity for the prerequisites of each rule is applied to the conclusions of each rule;
- composition. Fuzzy subsets, specified for each conclusion variable (or one variable), are combined together for formation of one fuzzy subset;
- reduction to crispness (defuzziness).

This method is used when it is necessary to transfer from the fuzzy conclusion to crisp output value.

Initial arc ignition and reliability of establishing of MMA and MAG welding processes were estimated by amount of continuous short circuits or arc extinctions up to establishing of the stable mode. The initial ignition is considered unsatisfactory, if amount of short circuits or arc extinctions exceeds 5. Hence, a linear membership function (Figure 2, *a*) is taken, in

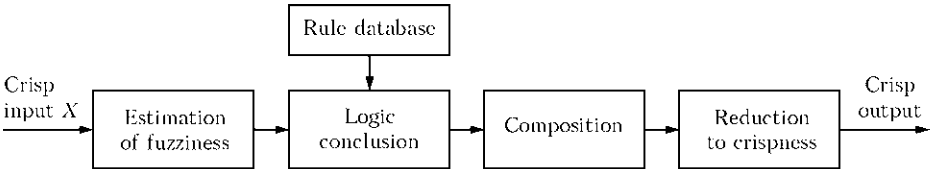

Figure 1. System of fuzzy logic conclusion

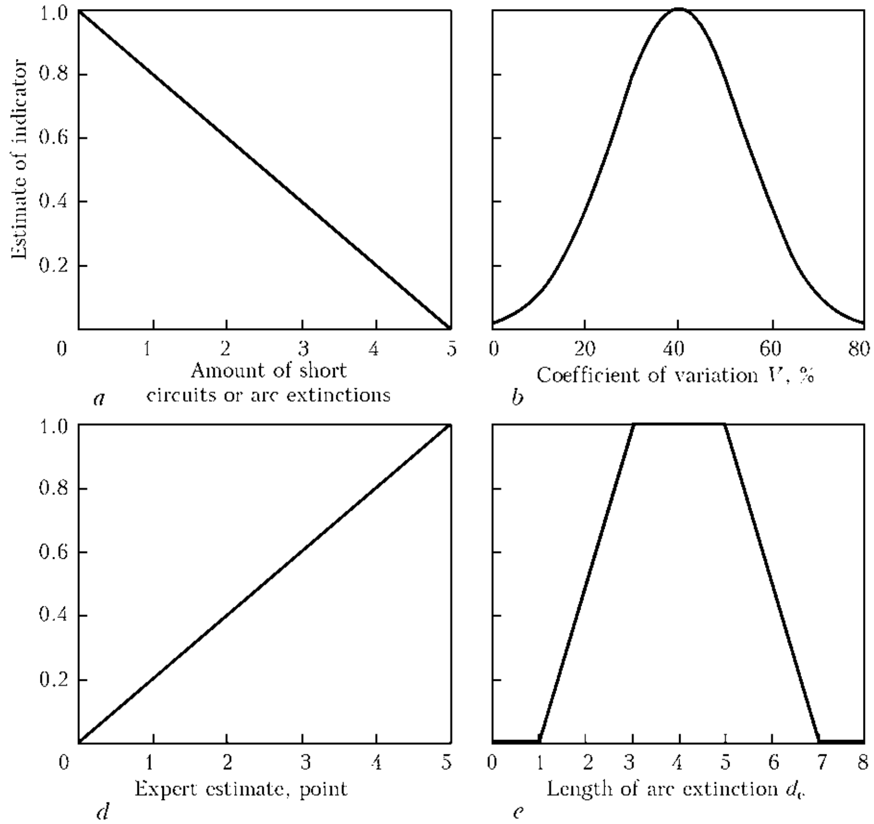

Figure 2. Membership function: *a* — initial arc ignition; *b* — stability of arcing; *c* — metal spattering; *d* — quality of weld formation; *e* — arc elasticity

which the maximum estimation corresponds with absence of short circuits or arc extinctions and the minimum if they make 5. Such a function follows the next equation:

$$\text{trim } f(x) = \max\left(\frac{5-x}{5};\ 0\right),$$

where x is the amount of continuous short circuits or arc extinctions.

The amount of arc extinctions in the process of welding was estimated in the similar way.

The stability of MMA welding process is usually estimated by arc vibration and noise. They, in-turn, are generated by variations of electric parameters. Thus, noise and vibration of the arc can be estimated by deviations of electric parameters of the arc, namely, current and voltage. The deviation of parameters is characterized by their coefficient of variation (standard deviation to mathematical expectation ratio). The power source has an external dropping characteristic in manual arc welding. In this case, the coefficient of variation of arc voltage is good to be used for estimation of arcing stability. A value of coefficient of variation at stable welding process was determined experimentally. Welding of samples from low-carbon steel at different parameters of the power source by ANO-21 and UONI-13/45 electrodes was carried out. Stability of arcing was evaluated by expert estimation from welder. Dependence of coefficient of voltage variation on welding current was obtained for manual arc welding at stable arcing. Deviation from this value towards the lower or higher values means reduction of arcing stability. In this case, roof or Gaussian function of membership can be chosen. The roof function estimation is adequate only at significant deviations of input volue (coefficient of variation of welding voltage) from optimum value. In case of small deviations (up to 10 %), the estimation, obtained with the help of roof function, are to be low, that will result in reduction of accuracy of system operation in total. Therefore, Gaussian function of membership is taken. Its value equals 1 at optimum input value x for set mode (Figure 2, *b*). An equation of such a membership function for manual arc welding with 100 A current will be

$$\text{gaussm } f(x) = \exp\left(-\left(\frac{x-40}{20}\right)^2\right),$$

where x is the coefficient of arc voltage variation.

Metal loss was estimated by furn-off loss and spattering coefficient K_l which is determined by formula

$$K_l = \left(1 - \frac{M_d}{M_m}\right) 100\ \%,$$

where M_d, M_m is the mass of deposited and molten electrode metal, respectively.

The coefficient of spattering up to 15 % [7] is considered to be acceptable in manual arc welding. A sigma function of membership (Figure 2, *c*) is built for specified quality indicator. Estimate 0.5 corresponds with input value x, equal 15 %. An equation of such a membership function is the following:

$$\text{sigm } f(x) = \frac{1}{1 + \exp(0.5(x - 15))}.$$

The quality of weld formation was determined by appearance of a bead and its height to width ratio equal arithmetic mean of three measurements, carried out in the beginning, end and middle parts. The estimate is set by expert using points from 0 to 5, membership function is linear (Figure 2, *d*). An equation, describing this function, is

$$\text{trim } f(x) = \max\left(\frac{x}{5}; 0\right),$$

where x is the estimate of weld appearance in points.

The arc elasticity was estimated by its extinction length. Minimum satisfactory length of the arc is a length equal two diameters of the electrode. The length exceeding three diameters of the electrode [2] is considered to be a good result. However, too high arc elasticity prevents performance of normal welding in vertical and overhead positions. Therefore, it is reasonable to set an upper limit for normal arc length for extinction at the level of five diameters of the electrode (for general-purpose power sources, if no specific requirements to arc elasticity are set) [8]. The membership function is trapezoid (Figure 2, *e*) and is described by equation

$$\text{trap } f(x) = \max\left(\min\left(\frac{x-1}{2}; 1; \frac{x-7}{-2}\right); 0\right).$$

In general, a set of membership functions is determined by customer's requirements to welding properties of the power sources and their operation conditions.

Operation of the system is performed by Mamdani algorithm [6]. Weight coefficients of each input are set depending on power source requirements. For example, the indicators of initial ignition and arc elasticity are more significant for manual arc welding in vertical and overhead positions. At that, the weight coefficients of given inputs are higher than in the others. The weight coefficient is higher for «metal spattering» indicator etc. in welding of face surfaces or surfaces with corrosion-resistant coatings. If such additional requirements are not specified, then the weight coefficients of all inputs are selected equal 1.

«Cut off» levels for each input of the system are determined based on rulebase:

$$\text{«IF» } (\text{Input}_1 - \text{MF}_1) \text{ and } (\text{Input}_2 - \text{MF}_2) \text{ and}$$
$$\ldots (\text{Input}_n - \text{MF}_n) \text{ «THEN» } (\text{Output} - \text{MF}_{\text{out}}),$$

where $\text{MF}_1, \ldots, \text{MF}_n$ are the membership functions of system inputs; MF_{out} is the membership function of system output.

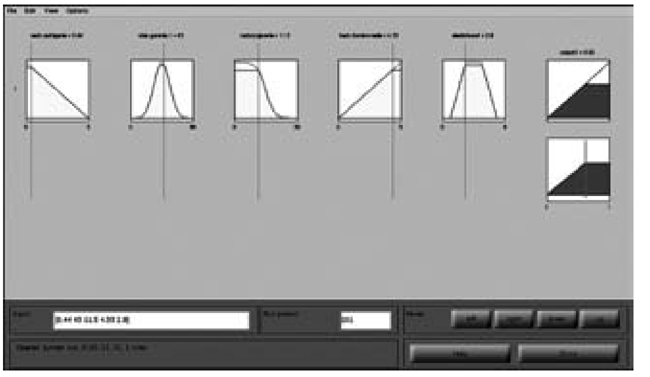

Figure 3. Fuzzy logic toolbox window with results of operation of system for estimation of welding properties

Further truncated functions of membership are determined. Joining of found truncated functions was performed using prod operation that results in obtaining of resultant fuzzy subset for output variable. Final stage is determining of crisp value of output variable by first maximum method. Membership function for output was assumed linear; 0 — when product of estimates of all outputs equal 0; 1 — when product equal 1. General estimate of all welding properties is determined as

$$\gamma = \prod_{n=1}^{N} x_n^{\varepsilon_n},$$

where N is the amount of indicators of welding properties; ε_n is the weight of n-th indicator; x_n is the value of estimate of each indicator.

As a result, the general estimate of welding properties of the power source which lies in the ranges [0, 1] (Figure 3) was obtained. The estimate is non-linear. The analysis showed that traditional estimate «excellent» corresponds with the value of general estimate in the range from 0.51 to 1, «good» — 0.28–0.50, «satisfactory» — 0.17–0.27 and «unsatisfactory» — 0–0.26. Construction of a system for estimation of welding properties was carried out in MatLab medium.

Table 1. Results of estimation of welding properties of «Fronius TPS 5000» power source by automated system

Parameter	Average value of parameter	Estimate by automated system
Initial arc ignition (amount of short circuits)	0.44	0.912
Stability of welding process (coefficient of voltage variation)	0.43	0.977
Metal spattering, %	11.5	0.852
Quality of weld formation (expert estimation)	4.33	0.866
Arc elasticity (diameter of electrode)	2.9	0.95
General estimate		0.62 (excellent)

Table 2. Comparison of results of estimation of welding properties (average values of indicators on results of deposition of several beads)

Parameter	Estimation by automated system	Average estimate of welder 1	Average estimate of welder 2
Initial arc ignition	4.6	4.5	5.0
Stability of welding process	4.9	4.0	4.0
Metal spattering	4.3	4.4	4.7
Quality of weld formation	4.3	4.1	4.0
Arc elasticity	4.8	4.7	4.6

Two methods were used for monitoring of system operation by comparison of results of estimation for «Fronius TPS 5000» inverter power source: in accordance with GOST 25616–83 standard, recruiting two high-qualified welders and using developed automated system. Estimation was carried out for the conditions of manual arc welding. Digital system for collection and recording of data was used for registration of welding current and voltage. It consists of current and voltage sensors based on Hall effect, analogue-to-digital transformer and PC. PowerGraph program was used for recording and analyzing of oscillograms.

As a result, the estimate of each welding property and general estimation by automated system were obtained (Table 1). Gathered data were transferred into a scale, regulated by GOST 25616–83 (Table 2) for comparison of results of automated system with results of welders' estimation. The result was multiplied 5 for transfer. The estimation of welding properties was carried out in accordance with test procedure, indicated in the standard.

CONCLUSIONS

1. Application of the automated systems based on fuzzy logic algorithms can solve a task of determination of windowed multicriteria estimation of quality indicators of the power sources.

2. Using of fuzzy logic and computer systems for data collection and processing provides the possibility of development of flexible systems for estimate of welding properties of the power sources for automatic arc welding. This allows reducing to minimum influence of the human factor on the estimation of welding properties.

1. *DSTU 60974-1–2003*: Arc welding equipment. Pt 1: Welding power sources. Valid from 01.07.2004.
2. *GOST 25616–83*: Arc welding power sources. Methods for testing of welding properties. Introd. 28.01.83.
3. Troitsky, V.A. (1981) Elements of defectology. In: *Nondestructive testing of welded joints*. Kiev: PWI.
4. Pokhodnya, I.K., Ponomarev, V.E., Zaruba, I.I. et al. (1992) Procedure of complex evaluation of welding-technological properties of power sources. In: *New welding power sources*. Kiev: PWI.
5. Troitsky, V.A. (1983) Quantitative evaluation of quality level of welding processes and equipment. *Avtomatich. Svarka*, **4**, 62–66.
6. Krichevsky, M.L. (2005) *Intellectual analysis of data in management*: Manual. St.-Petersburg: SPbGUAP.
7. Zhiznyakov, S.N., Sidlin, Z.A. (2006) *Manual arc welding. Materials. Equipment. Technology*. Kiev: Ekotekhnologiya.
8. Scotti, A., Ponomarev, V. (2008) *Soldagem MIG/MAG melhor entendimento, melhor desempenho*. SanPaulo: Artliber Editora.

UPGRADING OF ELECTRIC CIRCUIT OF A-1150 MACHINE FOR VERTICAL WELDING

V.I. STEPAKHNO, L.N. KOPYLOV and **G.S. ZELENCHENOK**
CJSC «PWI PPWE», Kiev, Ukraine

A-1150U machine designed in 1960s is still in demand in its upgraded form in shipbuilding, bridge and storage tank construction. Pilot Plant of Welding Equipment of the E.O. Paton Electric Welding Institute (PWI PPWE) developed a new control circuit based on modern components and control units. The new circuit provides substantial improvement of technical and service characteristics of the machine, and simplifies implementation of the welding process with forced weld formation. The machine with the new electric circuit is additionally designated by «K» index (A-1150K).

Keywords: *A-1150K machine, welding process with forced formation, weld metal, new electric circuit, small-sized panel-handle, electronic control circuit with feedbacks*

The industry of CIS and foreign countries has used A-1150 machine for welding vertical and inclined welds for more than 40 years now. During this period PWI PPWE has manufactured more than 150 equipment sets based on orders from users, which points to a high quality of the development and need for it in production.

Idea of development of a self-propelled machine for automatic welding of vertical butt welds, which could move directly over the butt without any guides of rack type, was put forward by Prof. B.E. Paton. Such equipment was required in ship-building, and bridge and tank construction. In these industries there is a need to perform large volumes of welding of extended vertical and inclined butt welds. Performance of this work required a large number of highly-qualified manual welders. Replacement of manual welding by automatic process was the only way to solve this important national economy problem.

Work on welding technology and machine design was performed at the PWI Design Bureau. A-1150 machine enabled realization of a highly efficient process of flux-cored wire welding with forced formation of weld metal using two copper water-cooled shoes, which are placed from the weld face and reverse side. Application of the above welding process enabled an essential improvement of the efficiency of welding vertical and inclined welds compared to manual welding. Thus, while in manual arc welding of 20 mm thick metal (09G2S steel) with UONI-13/55 electrodes (4 mm diameter, 140–150 A welding current) welding speed was equal to 0.4–0.5 m/h, the process of welding with forced formation by flux-cored wire of PP-AN5 grade allowed welding at currents of 400–420 A, achieving the welding speed of 4.8–5.2 m/h [1]. The main advantage of the proposed process consisted in that quality welding of critical welds could be performed by welders of a low qualification after short practical training.

First samples of A-1150 machine were introduced in the Kherson Shipbuilding Plant. After receiving positive practical results and approval of the technological process by the USSR Register, technology and equipment became widely applied in the shipbuilding plants [2], as well as in tank and bridge construction.

Machine design was continuously improved. Mainly the machine mechanical components were upgraded, which currently satisfy users of this equipment, unlike the electrical components. As a rule, changes in the electrical components were made at replacement of welding current source in the machine. In the first variant of A-1150 machine, welding arc and electric circuit were powered from welding generator converter of PSG-500 type. The next variant of the machine electric circuit (A-1150U) was developed after the industry has mastered manufacturing of welding rectifiers of VDU-504 (505, 506) type. In this variant power of machine control circuit was disconnected from the welding source, and it was powered independently from 380 V mains. Such a change noticeably improved the quality of welding process control. However, despite the made changes, electrical components of A-1150U machine do not meet the current requirements. In particular, the electric circuit is based on outdated components, electronic circuits for control of motors of machine displacement and electrode wire feed drives are absent. Change of motor rotation speed is performed by a simple circuit, without any feedbacks. In such a control system, most of the motor power is lost, particularly at motor operations at low revolutions. In addition, there is no possibility for visual control of the welding speed and electrode wire feed rate in machine preparation for operation and during welding. A certain inconvenience of machine control is related to the specifics of performance of the welding process with forced formation: the process requires continuous visual control of weld pool position relative to the upper edge of the forming shoe. This problem is solved by selection of the speed of machine movement using a resistor, which his traditionally located on the control panel. The only problem is that when looking for the resistor, the welder has to ignore the welding zone for a short time, which may lead to defects in welds.

Figure 1. Appearance of A-1150K machine

Considering the current need for machines of A-1150 type, a decision was taken to develop a new circuit based on modern components, which proved to be reliable in the equipment batch-produced by the plant. This work was performed when manufacturing two A-1150 machines for Bridge Construction Team of «Mostobud»(Dnepropetrovsk). Variant of A-1150 machine with a new electric circuit is marked by «K» index (A-1150K) (Figure 1).

New electric circuit was developed by plant specialists in keeping with the specification, which was prepared taking the above-mentioned drawbacks into

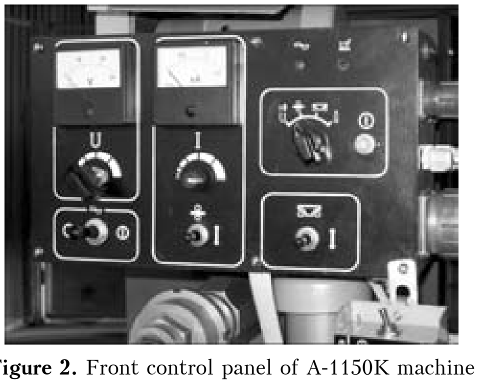

Figure 2. Front control panel of A-1150K machine

Figure 3. Small-sized panel-handle of A-1150K machine

account. Machine block-diagram includes the power unit, control panel, small-sized panel-handle, drive mechanisms and control drives. Electric circuit is independently powered from external 380 V, 50 Hz circuit. Control circuits are powered from 29 V constant voltage, which is generated in the power unit.

The front control panel (Figure 2) carries welding process controls: toggle switch and light indicator CIRCUIT ON; ammeter for welding current monitoring; voltmeter for visual monitoring of arc voltage U_a, electrode wire feed rate v_{el}, welding carriage speed v_c, button for monitoring shielding gas feed; switch for controlled parameter setting; two switches for setting the direction of electrode feed and carriage movement, and light indicator WELDING ON.

Visual monitoring of welding mode parameters at setting up is performed by readings of the voltmeter, which measures welding source voltage or armature voltage of motors of electrode feed and carriage movement mechanisms, when setting the mode parameter switch to the controlled parameter and pressing the button to switch on the reading. Welding mode parameters can be controlled both at setting up and in welding.

For convenience of process control in welding, the machine is fitted with a small-sized panel-handle (Figure 3), which carries the toggle switch for welding process switching on and off, STOP button for electrode feed and STOP for the carriage, button for switching on welding carriage travel speed, as well as a resistor to control the carriage speed.

The new electric circuit is arranged so that the controls used for machine setting up for welding, are located on the control panel and panel-handle, and all the controls used in performance of the welding process with forced formation of the weld metal, are located only on the panel-handle. During welding, the operator is holding the panel-handle in his hand, and its design enables performance of all the required operations with the fingers of the same hand, which is holding it. The following operations can be performed from the panel-handle: stop the machine travel carriage, switch on the travel speed of carriage movement, perform smooth adjustment of welding speed, stop electrode wire feed, switch the welding process on and off (switch on the welding source, electrode feed and shielding gas). All these operations are performed from the panel-handle without using the control panel. Thus, the welding process can now be controlled while keeping the weld pool in sight that is practically impossible, when operating the old variant of the equipment.

Main technical characteristics of A-1150U and A-1150K machines

Parameter	A-1150U	A-1150K
Mains voltage, V (50 Hz)	380	380
Control circuit supply voltage, V	29	29
Welding current at 100% duty cycle, A	500	500
Thickness of metal being welded, mm	8–30	8–30
Smooth adjustment of electrode feed rate, m/min	3.0–3.7	2.0–5.4
Smooth adjustment of welding speed, m/min	0.03–0.20	0.03–0.25
Electrode wire diameter, mm	2.5; 3.0; 3.5	2.5; 3.0; 3.5
Tractive force of movement mechanism, kg, not less than	120	140
Tractive force of electrode feed mechanism, kg, not less than	30	38
Machine weight (without cassette with electrode wire), kg, not less than	32	32

As drives of electrode feed and machine displacement mechanisms, the machine uses electric mechanisms with DC motors of 130 W power with permanent magnets in the excitation system (in A-1150U machine electric mechanisms with 90 W motors were used). For motor control the new circuit uses power units with feedbacks, providing minimum power losses at motor operation at low revolutions, and rotation stabilization at unauthorized load changes.

Testing of A-1150K machines showed that the used design solutions improved the service properties and simplified practical realization of the process of welding with forced formation of weld metal. Upgraded A-1150 K machine provides a high quality of welded joints and is recommended for application in different industries.

1. Pokhodnya, I.K., Dubovetsky, V.Ya., Shlepakov, V.N. et al. (1966) Vertical arc welding with weld forced formation. *Avtomatich. Svarka*, **11**, 67–70.
2. Voinov, S.V. (1982) *Automatic vertical welding*. Leningrad: Sudostroenie.